Faculdade de Engenharia da Universidade do Porto


# Can graphene be the missing piece to use human placenta in the treatment of myocardial infarction?

Maria Inês da Silva Passos Chaves Fernandes

DISSERTATION

Integrated Master in Bioengineering

Major Biomedical Engineering

Supervisor: Inês Gonçalves

Co-supervisor: Andreia Pereira

June, 2021

# Resumo

As doenças cardiovasculares são a principal causa de morte mundialmente. Quando as artérias coronárias que fornecem o sangue ao coração bloqueiam, o fluxo sanguíneo é comprometido levando a um enfarte do miocárdio que tem uma taxa de mortalidade de ~30 %. Para restabelecer o fluxo sanguíneo, um do procedimentos possivéis é uma cirurgia de revascularização do miocárdio que requer a utilização de enxertos autólogos, vasos recolhidos do paciente. No entanto, os enxertos autólogos nem sempre estão disponíveis, e alguns deles estão associados a elevadas taxas de mortalidade (até 50 %) devido à ocorrência de trombose ou infeção. Em caso de falha, os pacientes têm de efectuar uma segunda intervenção e/ou podem morrer. Assim, são necessárias novas soluções para substituir os enxertos autólogos na revascularização do miocárdio. Abordagens de tecidos, que visam promover a remodelação dos enxertos, têm sido frequentemente adoptados para conceber enxertos vasculares de pequeno diâmetro (SDVG). As matrizes descelularizadas representam uma scaffold de engenharia de tecidos interessante para SDVGs, uma vez que a estrutura e a maioria das propriedades bioquímicas do tecido original são preservadas. Contudo, as matrizes obtidas apresentam fracas propriedades mecânicas e baixa hemocompatibilidade. Assim, é importante afinar estas características das matrizes descelularizadas para se obter um desempenho semelhante ao do tecido original.

Uma das estratégias para melhorar estas propriedades é a utilização de materiais à base de grafeno (GBMs) nas diferentes matrizes descelularizadas. O grafeno é o material mais forte do mundo e tem sido descrito como citocompatível e antimicrobiano, o que pode ser interessante para aplicações biomédicas. No que diz respeito à hemocompatibilidade, estudos adicionais sobre o revestimento de tecido descelularizado com óxido de grafeno reduzido (rGO) e óxido de grafeno (GO) ainda precisam de ser realizados, uma vez que os resultados são contraditórios.

Neste trabalho de dissertação, foram propostas duas estratégias para desenvolver o SDVG: 1) descelularização da artéria do cordão umbilical (dArtery) e revestimento com GBMs no interior do lumen, já adquirindo scaffolds com geometria tubular, e 2) descelularização e digestão de tecidos da placenta humana e preparação de um hidrogel derivado de matriz extracelular (ECM) com GO incorporado, para uso futuro como bioink para produzir canais tubulares. Na primeira estratégia, a descelularização das artérias do cordão umbilical foi realizada com a promoção de lise celular e ruptura da membrana com ciclo de congelamento/descongelamento, pressão osmótica e solução de 1 % de Triton X-100 contendo ácido etilenodiamino tetra-acético (EDTA) para enfraquecer a adesão das células. Finalmente, a hidrólise do ácido desoxirribonucleico (ADN) e a sua remoção completa

foram realizadas utilizando DNase. A eficiência do processo de descelularização foi confirmada por microscopia de fluorescência após marcação de núcleos celulares e por quantificação do ADN, obtendo 94.7 % de diminuição na melhor condição (DNase a 4 ºC). A descelularização dos tecidos da placenta humana: âmnio e cório, foi realizada utilizando dois métodos diferentes, seja utilizando SDS ou de forma semelhante à descrita para as dArteries, mas com 3 ciclos de 2 % de Triton X-100 e 1.2 % de DNase ou 0.04 % de DNase. A quantificação do ADN confirmou uma maior eficiência (99.5 %) com Triton X-100 e 1.2 % de DNase. A incorporação GBMs nas diferentes matrizes descelularizadas foi então realizada. Foram incorporados diferentes tipos de GBMs, com tamanho lateral diferente, na dArtery usando várias estratégias: perfusão, pressão e pressão + perfusão. Apesar da microscopia electrónica de varrimento ter confirmado um revestimento homogéneo do lúmen interno, nenhum GBM foi capaz de melhorar as propriedades mecânicas das artérias descelularizadas. No que toca a hemocompatibilidade das dArteries, o tempo de coagulação foi avaliado adicionando plasma humano recalcificado a dArteries não revestidas e revestidas com GO, com e sem heparinização prévia. A heparinização parece ser necessária para evitar a coagulação do plasma, e tal como as dArteries sem revestimentos heparinizadas, as dArteries revestidas com GO heparinizadas também não induziram a formação de coágulos. Relativamente aos hidrogéis derivados de ECM, foram incorporados 1 % GO e 10 % GO, com a condição de 10 % GO levando a um reforço mecânico de 174 %, quando adicionado após a digestão do hidrogel derivado de ECM. Em conclusão, este trabalho de dissertação permitiu obter artérias descelularizadas revestidas de GO hemocompatíveis, apesar de não mostrarem melhoria das propriedades mecânicas, e hidrogéis derivados de ECM reforçados, contendo 10 % GO, que podem ser uma matriz promissora para a produção de SDVGs ou para utilização como hidrogéis injectáveis onde os hidrogéis fortalecidos são uma vantagem.

# Abstract

*Cardiovascular diseases are the leading cause of death worldwide. When the coronary arteries that supply the heart block, the blood flow is compromised leading to myocardial infarction, which has a mortality rate of ~30 %. To re-establish the blood flow, a coronary artery bypass grafting surgery (CABG) may be performed. The gold standard for this procedure requires the use of autologous grafts, vessels harvested from the patient. However, autologous grafts are not always available, and some of them are associated with high failure rates (up to 50 %) due to thrombosis or infection occurrence. In case of failure, patients have to perform a second intervention and, in worst case scenarios, die. Thus, new solutions are needed to replace autologous grafts in CABG. Tissue-engineered approaches, which aim to promote graft remodelling, have been under investigation to design small-diameter vascular grafts (SDVGs) for CABG. Decellularized matrices derived from different sources are interesting tissue-engineered scaffolds for SDVGs, once they preserve the structure and most of the biochemical properties of the original tissue. However, the matrices obtained show poor mechanical properties and low hemocompatibility. Thus, it is important to tune these characteristics of decellularized matrices to obtain a performance similar to that of the original tissue.*

*One of the strategies to improve these properties is the use of graphene-based materials (GBMs) in the different decellularized matrices. Graphene is the strongest material in the world and has been described as cytocompatible and antimicrobial, which is crucial for biomedical applications. Regarding the hemocompatibility, further studies on the coating of decellularized tissue with reduced graphene oxide (rGO) and graphene oxide (GO) still need to be performed since the obtained results until now are contradictory.*

*In this dissertation work, two strategies were proposed to develop SDVG: 1) decellularization of the umbilical cord artery (dArtery) and coating of the inner lumen with GBMs, already obtaining scaffolds with tubular geometry, and 2) decellularization and digestion of human placental tissues and preparation of extracellular matrix (ECM)-derived hydrogels with incorporated GO, for future use as bioink to produce tubular conduits. In the first strategy, the decellularization of the umbilical cord arteries was performed with the promotion of cell lysis and membrane disruption with freeze/thaw cycle, osmotic pressure and 1 % Triton X-100 solution containing* Ethylene-Diamine-Tetra Acetic acid *(EDTA) to weaken cells adhesion. Finally, DeoxyriboNucleic Acid (DNA) hydrolysis and complete*

*removal were performed using DNase. Efficiency of decellularization process was confirmed by fluorescence microscopy after staining the cell nuclei and by DNA quantification, revealing 94.7 % reduction in the best condition (DNase at 4 ºC). The decellularization of human placental amnion and chorion plate tissues were performed using two different methodologies, either using SDS or similarly to the described for the dArteries, but with 3 cycles of 2 % Triton X-100 and 1.2 % DNase or 0.04 % DNase. DNA quantification confirmed higher efficiency (99.5 %) with Triton X-100 and 1.2 % DNase. The incorporation of graphene-based materials (GBMs) in the different decellularized matrices was then performed. Different types of GBMs varying in lateral size were incorporated in the dArtery using several strategies: perfusion, pressure and pressure + perfusion. Despite scanning electron microscopy confirmed a homogeneous coating of the inner lumen, none of the GBMs improved the mechanical properties of the dArteries. For the hemocompatibility of the dArteries, the clotting time was assessed by adding recalcified human plasma to uncoated and GO-coated dArteries, with and without previous heparinization. Heparinization seemed to be necessary to prevent plasma coagulation, and like heparinised uncoated dArteries, heparinised GO coated dArteries did not induce clot formation. Concerning the ECM-derived hydrogels, 1 % GO and 10 % GO were incorporated with 10 % GO leading to a mechanical reinforcement of 174 %, when added after digestion of the ECM-derived hydrogel. In conclusion, this dissertation work allowed to obtain hemocompatible GO-coated decellularized arteries despite not showing improvement of the mechanical properties, and reinforced ECM-derived hydrogels containing 10 % GO, which can be a promising matrix for the production of SDVGs or for use as injectable hydrogels where reinforced hydrogels are an asset.*

**The work presented in this thesis was developed at:**

Bioengineered Surfaces Group

i3S – Instituto de Investigação e Inovação em Saúde; INEB – Instituo de Engenharia Biomédica

Universidade do Porto, Portugal






**Funding:**

This work was financially funded by Fundação para a Ciência e a Tecnologia (FCT) and Fundo Europeu de Desenvolvimento Regional (FEDER) through Projects PTDC/CTM-COM/32431/2017 SoftStrong), 01-0145-FEDER-007274 and UID/BIM/04293/2019 (i3S).





# Agradecimentos

Em primeiro lugar, gostava de agradecer à minha orientadora, Inês Gonçalves, por todo o acompanhamento que me fez durante estes meses. A Inês sempre foi uma professora incansável, disponível para aconselhar e que, por isso, desde as suas aulas na FEUP, vi como uma referência. Obrigada por me ter sempre levado a dar o meu máximo, tirando-me da minha zona de conforto, e de me ter dado a oportunidade de apresentar o trabalho que desenvolvemos em conferências – quanto stress senti, mas com uma sensação de realização no final. Cresci e aprendi muito nestes últimos 6 meses, graças a si. Depois, quero também agradecer muito à minha co-orientadora, Andreia Pereira, por todo o apoio tanto prático – no laboratório, onde me ensinou as diferentes técnicas – como moral – com todas as conversas de incentivo e de encorajamento ao longo destes meses. Andreia, obrigada por toda a tua ajuda e por também me teres feito crescer, acreditando sempre em mim. A tua disponibilidade para ajudar e aconselhar os outros é constante e é das coisas que mais admiro em ti. Gostava de agradecer por me teres sempre incentivado a manter toda a minha 'outra vida' (projetos de voluntariado, concursos, ballet) alertando-me que não devo parar a minha vida pessoal por causa do trabalho. Tive mesmo muita sorte de ter trabalhado com a supervisão desta dupla fenomenal que me apoiou incondicionalmente.

Do ponto de vista de execução, o trabalho que fiz apenas foi possível graças à Dra Carla Ramalho e Dra Manuela Lopes do Centro Hospitalar S. João por me terem cedido as placentas e cordão umbilical, ao Dr Artur Pinto e à Licínia Timoncheco, do LEPABE, por terem gentilmente cedido o nGO para incorporação nas artérias descelularizadas, ao Dr Karl Schneider e à Dra. Helga Bergmeister por me terem cedido material para produzir os hidrogéis e por estarem sempre disponíveis para responder às minhas questões, à Paula Magalhães e Tânia Meireles do Cell Culture and Genotyping pela grande ajuda que me deram ao longo destes 5 meses na deteção do DNA e, por fim, ao Ricardo Vidal da Biointerfaces and Nanotechnology platform, por todo o apoio que me deu com a utilização do reómetro.

Gostava também de agradecer o apoio e orientação que senti quer por parte do professor Fernão Magalhães quer da professora Cristina Barrias, que foram seguindo o trabalho desenvolvido e que me ajudaram a desbloquear em alguns momentos mais desafiantes com os seus inputs.

Agradecer também ao meu grupo, Bioengineered Surfaces, liderado pela professora Cristina Martins, por me ter integrado, mesmo sendo uma época mais difícil que vivemos, sentindo sempre o apoio de todos os membros enquanto trabalhava no laboratório. Em especial, o Duarte Moura e a Helena Ferreira que estavam sempre disponíveis e também me guiaram nesta aventura. Sara, Sandra, Manuela e António, futuros mestres, obrigada pela vossa boa companhia e por todos os momentos de desabafo e entreajuda.

Um agradecimento muito especial à minha família toda. Aos meus pais (Teresa e Pedro) e irmão, Francisco, que foram um apoio incondicional e que me ajudaram sempre a pensar com clareza e a não desistir. Tudo se faz. Obrigada por terem sido o ombro amigo e o puxão de orelhas quando precisei. Ao resto da minha família: primos (Ico, Xica, Rita, Fá, Maria, Gongui, António, Luisinho, Mi e Luís), tios (Xinha, Abel Tiago, Cristina, Joana, João, Tiago e Ana) e avós (Zita, Tójão e Paulo), obrigada por terem sempre estado presentes ao longo da minha vida e por serem sempre pessoas com quem eu sei que posso contar e a quem irei sempre pedir conselhos.

Obrigada aos meus amigos que fiz na faculdade, na Missão País e Tochas, que foram um auxílio gigante ao longo destes 5 anos e que preencheram o meu tempo como estudante na FEUP com memórias inesquecíveis. À Carolina, Catarina, Adriana e Filipa obrigada por todos os momentos que passamos juntas. Aos meus queridos amigos de Biomédica: Fátima, Miguel, Margarida, Rafaela, Patrícia, Catarina M., Catarina D. e Ritinha um obrigada gigante por terem sido a minha salvação. Aline, amiga, foste das pessoas mais importantes que o curso me deu. Obrigada por todo o teu apoio e por todas as nossas conversas. Martim, obrigada por teres sido o meu infatigável parceiro de curso nestes 5 anos, por todas as boleias e desabafos. Obrigada por me apoiares e aturares constantemente (até durante o meu ótimo humor matinal).

Aos meus grandes amigos e amigas da vida: do ballet (Rita, Bia, Joana, Mafalda, Luísa e Carlota), Lalala (Bernardo, Carminho, João, Carlos, Duarte e Afonso), Sitas (Kika, Cate, Mimi, Pipa e Né) e Bambora (Martim, Inês, Rita, Filipe e Cristiana) obrigada por fazerem parte da minha vida. Por me ajudarem a desanuviar nestes meses mais intensos, ao estarem constantemente disponíveis para irmos dar uma volta ou jantarmos. Acredito que ainda temos muito para viver juntos.

Inês Passos Fernandes

# Contents

# List of Figures

# List of Tables

# Abbreviations

| | |
|---|---|
| ACM | Acellular Cartilage Matrix |
| ADM | Acellular Dermal Matrix |
| ANA | Acellular Nerve Allograft |
| BMSCs | Bone Marrow Mesenchymal Stem Cells |
| BNDF | Brain-derived neurotrophic factor |
| CABG | Coronary Artery Bypass Grafting |
| CHAPS | 3-[(3-cholamidopropyl) dimethylammonio]-1-propanesulfonate |
| $CO_2$ | Carbon dioxide |
| dhpECM | Decellularized human placenta ECM |
| dArteries | Decellularized Arteries |
| dECM | Decellularized Extracellular Matrix |
| $dH_2O$ | Deionized water |
| DNA | Deoxyribonucleic Acid |
| DT | Decellularized Tissue |
| ECM | Extracellular Matrix |
| EDC | 1-ethyl-3-(-3-dimethylaminopropyl) carbodiimide hydrochloride |
| EDTA | Ethylene-Diamine-Tetra Acetic acid |
| ELISA | Enzyme-Linked Immunosorbent Assays |
| FLG | Few-Layer Graphene |
| FLGO | Few-Layer Graphene Oxide |
| GAG | Glycosaminoglycan |
| GBM | Graphene-based material |
| GO | Graphene Oxide |
| HCl | Hydrochloric acid |
| HFF-1 | Human Foreskin Fibroblast-1 |
| HUVEC | Human Umbilical Vein Endothelial Cell |
| ITA | Internal Thoracic Arteries |
| LVE | Linear Viscoelastic |
| MSC | Mesenchymal Stem Cell |
| nGO | Nanosized Graphene Oxide ~ |

| | |
|---|---|
| NaCl | Sodium Chloride |
| NHS | *N*-hydroxysuccinimide |
| PBS | Phosphate-Buffered saline |
| PTFE | Polytetrafluoroethylene |
| rGO | Reduced Graphene Oxide |
| RT | Room Temperature |
| SAOS | Small-Amplitude Oscillatory Shear |
| SDS | Sodium Dodecyl Sulfate |
| SDVG | Small Diameter Vascular Graft |
| SEM | Scanning Electron Microscope |
| sGAG | Sulphated Glycosaminoglycan |
| TEBV | Tissue-Engineered Blood Vessel |
| VB12 | Vitamin B12 |
| VEGF | Vascular Endothelial Growth Factor |

# Chapter 1

# Introduction

## 1.1 Motivation

Cardiovascular diseases are the leading cause of death worldwide. According to the world health organization, every year, around 32.4 million myocardial infarctions and strokes occur, having a mortality rate of 58 % [1]. Myocardial infarction happens when there is narrowing/blockage of the coronary arteries that irrigate the heart, decreasing/inhibiting oxygen, and nutrient supply, which irreversibly damage the heart muscle (Figure 1) [2, 3].

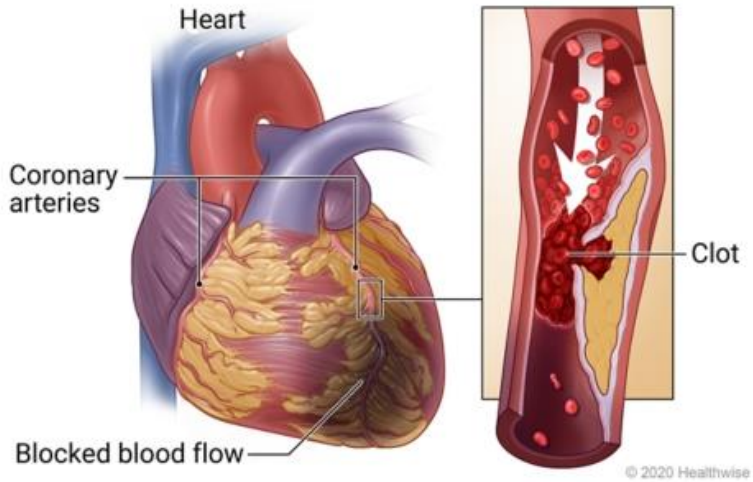


Figure 1 – Myocardium infarction - Formation of a clot in the coronary artery. Adapted from [2].

To reestablish the blood flow in the affected area, in some cases, a coronary artery bypass grafting surgery (CABG) is performed, being needed small diameter vascular grafts (SDVGs) (<6 mm inner diameter). The use of autologous grafts, which are vessels harvested from other places of the patient, is the current gold standard in CABG [4, 5]. However, they are not always available, have several comorbidities associated to their harvesting and some autologous vessels are associated with

high failure rates (up to 50 % at 10 years after surgery) due to thrombosis or infection occurrence (reviewed by [6]). The occurrence of a second occlusion leads to another myocardium infarction, which may require a second intervention or, ultimately, in a worst-case scenario, the patient could die [5, 7].

This raises the need for SDVGs that are always available and prevent thrombosis. Tissue-engineered approaches, such as the use of natural polymers (collagen and fibrin), which aim to promote graft remodeling by achieving a functional endothelium that prevents the thrombus formation, are being described as a promising strategy to design SDVGs [8, 9]. Within this strategy, the use of decellularized tissues as scaffold has been proposed in the literature, since they can preserve the natural tissue architecture, and the motifs and growth factors, promoting cell adhesion, colonization and proliferation (reviewed by [6]). Most times, the SDVGs are obtained from tubular human or animal tissues, namely arteries or veins. However, extracellular matrices (ECM) derived from 2D tissues can also present an interesting strategy to develop vascular grafts. Hydrogels derived from decellularized matrices may be promising scaffolds once most of the microstructure's components like collagen and glycosaminoglycans (GAGs), and biochemical properties are preserved [10, 11]. Unfortunately, both ECM derived scaffolds have limitations such as the lack of mechanical properties and, for the tubular derived arteries or veins, there is high incidence of thrombosis and infection due to collagen fibers exposure [12-14].

Graphene is the strongest material in the world [15] and is described as biocompatible and with antimicrobial properties [16, 17]. As such, graphene and graphene-based materials (GBMs) appear as interesting materials to enhance the mechanical and biological performance of decellularized matrices and ECM-derived hydrogels.

For grafts derived from tubular tissues, a previous work from our group showed that GO coating can increase the maximum force in 27 %, the burst pressure in 29 %, the strain in 25 %, and the compliance in 10 % of umbilical cord decellularized arteries. Moreover, graphene oxide (GO) coating did not compromise the endothelial cell adhesion and decreased platelet adhesion to decellularized arteries. However, when their hemocompatibility was tested *in vivo*, GO-coated decellularized arteries have a similar performance to uncoated, inducing the graft occlusion in the first 15 min. Thus, although the potential of this strategy, further improvements are needed.

In ECM-derived hydrogels (from 2D tissues), their use as SDVG is not reported in the literature which can be explained by the lack of mechanical properties. However, the incorporation of GBM is poorly reported and may present a good strategy to improve the mechanical properties of the ECM-derived hydrogel [15].

The source of the tissues used to obtain the decellularized matrices and gels is also important to determine the approach success. In arterial tissues, the decellularized tissues derived from other species (xenografts) have been described with higher immunogenicity than decellularized tissues derived from same specie (allografts) [18]. The use of human placental tissues and umbilical cord arteries present an interesting solution since these tissues are normally discarded after caesarean section birth. Hence, they would be reused and would always be available since, there are more than 30 000 births per year (2019) just in Portugal, from c-section [19].

## 1.2 Goals

The ultimate goal of this dissertation work is to understand if GBM can be used to reinforce placental decellularized matrices in order to develop a small-diameter vascular graft with similar or superior performance to autologous grafts. To achieve this, two different strategies are proposed: GBM incorporation in a) coating of decellularized umbilical cord arteries; b) ECM-derived hydrogels from chorion and amnion placental tissues.

For both strategies it was defined the specific objective of remove efficiently the DNA from the tissue (<10 % of initial) preserving as much as possible the microstructure of the native ECM. For this, different decellularization methods were attempted combining different components capable of promoting membrane disruption, weakening cell adhesion and hydrolyzing deoxyribonucleic acid (DNA).

For the GBM-coated decellularized arteries (dArteries) strategy, 2 additional specific objectives were defined, i) to achieve a higher improvement in the mechanical properties of decellularized arteries than the previously reported by our group and ii) to improve the hemocompatibility of GO-coated decellularized arteries. To enhance the mechanical properties, we hypothesized that a better penetration of GBM in the decellularized matrix through its porous (0.88 μm) will result in a better mechanical reinforcement. Nanosized GO (nGO) (~0.099 μm) was combined for the first time with decellularized arteries. Its smaller lateral size than the previously used GO (1.5 μm) could allow a better penetration in the decellularized matrix porous (~ 0.88 μm). Two different strategies for nGO incorporation were adopted, one just by coating the lumen with a nGO suspension and another inducing high pressure inside of the decellularized arteries to promote nGO particles penetration. To improve the hemocompatibility of the GO-coated decellularized arteries (dArteries) it was proposed their combination with an anticoagulant agent, heparin.

For the GBM reinforced ECM-derived hydrogel strategy, it was established the specific aim of achieving a moldable ECM-derived hydrogel with suitable mechanical properties to apply as SDVGs. For this, different amounts of GO were incorporated in ECM-derived hydrogels being the rheological properties studied. In this approach GBMs could be an advantage since they also present antimicrobial properties [16].

## 1.3 Dissertation Outline

Chapter 1 presents the motivation, main goals and the outline of this dissertation.

Chapter 2 contains an extensive literature revision of the topic of this dissertation. The first section describes the different tissue's decellularization methods: biological, chemical, and physical, and the characteristics and composition of the resultant decellularized extracellular matrices (dECM), being the end of this section dedicated to decellularization methods adopted in cannular tissues for SDVG. Then, the following section focuses on GBMs and their mechanical and biological properties. In the last section of chapter 2, it is described the interactions between GBMs and dECM for multiple applications.

Chapter 3 investigates the use of GBM to reinforce decellularized arteries. The efficiency of decellularization process was first evaluated. The effect of the use of GBMs differing in their lateral size in the coating of decellularized arteries was explored. In the case of GBMs with nano lateral size

(nGO), two different incorporation methods were tested: by perfusion and pressure of nGO dispersion. The burst pressure, compliance, strain and maximal force of the dArteries coated with the different GBMs were evaluated. Additionally, uncoated and GO-coated dArteries were combined with heparin to improve their hemocompatibility and coagulation time evaluated.

Chapter 4 explores the incorporation of GO in the ECM-derived hydrogels obtained from human placental tissues: amnion and chorion. Two different decellularization processes were explored to obtain the ECM-derived hydrogels and different concentrations of GO were incorporated before and after tissue digestion. The rheological properties of obtained hydrogels were evaluated.

Chapter 5 comprises the general discussion for the previous two chapters 3 and 4 in order to correlate them and compare the obtained results.

Chapter 6 highlights the main conclusions of the developed work and the future directions regarding the use of placental tissues in the CABG procedures.

## 1.4 List of Contributions

Under the scope of this thesis, 1 research article was published, and 2 oral presentations were performed in the conferences: XII Symposium on Bioengineering and IJUP 2021 - 14th Meeting of Young Researchers of University of Porto.

**Publications**

1. Andreia T. Pereira, Karl H. Schneider, Patrícia C. Henriques, Christian Grasl, Sofia F. Melo, **Inês P. Fernandes**, Herbert Kiss, M. Cristina L. Martins, Helga Bergmeister, Inês C. Gonçalves, Graphene Oxide Coating Improves Mechanical and Biological Properties of Decellularized Umbilical Cord Arteries. Acs applied materials and interfaces 2021;13(28):32662-72.

**Oral Communications**

1. **Inês P. Fernandes**, Andreia T. Pereira, Inês C. Gonçalves, Graphene oxide, heparin and decellularized arteries: a promising recipe to change the paradigm in cardiovascular diseases?. Symposium on Bioengineering – Science Under 5' 2021.
2. **Inês P. Fernandes**, Andreia T. Pereira, Inês C. Gonçalves, Graphene oxide, heparin and decellularized arteries: a promising recipe to change the paradigm in cardiovascular diseases?. IJUP 2021.

**Awards and Distinctions**

1. 3rd place Science Under 5' (Symposium on Bioengineering)
2. Best Oral Communication in the Health Sciences area (IJUP 2021)

# Chapter 2

# Literature Review

## 2.1 Decellularized Matrix

Decellularization of a given material (tissue or organ) happens when cells and cellular debris are removed from the extracellular matrix (ECM). This process aims to remove the immunogenic components of the native tissue (cells) while preserving the main constituents of ECM, namely collagen, proteins, proteoglycans, and GAGs. ECM composition, structure and biomechanical properties are specific to the tissue or organ [20, 21], and are very dynamic during development. The use of ECM-based scaffolds in tissue engineering approaches, such as decellularized matrices, aim to provide a similar microenvironment to the native tissue for cells, to facilitate their adhesion, migration, proliferation, and differentiation and enhance tissue regeneration [22, 23].

Decellularization of organs and tissues produces interesting biomaterials, decellularized ECM (dECM), since it preserves the most part of the original structure as well as the biochemical nature of the original tissue [24, 25]. Thus, the use of extracellular matrix-based materials in tissue engineering approaches is widely explored.

### 2.1.1 Decellularization Methods

There are multiple methods to decellularize tissues (natural or derived from cultured cells) and organs, as reviewed by Heath *et al* [26]. Depending on type of tissue or organ, the adopted decellularization method can generate different outcomes. Thus, decellularization protocols should be adjusted and optimized considering the source of tissue or organ, since there is no key theoretical framework.

Decellularization methods can be divided onto three categories depending on the strategy used in decellularization process: biological, chemical and physical (Table 1).

Table 1 – Impact and limitations of the decellularization methods on cells and ECM. Adapted from [26].

| Decellularization Method Category | Agents | Impact on cells and ECM | Limitations | References |
|---|---|---|---|---|
| Biological | Trypsin | Cleave cell's adhesive proteins | Long exposure can damage ECM (> 12 h) | [27-31] |
| | Dispase | Separate epithelia (cleave fibronectin and collagen IV) | Use of other treatments to complete decellularization | [32, 33] |
| | DNase/RNase | Digest residual genetic material | Use of other detergents to complete decellularization | [24, 25, 33, 34-40] |
| Chemical | Acids | Disrupt nucleic acid and solubilize cytoplasmic components | Denature ECM components, reduce matrix's strength | [41-44] |
| | Alcohol | Cell lysis and removal of residual nucleic acids and lipids | Increase matrix stiffness | [45-50] |
| | Alkalines | DNA denaturation | Damage collagen, reduce growth factor and GAG components | [51-53] |
| | Chelators | Weaken cell adhesion | Need to be combined with biological processes to remove cells in ECM | [54-55] |
| | Ionic Detergents | Disrupt cell membrane, solubilize DNA and denature proteins | Remove some GAGs and collagen | [47, 51, 56, 60-63, 65-72] |
| | Non-ionic Detergents | Disrupt cell membrane and lipid-lipid interaction | Use of other treatments to complete decellularization | [35, 59, 63-72] |
| | Zwitterionic Detergents | Greater ECM preservation collagen and elastin than ionic detergent, improved cell removal than non-ionic | Decrease of elastin | [57, 73] |
| Physical | Freeze/thaw cycles | Initiate cell's disruption – lysis and protein dissociation from DNA | Insufficient cellular residue removal | [74, 75, 78-80] |
| | Osmotic pressure | | | [50, 76, 77] |
| | Mechanical agitation | Facilitate penetration of agents, facilitate removal cellular components | Change mechanical properties | [52, 81-88] |
| | Pressure | | | [52, 81-90] |
| | Supercritical $CO_2$ | Few ECM modification | Poorly explored | [91-94] |

## a) Biological Decellularization Method

Biological decellularization methods consist of exposure of the tissue to enzymes, which are mostly proteases. Trypsin, for example, is capable of cleaving the cell's adhesive proteins, but a long exposure time can damage the ECM. The concentration and time exposure of trypsin vary depending on the application. For porcine coronary artery decellularization, 0.03 % and 0.05 % trypsin can be used without affecting the tissue's structure [27] whereas for human elastic cartilage [28], 0.25 % trypsin is used. For the decellularization of abdominal porcine fascial tissue [29], canine placenta [30] and bovine elastic cartilage [31], 0.05 % trypsin is the value optimized. Regardless of the concentration of trypsin, exposure time is the most important parameter to take into consideration. It should be less than 12h once Lin *et al* [27] tested for longer time points and observed several damages in ECM structure due to significant decrease in collagen and GAG content. Dispases are enzymes which are able to cleave fibronectin and collagen IV and are normally used to separate the epithelia. They are used in 560 units/L for 24h at 4 ºC for porcine skin. The time of exposition will depend on the size of the decellularized matrix. For small pieces of porcine skin which were 0.5 x 0.5 x 0.3 $cm^3$, dispase in 560 units/L was used for 12 h at 4 ºC and showed efficient removal of cells and complete cellular components [32]. They should be used in combination with other decellularization techniques, since they are not able to cleave laminin, collagen V, serum albumin nor transferrin [33].

Furthermore, there are other enzymes, such as DNase I and RNase, which are responsible to digest the residual genetic material [24, 25, 34-37]. There is no optimal concentration used, it can be 50 units/mL [38] or around 200 UI/mL [39] for DNase, and 1 unit/mL, for example, for RNase, depending on the exposure time which in this case, was 6h or 24 h, respectively. In most of the studies, the

concentration of these enzymes is not specificized. Nevertheless, the concentration used should be low to avoid ECM damage. These enzymes are normally used overnight and are used in combination with detergents, which are chemical agents [33, 40].

## b) Chemical Decellularization Method

In chemical decellularization methods, tissues or organs are immersed in a given solution with an acid, alcohol, alkaline base, chelating agent or detergent. An acid solution (e.g., peracetic acid) is able to disrupt the nucleic acids, resulting in the remotion of DNA, and solubilize the cytoplasmic components [41, 42]. The use of acids can denature ECM components and reduce the matrix strength [43, 44].

In the case of alcohol solutions such as ethanol and methanol, the solution will cause dehydration by replacing cytosolic water following lysis of the cells and removal of residual nucleic acids and lipids [45, 46]. Alcohol is also capable of crosslinking ECMs components, which leads to an increase in the stiffness of matrix [47-50].

Alkaline bases (ammonium hydroxide, calcium hydroxide) allow the denaturation of plasmid and chromosomal DNA [51, 52]. But, at the same time, can damage the collagen and reduce growth factor and GAG components resulting in the alteration of the mechanical properties [53].

Furthermore, chelating agents as ethylenediaminetetraacetic acid (EDTA), chelate divalent cations, needed for integrin binding, resulting in the weakening of cell adhesion. However, they may not remove all the cells in the ECM so, usually, they are combined with proteases (biological decellularization method) [54, 55].

Detergents (ionic, non-ionic or zwitterionic) allow the disruption of lipid-lipid and lipid-protein interactions that enable the membrane's cohesion [56-59]. The ionic detergent sodium dodecyl sulfate (SDS) is the most robust decellularization method used. It has the ability to disrupt the cell membrane, solubilize DNA and denature proteins. However, when an ionic detergent is used, it can also remove GAGs and growth factors from the ECM and leave some residual surfactant [47, 51, 60-62]. Non-ionic detergent, Triton X-100, is the gentlest detergent and is normally favored when capable to fully decellularized since it has a limited impact on the protein-protein interactions of the ECM. It can result in GAG deficiency and loosening of the collagen network [35, 59, 63, 64]. Nevertheless, Triton X-100 has minimal changes in tissue biochemistry with the less detrimental effect on GAG content comparing to SDS and trypsin treatments [63]. These results were also obtained in Fernández-Pérez and Ahearne [65] where 0.1 % (w/v) SDS or 1 % (v/v) Triton X-100 treatments were compared. The obtained decellularized porcine corneas showed a significant loss of sulphated glycosaminoglycans (sGAGs) for the SDS treatment (Figure 2). This decrease in sGAG with SDS treatment was also observed in decellularization processes by other authors for cornea [66-69], and also for other tissues cartilage [70, 71], ligament [72] and adipose [71]. Furthermore, the less effective DNA removal with Triton treatment was also observed.

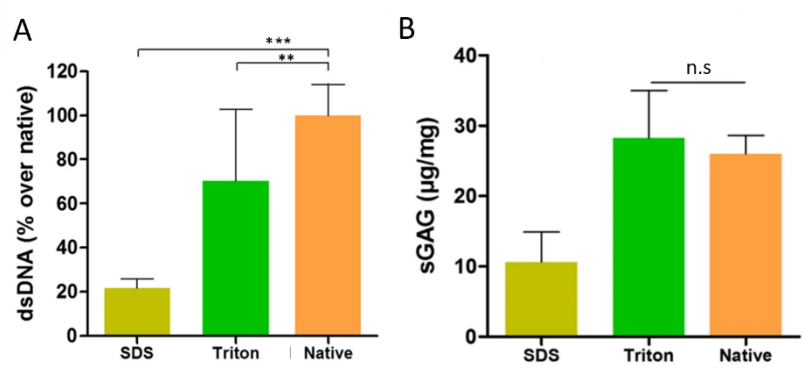


Figure 2 - Results of ECM-derived hydrogels quantification for different decellularization methods SDS and Triton: (A) dsDNA, (B) sGAGs,; *p < 0.05, **p < 0.01, ***p < 0.001. Adapted from [65].

Zwitterionic detergents for example, 3-[(3-cholamidopropyl) dimethylammonio]-1-propanesulfonate (CHAPS), which are the second most robust for decellularization, have zero-net charge on the headgroup, but carry a positively and a negatively charged group. Thus, this type of detergent combines the features of improved cell removal comparing to non-ionic detergents and greater ECM preservation of collagen than ionic detergents (SDS treatment had a loss of 80 % of collagen in [57]) leading to similar mechanical properties, tensile strength, and elastic behavior, to the native tissue. However, there is some elastin deficit of 60 % (similar to SDS treatment) which results in decrease of elastic functions [57, 73].

### c) Physical Decellularization Method

Physical decellularization methods are normally used in combination with other treatments. To initiate the disruption of cells, osmotic pressure [50] and freeze/thaw cycles [74, 75] are performed. Osmotic pressure is promoted in tissues using hypotonic solutions such as deionized water, which induce cells rupture and hypertonic solutions such as low ionic strength solution or sodium chloride (NaCl), which lead to cell lysis and proteins dissociation from the DNA. This method is capable of lysing cells effectively, but the removal of their cellular residues is not sufficient [76]. When this physical decellularization method is used, it is recommended to perform multiple cycles with the solutions [77]. The freeze/thaw cycles are able to disrupt cells by forming ice crystals. This process minimizes the use of other biological and chemical agents. It does not alter the mechanical properties of the tissue significantly and the addition of a cryoprotectant such as glycerol, propylene glycol and dimethyl sulfoxide (DMSO) [78], is capable of reducing the ECM disruption [79, 80]. However, when cryoprotectants are used in higher amounts, the formation of crystals is compromised inhibiting the hampering of cells.

During exposure to chemical or biological decellularization agents, mechanical agitation [81-83] and pressure gradients [52, 84] are also used to enhance the penetration of the given agents into the tissues and, with the improvement of the mass transport in the system, facilitating removal of the cellular components [52, 81-84]. Nevertheless, mechanical agitation and pressure can lead to changes in mechanical properties of the tissues [85-88]. The use of pressure when lower temperatures are used (starting pressurization with 10 ºC temperature), can also damage the ECM components such as collagen fibrils [89, 90].

The exposure to supercritical carbon dioxide ($CO_2$) leads to decellularization of the tissue by exposing it to inert $CO_2$ in short treatment times of 15 minutes [91, 92]. Normally, it results in very

few modifications of the ECM compared to the conventional decellularization methods using chemical solutions and the resulting biomechanical properties are less affected [93, 94]. The studies performed showed this method is very promising but, due to its novelty, further studies should be performed.

To increase the efficiency of the decellularization method maximizing the ECM components preservation, most of the protocols combine strategies of two or three different categories. Normally, physical methods such as freeze/thaw cycles and osmotic pressure are used to initiate cell disruption. Mechanical agitation and pressure gradients are able to facilitate the entrance of the biological and chemical agents used to dissolve the membrane and DNA remotion. Every agent has a different impact in the matrix. When designing a protocol, each outcome described previously, should be taken into consideration to make sure the resulting decellularized matrix has complete DNA removal at the same time as its decellularized matrix is capable of preserving its native microstructure and properties.

### 2.1.2 Decellularized Blood Vessels

In the context of the first approach studied in this thesis project (GBM-coated dArteries), resulting decellularized blood vessels will be assessed, comparing different methods. As previously mentioned, the decellularization method will directly affect the composition and mechanical properties of the obtained decellularized ECM. Most of the times, the glycosaminoglycans, collagen, elastin and proteoglycans components remain in the dECM. Normally, decellularization produces a material which maintains the ECM architecture, key structural components of the core and some of the mechanical properties of the native tissue [95]. In contrast, associated modulatory proteins and soluble factors which are needed to stimulate tissue-specific functions are eliminated during the decellularization process [96]. Thus, some molecular interactions are perturbed [95].

For blood vessel decellularization, Simsa *et al* [97] compared different detergents: 0.1 % SDS, 8 mM CHAPS and 1 % Triton X-100. Decellularization was performed with an initial freeze/thawing cycle and then, with agitation and perfusion of the 3 different detergents with DNase. All the methods allowed more than 99 % removal of native DNA. Most part of the ECM structure was maintained, except GAG content, which was significantly decreased in all groups, apart when treated with SDS. These results were not coherent with the ones described above, where SDS treatment would have a worst effect on GAGs. The basement membrane integrity showed alterations for all treatments comparing to the native tissue. Triton X-100 would appear less altered. In terms of mechanical properties, tensile strength and burst pressure were very similar to native tissue for all the protocols. Nevertheless, when treated with Triton X-100, the time of exposure to DNase needed to be longer for complete decellularization. Furthermore, when DNase was not used, blood vessels did not fully decellularize. However, it showed a higher mechanical stability and higher GAG content. This result suggested that DNase tend to have a harsh effect on ECM components, even though it is necessary to obtain efficient removal of DNA. Additionally, an important parameter decellularized tissue should have, is the capacity to recellularize. The tissue's ability to recellularize was more efficient when treated with Triton X-100.

Schneider *et al* [39] tested two decellularization methods for small diameter vascular grafts from human placenta where two solutions 0.5 % SDS and 1 % Triton X-100, were perfused. SDS and Triton X-100 were able to remove DNA resulting in values of DNA quantification very low comparing to native (8.51 ± 0.23 µg) 0.24 ± 0.02 µg and 0.29 ± 0.06 µg, respectively. Triton X-100 method preserved more proteins than when treated with SDS. Biomechanical properties of both treatments after decellularization reduced approximately 60-70 %. In fact, there was a significant decrease of maximum tensile strength (Native: 1.87± 0.49 N, SDS: 1.17 ± 0.36 N, Triton: 0.96 ± 0.44 N) and

compliance after decellularization (Native: 10.92 % ± 0.95, SDS: 6.276 % ± 1.56, Triton: 8.77 % ±1.27, $P < 0.001$). dECM was crosslinked with heparin to avoid formation of thrombus when implanted. For both methods, resulting grafts had low immunogenic potential and showed excellent biocompatibility *in vitro* and *in vivo*. After one month of implantation, the compliance increased, it was in the range of 6 % and the maximal strength and burst pressure had significantly increased for both treatments. Both treatments resulted in grafts with high patency rates, no formation of thrombus nor rupture and they presented cell migration which is important for the tissue remodeling and explains the improvement of the mechanical strength. Nevertheless, these results were obtained using a small animal model, a rat, which has a different hemodynamic and thrombogenicity from humans. Thus, further studies should be performed in larger animal models, such as sheep.

### 2.1.3 Decellularized Placental Tissues

In the context for the second strategy of this dissertation work (ECM-derived hydrogels), decellularization of placental tissues will be performed and different methods compared. These decellularized tissues can be used as ECM-derived hydrogels, which provide a good microenvironment for cell migration and proliferation [98]. They are able to reduce inflammatory response [99] and prevent formation of scar tissue [100], representing an interesting approach for tissue engineering strategies.

Francis *et al* [101] decellularized the chorionic plate for 16-24 hours with 2 % N-lauryl sarcosine, an ionic detergent. Afterwards, the detergent and cell debris were removed with multiple cycles of washing with water. The DNA quantification of the decellularized tissue was performed by Quant-iT PicoGreen™ (ThermoFisher Scientific, Carslbad, CA), and showed, in average, 116.69 ng/mg remaining DNA in the decellularized human placenta ECM (which represents 1 % of DNA remnant).

Leonel *et al* [30] compared multiple protocols for placental tissues decellularization with different temperature: -80 ºC, -20 ºC, 4 ºC or RT, reagents such as 1 % SDS, SDS + TRIS, 1 % Triton X-100, EDTA + penicillin-streptomycin, DNase I, 70 % ethanol or EDTA + 0.05 % trypsin + antibiotic and, finally, with different duration (1h30, 5 h, 2-10 days). These different protocols show the enormous possibilities of procedures, which can be done by combining the different methods of decellularization (biological, chemical and physical). The DNA quantification was assessed using Quant-iTTMPicoGreen$^{R}$ dsDNA reagent for two protocols. For the protocol where the reagents used were: EDTA + 0.05 % trypsin + 0.5 % antibiotic, showed less amount of remaining DNA (418 ± 373.7 ng/mL) than another protocol where the reagents used were: 5 mM EDTA + 50 mM TRIS + 0.5 % antibiotic with 1125 ± 787.1 ng/mL DNA remnant.

The decellularization process for the placental tissues still needs to be optimized in order to respect the minimal criteria to verify decellularization intent which needs to be close to 50 ng/mg of remaining DNA [25].

## 2.2 Graphene-based materials

Graphene is a single layer crystalline form of carbon comprising $sp^2$ hybridized atoms [102]. It is composed by hexagonal bonded carbon atoms that form a honeycomb lattice structure. It was firstly isolated from graphite in 2004 and since then has attracted a lot of interest due to its unique

structure, which provides to graphene exceptional mechanical, thermal and optical properties, as well as a hydrophobic and conductive nature [103].

Graphene-based materials (GBMs) are a very large class of materials which derive from graphene, exhibiting different features [16] (Figure 3). Their chemical properties such as functional groups and degree of oxidation, and physical properties as size, thickness, edge length and defect size, can vary depending on the method used to synthetize them [104-110]. In particular, graphene oxide (GO) is often obtained using a natural graphite powder via the modified Hummers' method [111] and reduced graphene oxide (rGO) can be produced by the reduction of GO [112]. GBMs can be used alone, as a powder or suspension or film, [113, 114] or in combination with other materials, generally, to enhance their native properties [115-117]. Surfaces containing GBMs can be divided into three categories: films, coatings and bulk composite materials. These GBMs containing surfaces have an enormous range of applications such as in electronic, optic, and biomedical field [16].

The mechanical and biological properties of GBMs will be described in the following sections to understand the potential of these materials' application in biomedical field.

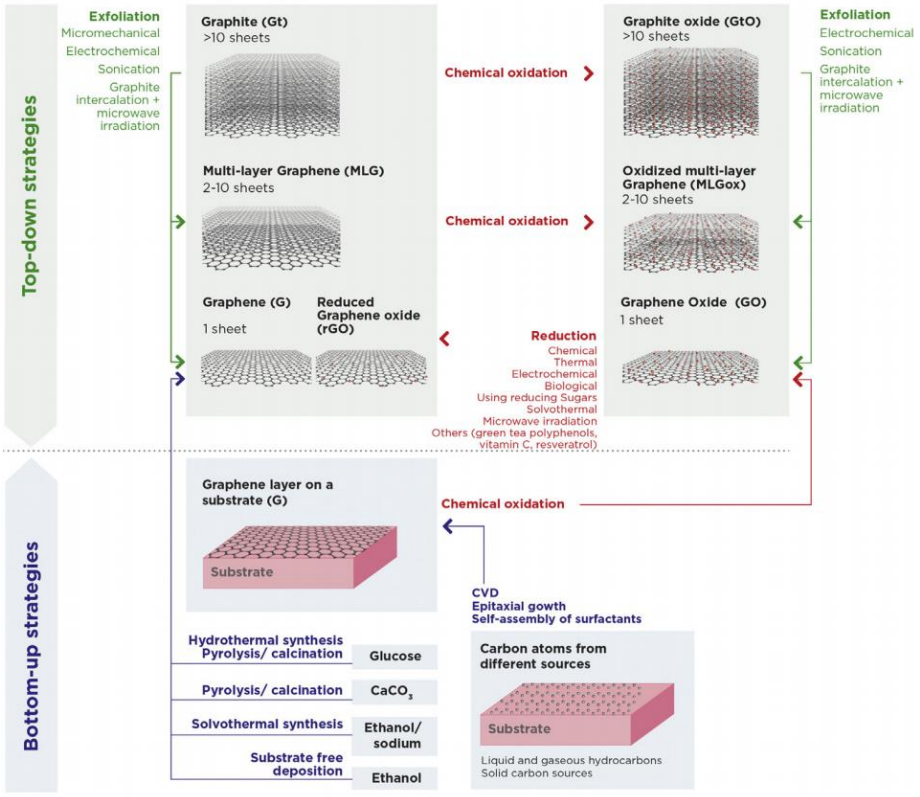


Figure 3 – Graphene based materials (GBMs) and production methods from [16].

## 2.2.1 Mechanical Properties

### a) Strength and Stiffness

Graphene is the strongest material in the world [118]. Hence its usage, as well as GBMs, by itself or to reinforce other structures, have been explored. Hone *et al* [118] showed that the intrinsic strength of a monolayered defect-free graphene membrane is 130 GPa. This outstanding strength can

be explained by its structure, where the $sp^2$ bonds forming the hexagonal lattice give stability and opposition to a variety of in-plane deformations [15].

Oxidation of graphene, renders materials with worse mechanical properties but more stable, being an attractive solution for multiples applications. Dikin *et al* [119] showed that the stress distribution of GO would be spread homogeneously, and the stiffness was 40 GPa whereas the strength was about 120 MPa. The strength obtained for GO is in the megapascal order, which is significantly lower than the strength of graphene, that is in the order of the gigapascal. The reduction of the mechanical properties can be explained since GO has multiple physical and chemical features as $sp^2$ bonds disturbed, by the presence of oxygen and a large number of defects. This can also lead to a reduction in electrical conductivity and poor thermal stability. However, when GO fibers were produced and the crosslinking between the interlayers and intralayers was performed, the strength value raised to 0.5 GPa [120].

In some recent studies, comparing to the value of GO paper, GO fibers would also present similar values of strength [121-123] to the ones obtained in Xu *et al* [120] research. However, the Young's Modulus value of GO fibers would increase in some studies [124]. Suk *et al* [125] showed that the Young's Modulus values of a monolayer of GO were about 208 ± 23 GPa with atomic force microscopy and finite element method. In Gomez-Navarro *et al* [126] experiment, the value of the Young's Modulus of GO sheets was of 250 GPa. Even in the case of high densities of $sp^3$-type defects, the strength and stiffness of graphene were preserved whereas the breaking strength lowered 14 % comparing to the pristine graphene [127].

In the literature, GBMs are mostly used as composites in polymeric matrices where a more effective mechanical action is expected since its mechanical properties will be dependent of the covalent and non-covalent bond configuration between the graphene sheets and the matrix. The Van der Walls forces and hydrogen-bond interactions of GBMs composites in polymeric matrices show improved mechanical properties [128, 129]. For example, GO-PVA composite with 0.7 wt% GO sheets [130] showed an improvement of 76 % elastic modulus and 62 % strength. However, GBMs can also be used, more rarely, as coatings. In Papageorgiu *et al* [15] review it was shown that GBMs were used as fillers of multiple polymers like epoxy, Polytetrafluoroethylene (PTFE), polypropylene, and were able to enhance the ultimate tensile strength and Young's Modulus of most polymers up to 15-250 %. The mechanical reinforcement provided by GBMs depends on their physical and chemical properties, the method performed to obtain the specific GBM and the incorporation process of the given GBM.

### b) Toughness

Fracture toughness is an important parameter for engineering applications. In Zhang *et al* [131], a crack in the graphene films was done and a certain load applied. This research allowed to define that the fracture stress would decrease when the crack's length increased. Moreover, the value for the critical strain energy release rate was 15.9 $J/m^2$ whereas the critical stress intensity factor was of 4.0 ± 0.6 MPa. These results demonstrated that the toughness of graphene would depend immensely on its weakest link where the failure begins [131-135].

## 2.2.2 Biological Properties

### a) Biocompatibility

Carbon derived materials can be found in multiple applications of the daily life such as pencils and biomaterials. These latter, need to be biocompatible to ensure that no damage is caused to the individual who is handling them.

Due to their novelty, the biological response mechanisms to GBMs are still not completely understood even though there are several studies on them [136-140]. Nevertheless, it is known that the outcomes of GBMs interaction with the biological system depend on GBM features, such as number of layers, lateral size, and oxidation degree.

The cytotoxicity of GBMs depends on concentration, exposure period, oxidation degree, lateral size and the cell type used [137, 141-143]. The dose of GBM is one of the main features that will influence the viability of the cells, *in vitro*. In Cheng *et al* [144], the viability of HUVECs in contact with GO and rGO with a concentration of 20 μg/mL is 95 %, while for a concentration of 100 μg/mL, the viability decreases to 60 %. Other important characteristics are the oxidation degree and the size [137]. It was reported that smaller and more oxidized GBMs have a better biocompatibility towards HFF-1cells [145]. Furthermore, oxidized GBMs were able to better interact with the cell membrane, being more internalized and having a better cytocompatibility. The graphene nanosheets accumulation in cellular plasma membrane result in the blockage of membrane channels and disturbance of intracellular balance [146-148].

GBMs are able to adsorb medium components as nutrients and cell growth factors on their surface which enables them to be a good support for cell attachment, growth and proliferation [149]. GBMs are also a good assistance for cell differentiation of mesenchymal, neural, and induced pluripotent stem cells [149].

The biodegradation of a material is an important feature to evaluate given that it will allow to understand its possible applications. Furthermore, its biodegradation is crucial since graphene being a nanomaterial, its accumulation in the reticular organs such as kidney and lungs, can be prevented. Recently, applications of GO and rGO are being discovered, thus the importance of studying their chemical properties as well as to minimize their environmental impact on human cells and tissues. Kotschey *et al* [150] demonstrated that, when in contact with low quantities of horseradish peroxidase, from plant, fungal and bacterial peroxidases superfamily, GO is susceptible to degradation. In contrast, reduced GO is not affected by this metalloenzyme. Furthermore, the number of layers will also affect the result of the degradation. In fact, while thicker oxidized single layer GBMs (reaching 20 nm thickness) did not show after 15h and 24h signs of degradation alteration and stayed almost intact when in contact with myeloperoxidase, which belong to mammalian peroxidase superfamily, thinner GBMs (around 1 nm thickness) suffered complete degradation [151]. Mukherjee *et al* [152] demonstrated that GO sheets with different lateral sizes (100 ± 50 nm and 10 ± 8 μm) were degraded by neutrophils, being a non-genotoxic material to human lung cells. Moreover, depending on the oxidation level, GO after blood plasma treatment sheets (3.31 ± 0.66 nm thickness) is degraded after 14 days [153] since the active substances in blood plasma can attack the carbon atoms which are connected to oxygen-containing groups. Hence, GBMs with less oxygen, lower number of active sites, have a slower biotransformation.

In addition, macrophages which have crucial role in inflammatory response, have capacity to phagocyte GO, despite depending on the lateral size. The M1 macrophage (pro-inflammatory) polarization [154, 155] is induced with larger GO sheets and their apoptosis promoted with a GO concentration over 50 μg/mL [156-159].

Liu *et al* [160] evaluated the biodistribution of GO *in vivo* with the injection of GO samples, intravenously, in mice. Small GO particles (148-160 nm) accumulate in larger quantities in the liver whereas larger GO (556-780 nm) tend to be retained in the lungs. Moreover, it was also observed in this study that small GO had a tendency to stay for a longer time in the circulation, with 170 min as a terminal elimination half-life, in comparison to larger GO (with terminal elimination half-time of 102 min). Additionally, Zhang *et al* [161], have shown that when exposed to GO (10-800 nm) for 14 days, the examined organs did not present pathological changes.

### b) Hemocompatibility Properties

GBMs have been envisaged for biomedical applications that are in contact with blood. Thus, the hemocompatibility is an important property to study. In the literature, there are many studies that observed the interaction between GBMs and blood (proteins and cells) [142, 162-165]. Regarding the interaction of GBMs with red blood cells, the results obtained in the literature are contradictory [145, 166].

The study of platelets and coagulation was also performed. In Sasidharan *et al* [156], the hemolytic potential assessment was performed for concentrations of GBMs varying between 0–75 μg/mL treated in whole blood. The hemoglobin release from graphene treated and not treated was compared with optical photographs, not being observed visual differences. The analysis of platelet activation was performed by flow cytometry. This experiment demonstrated that GBMs did not interfere with the normal platelet functioning. Coagulation studies showed that GBMs did not hinder intrinsic nor extrinsic pathways of coagulation. Furthermore, Feng *et al* [166] studied the effect of GO with different concentrations (0.001, 0.01, 0.05, 0.1, and 0.5 mg/mL). *In vitro* results demonstrated a thrombogenic effect for GO with 0.5 mg/mL concentration [166]. This was assessed by detecting the concentration of complement fragments with Enzyme-Linked Immunosorbent Assays (ELISA) assays. Further experiments *in vivo* need to be performed for both studies. Yang *et al* [167] showed that GO coating of a stent induced longer activated partial thromboplastin times and had lower platelet adsorption than other coatings.

Henriques *et al* [168] showed that GO and rGO films do not induce hemolysis when in contact with red blood cells, according to ISO 10993-4. Furthermore, blood components, in specific, red and white blood cells and platelets, adhered onto all surfaces when GBMs films were incubated with human whole blood. These blood components tended to adhere in higher amount to reduced surfaces, rGO than to oxidized surfaces, GO. Moreover, platelets appeared in more activate states when rGO films were used. These results were explained due to the reduced protein adsorption on GO since its surface is more hydrophilic than rGO.

The protein adsorption to GBMs depends on the protein and the GBMs features. In fact, albumin is better adsorbed by hydrophobic GBMs through $\pi - \pi$ interactions [169]. This was also corroborated by Palmieri *et al* [163], where it was shown that GO would better adsorb fibrinogen whereas non-oxidized GBMs would adsorb higher quantities of albumin. Moreover, larger particles of GO (1 μm) have higher capacity to adsorb albumin (small protein) than smaller particles (100 nm) while an opposite outcome is seen for fibrinogen (larger protein) where its adsorption increases with the decrease of the GO nanosheets lateral size [170].

The complement system seemed also to be activated by GO leading to the expression of pro inflammatory cytokines. These latter are more activated for smaller GO particles (< 1 μm) [171].

### c) Antimicrobial Properties

Bactericidal effect of GBMs is explained by their capacity to induce oxidative stress and membrane damages on bacteria. GBMs are capable of initiating molecular events such as redox reaction with biomolecules, mechanical destruction of the membranes and catalysis of extracellular metabolites, which culminates with bacteria death. Their antimicrobial properties depend on the GBM and the used amount, production technique and if they are in colloid form, coating or composite. The antimicrobial properties will be higher when the GBM's exposure is greater [16].

When GBMs are in the form of colloids, GO has a higher antimicrobial property than rGO [172, 173]. In the literature contradictory results were obtained for the effect of GO nanosheets size in their bactericidal effect. Some studies showed that larger GO nanosheets would have stronger antibacterial properties while others showed that smaller GO nanosheets would have higher oxidative and antibacterial capacity [174, 175].

Besides lateral size, oxidation degree also has an impact in the antimicrobial property when GBMs are used in 2D films (coatings). Smaller GO particles induce higher oxidative stress in bacteria and have stronger antimicrobial properties than when compared with films containing larger particles or rGO [16, 176]. Moreover, Hu *et al* [114] demonstrated that GO and rGO films, the latter being obtained by reduction of the GO film, presented similar results and inhibit bacterial growth. GO is able to completely suppress *E. coli* growth whereas rGO limits the number of colonies present. In addition, smooth surfaces tend to promote bacterial adhesion while rough surfaces have the opposite result [16, 177].

In the case of GBMs-containing composites, the roughness and wettability are the parameters which will influence the most the adhesion of bacteria. When the surface is more hydrophilic, it will prevent the adhesion of hydrophobic components [16]. However, bacteria are a mixture of hydrophobic and hydrophilic proteins and its ratio depend on the species. Thus, the interaction with the bacteria is not the same. In summary, the bactericidal effect of GBMs is potentiated when their exposure is higher. Then, the type of GBM used influences the outcome once small GBMs with more oxidized groups have more active antimicrobial properties due to their oxygen-containing functional groups whereas rGO are more active because of their edges being sharper. The wettability of GBMs must be taken into consideration as well as the bacteria specie. And, finally, the GBM coated decellularized matrix surface topography and its roughness (nano or micro) will affect the number of adhesive areas for bacteria [16].

## 2.2.3 Biomedical Applications

As previously mentioned, there are several studies that show the potential use of GBM in a wide range of biological applications. When used for drug delivery and as antimicrobial agents, the form of colloids is used given that the loading capacity and the dispersibility in aqueous solvent are high [178].

The development of biosensors is possible with free-standing films [179] or graphene/carbon nanotubes aerogels [180]. This application is possible due to GBM high surface area and electrical properties. GBMs antimicrobial properties, electrical conductivity, surface area and electron transfer potential are optimal for applications as cardiac, orthopedic, neurological, bone and muscle tissue engineering, and skin wound healing [178, 181, 182].

GBMs coatings can be dispersed in a flat or random orientation depending on the method used to perform the coating. Coatings are useful for multiple applications: biosensors, orthopedic implants, catheters, contact lenses and, cardiac and bone tissue-engineering [182, 183].

GBMs can also be used as composites when combined with polymers, ceramics, or metals. The resulting GBMs composites are produced with different techniques [15, 184]. The final characteristics of the composite depend on the GBM, the method and the polymer used. Hence, a great variety of applications are possible: drug delivery, antimicrobial properties, mechanical heart valves and multiple domains of tissue engineering (cardiac, bone, cartilage, neuronal and muscle).

## 2.3 Incorporation of GBM in Decellularized Matrices

Graphene-based materials (GBM) can be incorporated in decellularized matrices to enhance their original properties. There are few studies in the literature that evaluated the use of GBM such as graphene oxide (GO) and reduced graphene oxide (rGO), combined to decellularized matrices. Furthermore, neither the decellularized tissue, its decellularization method, GBMs nor the incorporation method used were the same for all the studies. Table 2 shows all the studies that report the incorporation of GBM in decellularized tissues and the observed outcomes. These studies were grouped and are further discussed considering their biomedical application.

Table 2 – Biomedical applications of decellularized matrices containing graphene-based materials (GBM) such as graphene oxide (GO) and reduced graphene oxide (rGO). The decellularized tissue, decellularization method, GBM type, the purpose of adding and the incorporation method and the obtained outcome, are summarized.

| Application | Decellularized tissue | Decellularization Method | GBM | | Incorporation method | Results | | Reference |
|---|---|---|---|---|---|---|---|---|
| | | | Type | Purpose | | Biological performance | Mechanical performance | |
| Nerve Regenaration | Nerve Allograft | tris-HCl, DNase and RNase, 3 % Triton-100, Tris-HCl | GO (20 mg/ml) | Improve conductivity, absorbability and biocompatibility | Dip coating on solution of GO | *In vivo* - no toxic reaction, good healing, no inflammation; Higher action potential, thickness myelin, axon diameter. | Not evaluated | [186] |
| | Nerve Allograft | Not specified | GO-VB12 (20 mg/ml) | Adsrob VB12, promote growth neurites and strong electrical conductivity | Dip coating GO-VB12 solution | *In vivo* - no toxic reaction; GO-VB12-ANA group rats not paralyzed, nerve action potential higher. | Not evaluated | [187] |
| | Leek (*Allium porrum*) Cellulose-based scaffold | 1.0 % SDS treatment, dH20 | GO (0.5 mg/ml) | Enhance cell attachment and viability | DT surface activation with UV-Ozone dip coating in GO solution | *In vitro* - normal neuroblastic morphology. | GO reduces stifness (elastic modulus) and icreases tensile strength. | [196] |
| Skin Repair and Replacement | Dermal Matrix | 0.25 % Dispase, 0.3 % Triton X-100, 0.25 % trypsin, fat digestion solution of chloroform methanol (v/v = 1:1) | rGO ( 10, 20, 40, 80, 100 and 200 mM) | Induce angiogenesis, reduce toxicity,excellent electroconductivity and biocompatibility | ADM freeze-dried, rehydrated and prepared with EDC/NHS. Solution immersion to obtain ADM-rGO and ADM-GO | *In vitro* - ADM-rGO had better cell viability, cells migrated deeper; *In vivo* - ADM-rGO-MSC promoted faster wound closure, more collagen regeneration in wound sites, better neovascularization and diamter of blood vessels. | ADM-rGO had better Young's Modulus, ultimate tensile strength- and strain at failure. | [198] |
| | | | GO ( 10, 20, 40, 80, 100 and 200 mM) | Comparision | | | | |
| | Bovine Heart Tissue | Chemical and Enzymatic agent (1 wt % SDS) | GO (0, 1, 3, 5 wt%) | Improve mechanical properties | After decellularization, sample is lyophilized creating DT powder which is then dissolved and % GO is added to the solution (crosslinking possible with EDC/NHS) | DT/GO 3 % - improved cell viability up to 25 %. | *SEM* - porous 3D structure with interconnectivity; DT/GO 3 % - improved mechanical strength up to 25 %. | [207] |
| Cartilage Regeneration | Cartilage of distal femoral condyle | Freeze/thaw, 1 % SDS, ddH20, DNase and RNase | GO (0, 1, 2, 4 , 6 mg/mL) | Improve mechanical properties | ACM particles and diffferent % GO mixed and put through gradient freezing. Then, some suffered crosslinking with EDC/NHS. | *In vitro* - ACM-GO (2mg/mL) promoted cell adhesion and proliferation, and chondrogenic differentiation. *In vivo* - good biocompatibility and mild inflammatory response. | Scaffolds with crosslinking had a more ideal structure and mechanical properties. Increasing GO concentration, increased gradually the ACM-GO elastic modulus. | [210] |
| Cardiovascular Disease | Common carotid artery | 0.15 % Trypsin, RNase, DNase and lypase | rGO-enzymes ( 10, 20, 40, 80, 100 and 200 mM) | Provide platform for cascade reaction and enhance stability of: apyrase and 5'-nucleotidase | Vascular matrix activated with EDC/NHs, rGO-enzymes complexes added | *In vitro* - rGO-enzyme coating have antithrombotic behavior, no significant aggregations; *In vivo* - rGO-enzyme unobstructed proportion high and high blood flow volume. rGO coated results similar to control group (no coating). | Not evaluated | [214] |
| | Pulmonary Valve Tissue | 1X trypsin/EDTA, 0.5 % SDS | rGO (100 µg/ml) | Less thrombogenic | Acellular discs immersion in rGO solution | *In vitro* - coating did not cause oxidative stress to fibroblasts, DNA not damaged rGO coating shows thromboresistance. | Not evaluated | [217] |

ACM = acellular cartilage matrix, ADM = acellular dermal matrix, ANA = acellular nerve allograft, DT = decellularized tissue, EDC = 1-ethyl-3-(-3-dimethylaminopropyl) carbodiimide hydrochloride, EDTA = Ethylene-Diamine-Tetra Acetic acid, MSC = mesenchymal stem cell, NHS = N-hydroxysuccinimide, SDS = Sodium Dodecyl Sulfate, VB12 = Vitamin B12.

### 2.3.1 Nerve Regeneration

As can be seen in Table 2, three works were found exploring the capability of nerve regeneration using decellularized matrices combined with a GBM, graphene oxide (GO). Nerve regeneration is an important field in the scientific research since peripheral nerve injury can lead to paralysis. The quest for a material capable of replacing the nerves and allow the total function recovery of the affected limbs is crucial [185].

#### a) Acellular Nerve Allograft (ANA)

Wang *et al* [186] and Niu *et al* [187] decellularized the sciatic nerve of rats and incorporated GO. Decellularization of the sciatic nerve of rats [188, 189] was obtained by the hypotonic-detergent method, resulting in a 3D scaffold. This scaffold maintained extracellular components, namely vessels of Schwann basilar membrane, epineurium and perineurium. Wang *et al* [186] and Niu *et al* [187] used GO for its electrical conductivity property and aqueous solution stability. In addition, Niu *et al* [187] also used GO for its ability to adsorb Vitamin B12 (VB12) and concentrate it on the nerve injury site. VB12 is the most common drug used for the treatment of neurological disorders such as facial nerve paralysis, neuroticism, and memory loss [190, 191]. The final scaffolds were obtained by dip coating the ANA in a dispersion of GO (20 mg/ml) [186] or of GO-VB12 (20 mg/ml) [187].

In both cases, *in vivo* results, showed that the implanted scaffolds were not toxic and there was no inflammatory response. Wang *et al* [186] showed that the sciatic nerve action potential was significantly higher on the group with GO combined to the decellularized scaffolds, as well as the thickness of myelin sheath and the diameter of the axon. Additionally, the rehabilitation of the muscle was also more evident on the GO group. The results obtained by Niu *et al* with ANA coated with GO-VB12 were not compared with ANA coated with only GO. Hence, the results obtained do not allow to specifically determine the role of GO on a decellularized matrix to facilitate nerve regeneration. Nevertheless, the combination of the decellularized matrix with GO or GO-VB12 showed to be a good treatment option for nerve injury. Even though the Wang *et al* study was not referred in the Niu *et al* study, both experiments were performed in the same laboratory and Wang co-author in the second study. Given that in the second experiment, GO was combined with VB12, it could be possible to deduct that another approach was studied to assess the resulting nerve regeneration capacity.

#### b) Cellulose-based scaffold

Cellulose-based materials are very promising in the biomedical field since its properties such as abundancy, accessibility, low cost, and biocompatibility are very interesting [192]. These types of materials are used in multiple applications like wound dressings, drug release, implants, neural and cardiovascular applications. It can also be used in the form of nanoparticles, fibers, and composites in tissue engineering of bone and cartilage [192-195].

Toker *et al* [196] evaluated the potential application of a decellularized vegetal matrix as a scaffold for nerve regeneration. Leek samples were decellularized using a chemical decellularization method with SDS treatment (ionic detergent). After decellularization, the scaffolds maintained the cellulosic structure. GO dispersion (0.5 mg/ml) was added to the surface after the leek decellularized scaffolds were treated with UV-Ozone to activate the surface. GO was used to enhance cell attachment and viability to decellularized leek matrix (Figure 4) and GO coatings were found stable. The *in vitro* results demonstrated that cells had a normal neuroblastic morphology in the GO coated samples producing filopodia and lamellipodia enabling the adhesion and elongation in the surface.

Moreover, in the study, it was shown that decellularized leek samples coated with GO have an elastic modulus (1.50 ± 0.007 kPa) lower than the native samples (4.05 ± 1.11 kPa) and decellularized sample (4.42 ± 0.50 kPa), resulting in a reduced stiffness, and an increased tensile strength (1.93 ± 0.10 MPa) in comparison to the native samples (1.54 ± 0.28 MPa) and the decellularized sample (1.89 ± 0.25 MPa). However, contrarily to the expectations, the values of elastic modulus and tensile strength were higher for the decellularized samples in comparison to the native ones. Even though the authors of this study do not comment these results obtained, this may be a result from the decellularization method or from storage, but further studies should be performed.

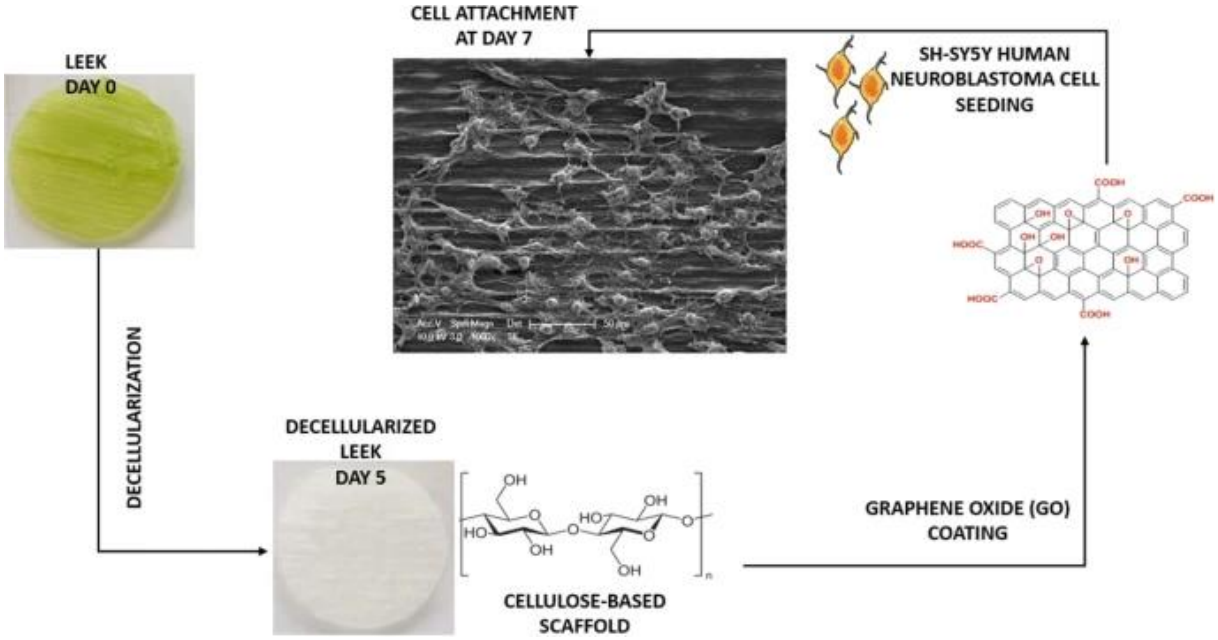


Figure 4 – Representation of the experiment results along the processes: decellularization of leek resulting in a cellulose-based scaffold, graphene oxide coating and cells attachment at day 7. Adapted from [196].

## 2.3.2 Skin Repair and Replacement

Skin substitutes to replace and repair are another very important domain of tissue engineering for healing dermal wounds. Hence, there are already several studies in the literature to find them (reviewed by [197]). However, only two works combine decellularized matrices with GBM (Table 2).

### a) Acellular dermal matrix (ADM)

Fu *et al* [198] obtained acellular dermal matrix (ADM) by the decellularization of skin treated with 0.25 % dispases solution, 0.3 % triton solution, 0.25 % trypsin solution and a fat digestion solution of chloroform-methanol (v/v = 1:1). ADM is composed of an extracellular matrix of proteins and collagen capable of retaining the basic dermal architecture and has excellent properties such as biocompatibility, bioactivity and a controllable biodegradability [199]. ADM was freeze-dried, rehydrated and crosslinked with Ethylene-Diamine-Tetra Acetic acid (EDC) and *N*-hydroxysuccinimide (NHS) solutions. Then, it was combined with reduced graphene oxide (rGO) or graphene oxide (GO) by immersion of the ADM scaffolds in the respective suspension with different concentrations (10, 20, 40, 80, 100 and 200 mM), fabricating ADM-rGO and ADM-GO hybrid scaffolds. ADM-rGO scaffolds

achieved high stability. Its application was to locally deliver mesenchymal stem cells (MSC) to accelerate diabetic wound healing, as ADM provide an analogous niche to the MSC. rGO was used since it should decrease the cellular uptake and reduce the toxicity of the ADM [200, 201]. In fact, when used in a certain concentration (at higher concentrations 50 ng/mL [202] and 0.0075 % (w/v) [203]), rGO promotes angiogenesis by the concentration increase of intracellular reactive oxygen species [202, 203]. Additionally, due to its excellent electroconductivity, lipophilicity and biocompatibility, it is beneficial for cell adhesion and proliferation [204-206].

The results showed a slower degradation rate for the ADM-rGO scaffold comparing to ADM, which is beneficial for wound healing. Moreover, the higher mechanical properties were obtained for the ADM-rGO scaffold, which had a Young's Modulus of 19 kPa, ultimate tensile strength of 5.55 MPa and strain at failure of 28.27 %. These values were compared to the ADM-GO scaffolds (13 kPa, 4.55 MPa, and 20.33 %) and ADM scaffold (9 kPa, 4.11 MPa, and 15.13 %). Still, the ADM-GO scaffolds presented better mechanical properties than the ADM scaffold (Figure 5).

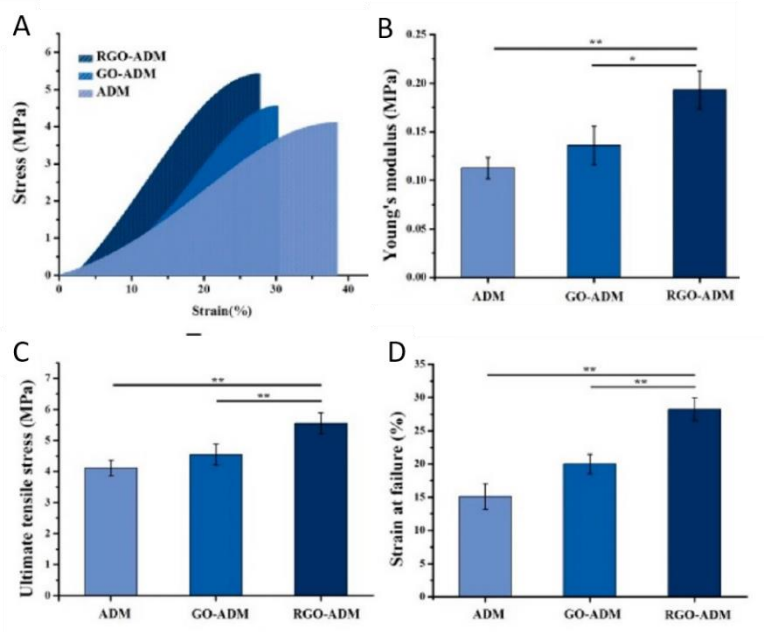


Figure 5 - Results of the ADM, GO-ADM and rGO-ADM mechanical properties: (A) Stress-strain curve, (B) Young's Modulus, (C) Ultimate tensile stress, (D) Strain at failure for the three scaffolds: ADM, ADM-GO and ADM-rGO; *p < 0.05, **p < 0.01. Adapted from [198]. ADM = acellular dermal matrix, GO = graphene oxide, rGO = reduced graphene oxide.

Regarding biological interactions, ADM-rGO scaffolds presented higher amount of MSC cells and they migrated for deeper regions, revealing the scaffold ability to capture and provide an environment more suitable for cell growth. For this reason, ADM-rGO scaffold proved to have little cytotoxicity and excellent biocompatibility. ADM-GO showed a lower cell viability than ADM-rGO for the highest tested concentrations. *In vivo* results showed that ADM-rGO-MSC would promote a faster wound closure with a higher rate of collagen regeneration than other treatments. Additionally, it also increased the vascular density and enabled the extracellular matrix deposition enabling the vascularization and re-epithelization of the tissue. Finally, neovascularization was more abundant, and the vessels diameter was larger, in the ADM-rGO-MSC scaffolds being capable of inducing angiogenesis in the wounds. Fu *et al* [198] established the ADM-rGO-MSC scaffold as a promising solution on the tissue engineering field for diabetic wound healing.

### b) ECM derived porous scaffold

Jafarkhani *et al* [207] used ECM derived porous scaffolds obtained from bovine heart tissue through its decellularization (SDS treatment), following its lyophilization to obtain decellularized tissue (DT) powder. Afterwards, the powder was dissolved and different amounts of GO (0, 1, 3 and 5 %) solution was added. The final porous scaffold was obtained by a freeze-drying technique in the resulting mixture. Then, to allow crosslinking between DT and GO, the samples were immersed in 1-ethyl-3-(-3-dimethylaminopropyl) carbodiimide hydrochloride/*N*-hydroxysuccinimide (EDC/NHS) where EDC is capable of activating the carboxyl groups (-COOH) of GO which reacted with the amine groups ($-NH_2$) of DT. In this case, GO was used to improve the mechanical properties and promote skin cell proliferation [111]. The scaffolds presented a porous and interconnected structure. The pore sizes decrease inversely with the increase of the amount of GO incorporated into the DT. The stability increases with GO concentration increase. DT/GO 3 % scaffold showed an increase in mechanical strength of up to 25 % in comparison to pure DT, which had mechanical properties poorer than the natural extracellular matrix of the skin. The Young's Modulus increased in proportion to the percentage of GO used, achieving values of 10.18 ± 1.77 kPa for DT/GO 3 % and 12.75 ± 2.5 kPa for DT/GO 5 % comparing to a Young's Modulus of 8.45 ± 1.3 kPa for pure DT. The values of the Young's Modulus are very similar to those obtained by the Fu *et al* [198] study.

For the results *in vitro*, the DT/GO 3 % scaffold was able to support the growth of cells, increasing their viability by 25 % compared to pure DT (Live/Dead staining). A higher percentage of GO (5 %) would lead to cytotoxic scaffolds. Hence, in this study the DT/GO 3 % was defined as a promising scaffold for tissue engineering with an average pore size of 200-230 μm, a porosity of 51 ± 11 % and a Young's Modulus of 10.18 ± 1.77 kPa, a value higher than the scaffold without GO (8.45 ± 1.3 kPa).

## 2.3.3 Articular Cartilage Regeneration

Articular cartilage injury is difficult to heal since it consists of hyaline cartilage, which does not have much blood supply [208]. In a clinical field, tissue engineering represents one of the most effective strategies to repair cartilage defects [209].

### a) Acellular cartilage extracellular matrix (ACM)

Gong *et al* [210] used cartilage from the distal femoral condyle was decellularized after being cut in slices, obtaining an ACM, with freeze/thaw cycle, 1 % SDS treatment, $ddH_2O$, DNase and RNase. The decellularization was verified since DNA content was not present in the ACM particles whereas GAGs and collagen II were preserved which are able to promote the chondrogenic differentiation [211]. The ACM is able to provide an optimal microenvironment for cell growth and differentiation of cartilage [212], having a similar composition to the natural tissue [213]. The incorporation of different concentrations of GO (0, 1, 2, 4 and 6 mg/mL) was performed with the mixture of both ACM and GO with gradient freezing. For some scaffolds, crosslinking was performed using EDC/NHS solution. Afterwards, lyophilization was performed, obtaining a composite scaffold. In this study, GO was used in order to improve the mechanical properties of the ACM scaffold. The Young's Modulus of the ACM-GO scaffolds crosslinked increased gradually with the increase of the GO concentration having 42.9 ± 0.24 kPa for ACM compared to 87.1 ± 0.45 kPa for ACM-GO (1 mg/mL), 151.8 ± 0.67 kPa for ACM-GO (2 mg/mL), 192.6 ± 0.52 kPa for ACM-GO (4 mg/mL) and 216.9 ± 0.73 kPa for ACM-GO (6 mg/mL).

When tested *in vitro*, the ACM-GO (2 mg/mL) had the best outcome, promoting cell adhesion and proliferation as well as chondrogenic differentiation. Moreover, this GO concentration revealed to be the less cytotoxic, capable of maintaining the activity of Bone marrow mesenchymal stem cells (BMSCs) adhered to the scaffold. The rat subcutaneous implantation of the scaffold showed the ACM-GO (2 mg/mL) had good biocompatibility and mild inflammatory response.

### 2.3.4 Cardiovascular Disease

Autologous grafts for blood vessels are the gold standard, but they are not always available, and some of them are associated with high failure rates (up to 50 %) due to thrombosis or infection occurrence [5, 7]. Thus, there are some studies in the literature to search for other solutions.

#### a) Tissue-engineered blood vessel

Huo *et al* [214] obtained tissue-engineered blood vessels (TEBVs) by decellularization the rat carotid artery using trypsin and RNase, DNase and lipase. The decellularized matrix preserved the vascular collagen fibers and elastic fibers signs. Then, the addition of EDC and NHS solutions is done to introduce active sites onto the surface and the prepared rGO-enzymes complexes dispersion added. rGO should act as barrier to separate the collagen of the blood and as enzyme carrier, enhancing stability and providing a good platform for the coagulation cascade reaction. The enzymes (Apyrase and 5'-Nucleotidase) should be capable to convert the released ADP which normally activates platelets into antiplatelet AMP and adenosine (Figure 6). Hence, this enzyme will fabricate an antithrombotic TEBV. It was believed that rGO had better biocompatible, biological stability [215, 216] in comparison to GO, that has oxygenic functional groups on the surface which will lead to platelet aggregation [165]. These findings are contradictory to the ones obtained in Pinto *et al* [145] and in Henriques *et al* [168] studies where smaller and more oxidized particles were found to be more biocompatible.

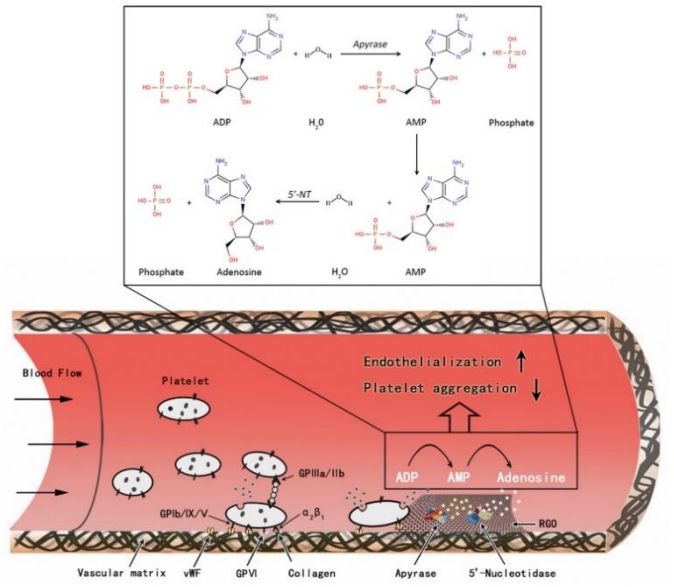


Figure 6 - Scheme of the incorporation of rGO-enzyme coated tissue-engineered blood vessels and mechanisms. Adapted from [214].

*In vitro* results showed the antithrombotic capacity that rGO-enzyme complexes provide. Moreover, the rGO-enzyme complexes promoted a proliferative activity of endothelial cells which was not found on the rGO coated decellularized matrices. In this study, the *in vivo* results, showed the rGO-enzyme complexes group had accelerating proliferation and migration of endothelial cells. Additionally, scattered platelets were not abundant in the surface. The microcomputed tomography angiography showed that TEBVs occluded due to thrombus formation after 7 days in the control and rGO groups whereas in rGO-enzyme group, they were open (Figure 7). It was demonstrated that only rGO-enzymes complexes were able to provide an antithrombotic characteristic to the TEBV. Thus, rGO coated TEBV are not sufficient to avoid thrombosis.

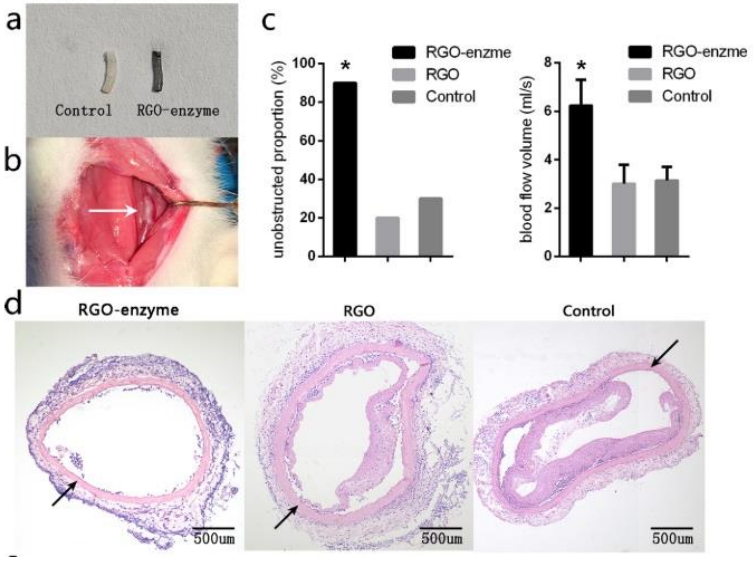


Figure 7 - Transplantation of carotid artery of rat using TEBVs: (A) RGO-enzyme coated and collagen-coated as control, (B) Arrow - implanted TEBV at 7 days, (C) Unobstructed proportion of TEBV at 7 days and blood flow volume obtained with ultrasonic Doppler, (D) H&E staining of TEBVs at 7 days; *$p < 0.05$ (n=10). Values are the mean ± SD. Adapted from [214].

Furthermore, in unpublished work previously performed by our group, small diameter vascular grafts were obtained from decellularized placental and umbilical cord arteries. The decellularization method performed used hypertonic/hypotonic solutions, 1% Triton X-100/0.02 % EDTA and 0.04 % DNase. DNA removal was observed after decellularization, as can be seen in Figure 8.

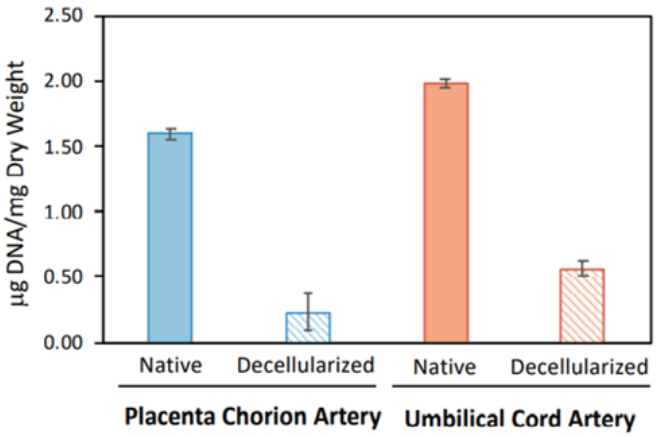


Figure 8 - DNA quantification in dried tissue (unpublished data by our group).

GO coating was then performed in the lumen of the decellularized arteries by perfusion. GO was able to cover the exposed collagen fibers of the decellularized matrices (Figure 9) and to improve the mechanical performance (by increasing 29 % the burst pressure, 25 % the strain and 10 % the compliance) of umbilical cord decellularized arteries. Regarding hemocompatibility, GO coating decreased platelet adhesion but was not able to avoid coagulation, when in contact with whole blood. Despite promising, further modifications have to be performed to enable the use of this GO-coated decellularized arteries as small diameter vascular grafts.

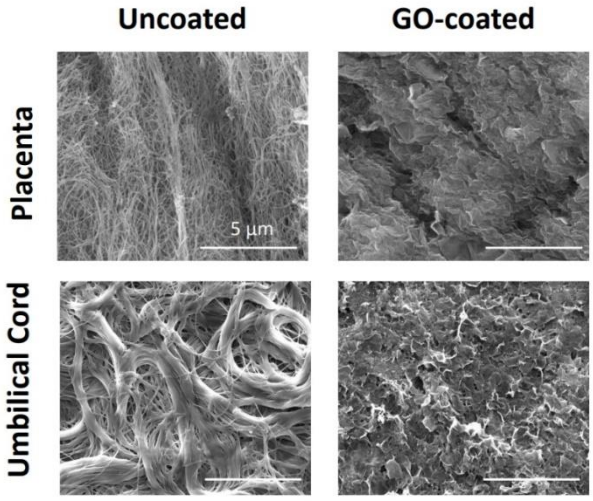


Figure 9 - SEM images of uncoated and graphene oxide (GO) coated decellularized placenta and umbilical cord arteries.

## b) Acellular pulmonary valve tissue

Acellular pulmonary valve tissue coated with rGO was developed for heart valve replacement by Wilczek *et al* [217]. Pulmonary valve tissue was decellularized with trypsin/EDTA and SDS solutions. Then, the obtained acellular discs were submersed in rGO dispersion (100 µg/ml). In this case, rGO

was used to decrease the thrombogenicity of acellular pulmonary valve tissue [218]. *In vitro* results showed a decreased cell fibroblast density on rGO coated acellular pulmonary valve tissue comparing with the uncoated matrix. This effect was associated with a mechanical damage of cell membrane. No damage in DNA, morphological alterations and oxidative stress were observed in the seeded fibroblasts. Additionally, the rGO modification did not cause significant platelet activation, which showed its thromboresistance.

### 2.3.5 Discussion

The previous studies showed that decellularized matrices combined with GBM have an improved biological and mechanical performance enabling their use in multiple applications. However, some refinements in the experimental steps should be performed to address some key questions that remain unanswered regarding the interaction between decellularized matrices and GBM.

The adopted decellularization method is not identical, which unable to obtain a direct correlation between the used method and the outcome obtained.

In most of the studies, the GBM choice, reduced graphene oxide (rGO) and graphene oxide (GO), is based in other studies and their properties. However, the explanation is not always coherent between studies. Thus, studies which compare the features of the different GBMs using the same base matrix and for different specific applications should be carried out. In this manner, it may be possible to choose the most suitable GBM to a given application, potentiating the outcomes. The same happens with the incorporation method of GBMs. There remains a lack of information to correlate and have any conclusion.

For nerve regeneration, Wang *et al* [186], Niu *et al* [187] and Toker *et al* [196] used GO as a coating of the decellularized matrix. However, in Niu *et al* [187], the coating was GO combined with VB12. The results were not compared to a coating of only GO. Toker *et al* [196] activated its surface before the addition of GO dispersion and the decellularization method was different since it is derived from a plant. Cellulose-based materials can have multiple applications. In this study, the *in vitro* tests were made with neuroblastic cells. In the future, it would be interesting to test other different cells to evaluate the use of cellulose-based materials for nerve regeneration.

For skin repair and replacement, Jafarkhani *et al* [207] tested different concentrations of GO being capable of deciding the better one (GO 3 %) to improve mechanical properties and cell viability. Fu *et al* [198] study was very complete since rGO and GO, with multiple concentrations, were tested. In this case, the ADM was crosslinked with the coating whereas in the previous study [207], the decellularized tissue was lyophilized and turned into a powder which then was solubilized and mixed with the GO dispersion resulting in a composite. For both, the mechanical properties would increase with the incorporation of the GBMs. However, Fu *et al* [198] showed that the ADM-rGO scaffolds had better mechanical properties than ADM-GO scaffolds. This property is very important in this application since skin needs to be very elastic and resist to tensile strength.

For cartilage regeneration, Gong *et al* [210] also tested different concentrations of GO. Their mechanical properties increased with the gradually increase of the GO concentration used. However, the ACM-GO scaffold showed to have better cell adhesion and proliferation for the 2 mg/mL GO concentration whereas for concentrations > 4 mg/mL, the scaffolds appeared to be more cytotoxic. Hence, the resulting composite scaffold had good mechanical properties and presented a good microenvironment for cells, being a good future tissue engineering strategy for cartilage injury treatment.

Finally, in the cardiovascular disease's domain, the available published studies used rGO. Huo *et al* [214] studied the need of forming complexes with two enzymes (apyrase and 5'-nucleotidase) to avoid obstruction and promote an antithrombotic behavior for the design of a tissue engineered vascular graft. In this experiment, the coating with rGO alone was not enough to prevent thrombus formation, *in vivo*. On the other hand, Wilczek *et al* [217] showed that rGO coating prevents the platelets adhesion to acellular pulmonary valve tissues, *in vitro*. Further studies should be performed to better understand the thrombogenic potential of rGO. In unpublished study by our group, GO was incorporated in decellularized arteries and was able to improve mechanical properties. However, the hemocompatibility properties were still not appropriate since even though platelet adhesion decreased in coated arteries, in whole blood, coagulation was not avoided.

## 2.4 Summary

This literature review provided knowledge and understanding of the impact of the decellularization methods used in extracellular matrix (ECM) by dividing the decellularization method into three categories, biological, chemical, and physical. The biological decellularization method uses proteases such as trypsin and dispases to detach cells from their ECM and DNase/RNase to degrade the genetic material. Chemical decellularization methods use a great variety of chemical agents: acid, alcohol, alkalines, chelators, ionic detergent, non-ionic detergent and zwitterionic detergent, each have a different impact on ECM components. Most of these chemical agents can damage and modify the ECM's structure. However, they can eliminate the genetic material avoiding immunological response of the host. Finally, physical decellularization methods like mechanical agitation, freeze/thaw cycles, osmotic pressure, pressure and, more recently, supercritical $CO_2$, are capable of rupturing cells and promote access for other decellularization agents. In the end, the process of decellularization should be a combination between the different categories in order to completely remove the cells' DNA, while preserving the original mechanical properties and composition of the matrix.

Graphene-based materials (GBMs) can be used in different forms such as: free-standing films, powders, dispersions, coatings and composites. Their mechanical properties are very attractive, once graphene is the strongest material in the world. Furthermore, their biological properties are very interesting for future biomedical applications given that GBMs are biocompatible, hemocompatible and, provide antimicrobial properties.

The interaction between dECM and GBMs is still poorly explored. There are a few studies in the literature that report the impact of GBMs incorporation in the mechanical and biological properties of dECM. Such lack of information prevents the correlation between the tissue source, decellularization method and the GBM type and its incorporation method and their biological and mechanical performance. Nevertheless, GBMs are capable of reinforcing decellularized extracellular matrices (dECM) improving their mechanical properties such as tensile resistance and Young's Modulus. Moreover, the incorporation of GBMs in dECM proved to be biocompatible showing a good cell viability.

The tissue-engineering blood vessels (TEBVs) showed that, in order to avoid coagulation, the reduced graphene oxide (rGO) used had to be combined with an enzyme. When used by itself, the incorporation of rGO outcome is not clear since in one study it is not sufficient and in the other one it is. This may be explained by the different decellularization and GBM incorporation methods. Previous work from our group used GO coating in decellularized arteries which resulted in a good

mechanical reinforcement. However, there remains the need to improve hemocompatible properties. Further studies should be performed testing GBMs used once the outcomes are still unclear.

# Chapter 3

# GBM-coated decellularized arteries

## 3.1 Introduction

Coronary (CABG) and peripheral artery bypass are the most common cardiovascular procedures worldwide (reviewed by [219]), being performed per year 200 000 in the US [220]. Large caliber vessels, with an inner diameter > 5 mm, like the aorta, arch vessels, and femoral artery, may be replaced with commercially available synthetic grafts such as expanded polytetrafluoroethylene and polyethylene terephthalate, which have demonstrated reasonable outcomes (reviewed by [219]). However, for small diameter vascular grafts (SDVGs) (< 5 mm) like coronary arteries and arteries below the knee these synthetic grafts tend to fail due to thrombus [221-223], intimal hyperplasia and/or chronic inflammation [224]. Even though several strategies were attempted to obtain a SDVG [4, 12, 225, 226], the gold standard procedure for peripheral artery bypass and CABG remains the use of autologous grafts, vessels harvested from the patient, such as mammary and radial arteries or saphenous veins [4, 5]. Despite the good performance of the available two mammary arteries, in most CABG procedures more than three grafts are needed, being used radial arteries or saphenous veins that are associated with failure rates of up to 50 % [5]. The failure of these grafts may require a second intervention and/or induce a second myocardium infarction culminating in patient death [5, 7]. Moreover, the harvesting of autologous graft is associated with several problems, such as anatomical limitations, wound complications which result in infections [5] and they are not always available, due to diseases progression or previous harvesting. Hence, there remains the need to find a substitute of the autologous grafts for CABG and peripheral artery bypass. By definition, an ideal small diameter vascular graft should be “off-the-shelf”, have similar mechanical properties to the vessels from the person which receives the bypass, give low inflammatory and thrombogenic response as well as antimicrobial properties.

Decellularized arteries may present an interesting solution since most of their original structure and biochemical properties such as growth factors are preserved [227]. These cues allow cell migration and vascular remodeling [39]. In the literature, several studies proposed the use of

decellularized xenografts and allografts arteries as SDVG [228, 229]. However, it was known that decellularization procedure tended to damage the microstructure of the original tissue matrix, deteriorating the mechanical properties of the dECM, which are a crucial feature to achieve a suitable SDVG, since they should be strong to withstand the blood pressure and mimic the compliance and strain of the native recipient vessel [225]. An incorrect match of these features can lead to perturbation of the hemodynamic flow, which causes turbulence that can promote thrombus formation, endothelial cells injury and stimulation of differentiation and migration of the vascular smooth muscle cells leading to intimal hyperplasia [230].

In order to promote rapid endothelization, many studies were developed by modifying the surface with brain-derived neurotrophic factors (BDNFs), vascular endothelial growth factor (VEGF) and heparin [231-233]. Despite the improved endothelization capacity, these decellularized arteries remained still far from the required mechanical properties of host vessels.

Graphene is described as the strongest material in the world with outstanding mechanical properties [15, 234]. Graphene and graphene-based materials (GBMs) have been described as cytocompatible and with antimicrobial properties [16, 17], which make them attractive for biomedical applications [16, 17]. There are few works which studied the incorporation of GBMs in decellularized arteries. Some of them show that GBM, more specifically GO and rGO, can improve the mechanical properties of decellularized matrices as reviewed in chapter 2 (section 2.3).

Previous work in the laboratory showed that the incorporation of GO in decellularized umbilical cord arteries (dArteries) was able to improve the mechanical properties by 27 % for the maximum force, 29 % the burst pressure, 25 % the strain and 10 % the compliance. Additionally, the resulting GO-coated dArteries allowed endothelial cell adhesion and were able to decrease the adhesion of platelet. However, the achieved burst is not similar to the mammary arteries and despite decreasing platelets adhesion when tested *in vivo* it was not possible to prevent clot formation. In order to improve the hemocompatible properties, the heparinization of uncoated and GO-coated dArteries may be performed. Heparin is capable of reducing platelet adhesion by reducing fibrinogen deposition [235].

In this first experimental part of this dissertation, we aimed to achieve a higher improvement in the mechanical properties of decellularized arteries than the previously reported by our group and to improve the hemocompatibility of GO-coated decellularized arteries. For this, we combined for the first time nanosized GO (nGO) (~0.099 μm) with decellularized arteries, hypothesizing that a better penetration of GO in the decellularized matrix through its pores (0.88 μm) could lead to a better mechanical reinforcement. Furthermore, the heparinization of the dArteries coated and uncoated will be tested in order to assay the resulting hemocompatibility.

## 3.2 Methodology

### 3.2.1 Decellularization of Umbilical Cord Arteries

#### 3.2.1.1 Isolation

Human placenta and umbilical cord tissues of cesarean births were obtained from Centro Hospitalar de S. João, Porto with the ethical committee approval and donor's informed consent. The umbilical cord was cut from the placenta and the two umbilical cord arteries were separated by using

tweezers. Then, in order to remove the residual blood in the vessels, they were connected by a surgical thread to a 14GA BD Venflon™ and rinsed with PBS.

### 3.2.1.2 Decellularization

After isolation, arteries were decellularized as previously described [13, 39]. Briefly, the isolated vessels were frozen at -80 ºC, for at least 18 h, and thawed in PBS at room temperature. The arteries were connected through the Venflon to a recirculating perfusion system, at 40/50 rpm, being perfused with hypertonic solution 1.4 % NaCl for cell lysis, 1 % Triton X-100 for cell membranes disruption, and 0.02 % w/w ethylene-diamine-tetra acetic acid (EDTA) in phosphate buffered saline (PBS) to allow dissociation of cells from the matrix (Figure 10). Then, the vessels were perfused with 0.04 % DNase (200 IU/mL, Roche) solution and incubated overnight with 0.04 % DNase solution under different conditions for DNA digestion:

i) Room Temperature under static conditions,

ii) Room Temperature with agitation in a roller,

iii) 4 ºC under static conditions.

Afterwards, the vessels were rinsed for 30 min in PBS at room temperature in a roller. Finally, the decellularized arteries were chemically sterilized by perfusion of 4.8 % (v/v) ethanol and 0.2 % (w/v) peracetic acid solution with a syringe and their incubation in the same solution in a roller at room temperature for 90 minutes, followed by rinsing with sterile PBS.

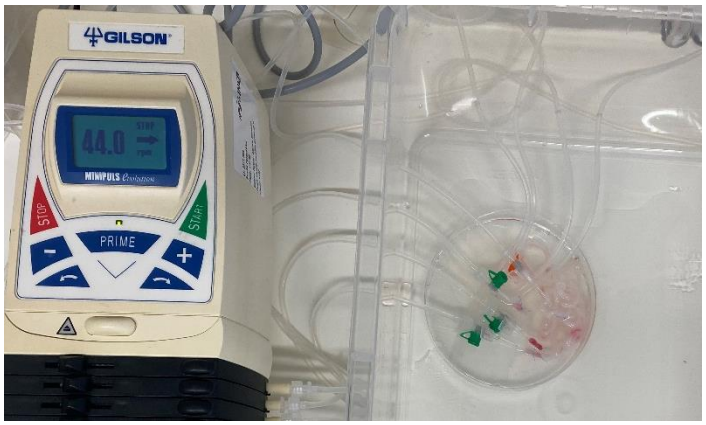


Figure 10 – Automatic decellularization set-up.

### 3.2.1.3 DNA identification and quantification

The presence of DNA in the native and decellularized arteries was visualized by microscopy upon staining of their lumen with Hoechst. For that, the native arteries and dArteries were cut longitudinally to expose their lumen and incubated with a 0.1 % Triton X-100 solution for 5 min at 4 ºC to permeabilize the membrane, allowing better staining penetration. Then, they were rinsed with PBS and incubated in a 3 µg/ml Hoechst solution for 15 min in the dark. Finally, samples were rinsed with PBS and visualized with confocal fluorescence microscope, being placed in microscope slide and excited with laser at 350 nm.

DNA content of native and decellularized arteries was quantified after tissue digestion with Qubit or after tissue digestion and DNA isolation with Nanodrop or Qubit. For tissue digestion and DNA

isolation, the protocol was performed as previously described in [236]. Briefly, the tissues were incubated overnight with a buffer solution composed by Tris, NaCl, EDTA, Proteinase K and SDS at 55 ºC to disrupt the membranes and cells and digest the tissue. Then, the DNA was isolated by adding a saturated solution of NaCl, vortex and centrifugation. The supernatant was collected, and DNA precipitated in an ethanol solution of 99 %. After centrifugation, the supernatant was discarded. After that, 70 % of ethanol was added to the pellet, being centrifugated and supernatant discarded. Finally, the DNA pellet was dried at RT for 5-10 min and then resuspended in water. The DNA was quantified after extraction with Qubit dsDNA HS Assay Kit (Life Technologies, Carlsbad, California, US) and Qubit 3.0 Fluorometer and Thermo Scientific™ NanoDrop 2000. It was also quantified before tissue digestion using Qubit™ 1X dsDNA HS Assay Kits assay, according to the instructions of the producer. When quantified with Qubit, before and after DNA extraction, values of Nanodrop are used as a reference to ensure that the limit of the equipment, 100 ng/µL of DNA concentration, is not surpassed and dilute samples to allow measurements.

## 3.2.2 Graphene-based materials (GBM) incorporation in dArteries

### 3.2.2.1 GBM synthesis and characterization

GO and few-layers GO (FLGO) were obtained from commercial graphite and a few-layer graphene (FLG) using the modified Hummers' method, respectively, as previously described [145]. nano GO (nGO) was kindly provided by our collaborator, Dr Artur Pinto from LEPABE [237]. The used GO and FLGO were characterized in the previous work performed by our group (unpublished data) and nGO by our collaborators. TEM images show the exfoliation degree of GBM (Figure 11). The lateral size of GO, FLGO and nGO were analyzed using Coulter (Coulter, LS230 Laser, USA) being 11.25 ± 8.26 µm, 26.58 ± 19.49 µm (unpublished data) and 0.099 ± 0.043 µm [237], respectively.

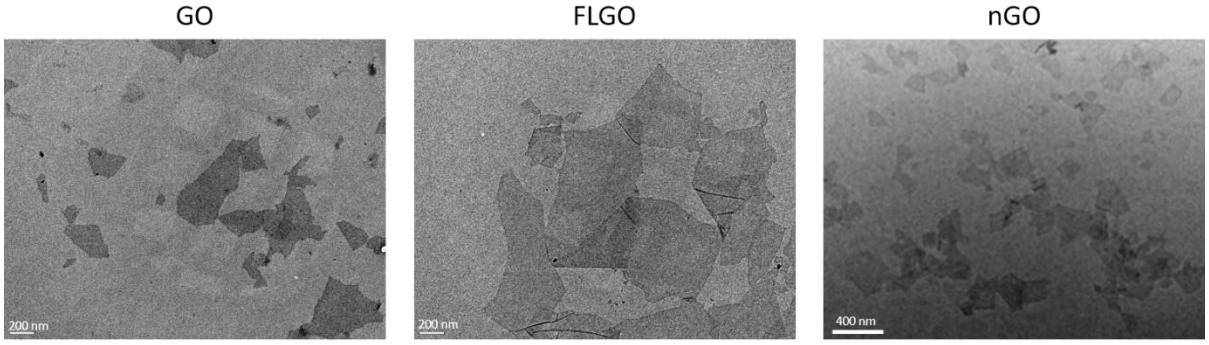


Figure 11 - TEM images of graphene oxide (GO), few-layers GO (FLGO) and nano GO (nGO). nGO images adapted from [237].

### 3.2.2.2 Preparation of GBM-containing dArteries

GBM were incorporated in the decellularized arteries (dArteries) using three different approaches:

### a) Perfusion

GO, nGO and FLGO were used to coat the inner lumen of decellularized arteries. GO, nGO or FLGO suspensions (0.5 mg/mL in $H_2O$) were perfused through the lumen of dArteries at 8 rpm overnight. 8 vessels from more than 5 donors were used. After that, each coated dArtery was perfused during 1 h with PBS to eliminate the unattached material.

### b) Pressure

A constant pressure inside of dArtery was promoted using a nGO suspension (0.5 mg/mL) (nGO-pressure) or PBS (Uncoated pressure). 5 vessels from more than 3 donors were used. The dArteries were sutured in the end and the suspension was infused in the lumen of dArteries with a syringe, being kept a constant pressure inside of the artery for 1h by pressing its embolus with a syringe pump.

### c) Pressure and perfusion

This strategy combines the procedure described in b), followed a). Thus, a constant pressure is promoted inside of the vessel for 1 hour and after, the dArtery was connected to a perfusion system, to allow the perfusion of nGO suspension More than 3 vessels from 2 donors were used.

## 3.2.2.3 Characterization of GBM-containing dArteries

### a) Topography

Scanning electron microscopy (SEM) was performed to evaluate surface topography of dArteries and GBM-containing dArteries lumen. Arteries were longitudinally cut being their lumen exposed. The different grafts were fixed with a 1.5 % glutaraldehyde in 0.14 M sodium cacodylate solution for 30 min at room temperature followed by washing with water. Then, the dehydration was attained by incubating the grafts with a growing ethanol/water gradient, 50, 60, 70, 80, 90 and 99 % (v/v), for 10 min each. Samples were then put in a hexamethyldisilazane ($C_6H_{19}NSi_2$; Sigma) and were left overnight in the fume hood to dry. The samples were mounted on carbon tape in SEM stubs and coated with a thin layer of gold/palladium by sputtering, to improve samples conductivity and consequently visualization. The samples were visualized in FEI QUANTA 400 ESEM (ThermoFischer, USA) or Phenom XL Desktop SEM.

## b) Mechanical Properties of GBM-containing dArteries and dArteries

Mechanical properties of the grafts were evaluated as described in [39, 238]. Tensile properties, compliance and burst pressure were measured in a circumferential hoop tension mode, using 3 mm rings cut uniformly as shown in Figure 12.

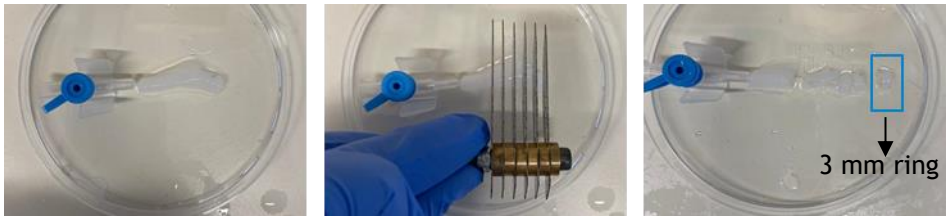


Figure 12 – System to cut the GBM-containing dArtery and dArtery rings.

A new set-up was established in the lab adapting the Texturometer (TA.xt plus, Texture Analyzer) with a system customized by us, that allows the measurement of the mechanical properties in circumferential hoop tension mode (Figure 13). In this system, the rings were placed around two stainless pins that were in contact in the beginning of the test, being the initial force normalized to 0 N. One of the pins was pulled apart until rupture of the ring. The inner diameter was determined by the displacement value where the F > 0 N.

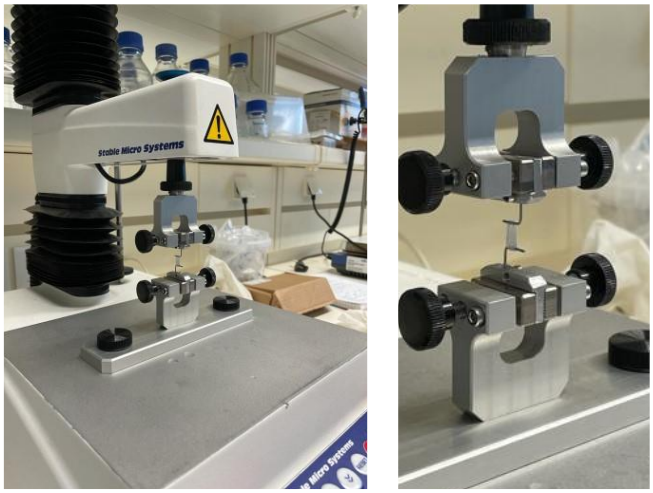


Figure 13 - Texturometer with the customized adapter during a tensile test.

To quality control of our customized system, some rings were sent to Center for Biomedical Research, Medical University of Vienna, Austria where the samples were analysed with the same parameters using a uniaxial BOSE electroforce LM1 test bench system (Bose corp, MN, USA).

For both settings, maximal loaded radial force (Fmax) is obtained directly, the theoretical burst pressure at rupture which was calculated using Laplace's Law (Equation 1), the compliance which is the ability of arteries to distend or contract with pressure variations (80-120 mmHg) was also calculated (Equation 2) and, finally, strain (percentage of elongation) was obtained from Equation 3.

$$\boldsymbol{p} = \frac{\boldsymbol{F}}{2 \times \boldsymbol{l} \times \boldsymbol{r}} \qquad \text{Equation 1}$$

With $F$ as the load (for burst pressure is Fmax), $l$ is the length and $r$ as the luminal radius.

$$\boldsymbol{Compliance} = \frac{\frac{\boldsymbol{D_{120}-D_{80}}}{\boldsymbol{D_{80}}}}{\boldsymbol{\Delta p}} \times \boldsymbol{10^4} \quad \text{Equation 2}$$

Where $D_{120}$ will be the systolic diameter at 120 mmHg, $D_{80}$ the diastolic diameter at 80 mmHg and $\Delta p$ the pressure difference [238].

$$\boldsymbol{Strain} = \frac{\boldsymbol{D_{Fmax}-D_{30}}}{\boldsymbol{D_{30}}} \times \boldsymbol{100} \quad \text{Equation 3}$$

Where $D_{30}$ will be the systolic diameter at 30 mmHg and $D_{Fmax}$ the diastolic diameter when maximal radial force is obtained.

Mechanical properties were evaluated using 10 arteries from 5 different donors for the following conditions:

- Uncoated: 110 rings
- GO-perfusion: 42 rings
- FLGO-perfusion: 24 rings
- nGO-perfusion: 38 rings
- Uncoated pressure: 14 rings
- nGO-pressure: 34 rings
- nGO-pressure-perfusion: 16 rings.

## 3.2.3 Hemocompatibility of GBM-coated dArteries and dArteries

### 3.2.3.1 Heparinization

Heparin was covalently linked to dArteries and to GO-coated dArteries. Briefly, 1 M hydroxylamine sulfate was manually perfused into the lumen of the grafts and the grafts were then incubated in the solution for 18 h in a roller at room temperature. Then, the grafts were rinsed with water for 1 h in the roller at room temperature, followed by perfusion with a syringe and 48 h incubation with heparin (25 IU/mL)/1- ethoxy-3(3-dimethylaminopropyl)carbodiimide (EDC, 84 mg/mL) solution at pH 1.5 in an orbital shaker [239]. Finally, the grafts were rinsed with water by perfusion with a syringe and for 90 min (roller, RT) and a final rinse with PBS for 30 minutes. The grafts were then preserved in PBS at 4 ºC until use.

### 3.2.3.2 Coagulation test

The clotting time was evaluated by measuring the time that the human recalcified plasma takes to clot when in contact with dArteries.

Briefly, the grafts were cut in order to expose the lumen and put in 48 well plate. The citrated plasma obtained from the Immunohemotherapy service of Centro Hospitalar S. João was thawed, and a 1 M calcium chloride solution was added. This allowed to activate the previously inactivated coagulation cascade of the plasma. Afterwards, the recalcified human plasma was added to the 48 well plate containing: uncoated, uncoated-heparinized, GO-coated and GO-coated-heparinized, using glass as a positive control. The well plate was immediately put in an orbital shaker in an incubator at

37 ºC and the time started to count. This event was visually observed by detecting the loss of movement of the plasma in response to rotation and shaking [240]. This experiment was repeated two times.

## 3.3 Results and Discussion

### 3.3.1 dArteries

Human umbilical cord arteries were decellularized as previously described [13, 39]. The decellularization process was verified macroscopically as the matrix is transformed from red aspect (indicative of cells presence) to a white matrix (Figure 14).

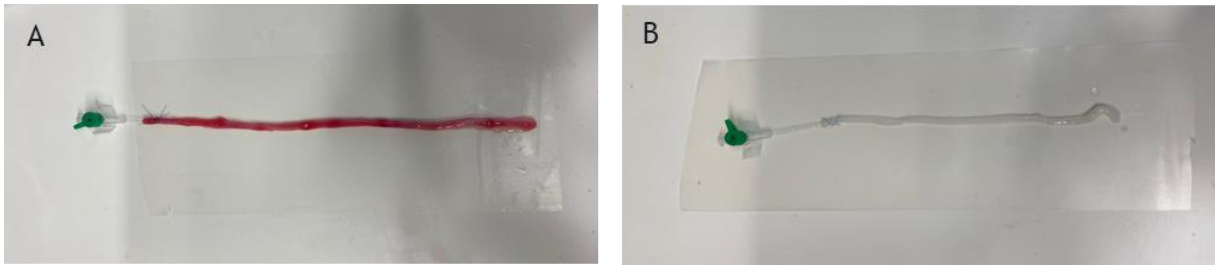


Figure 14 - Isolated umbilical cord artery connected to a Venflon: A) before decellularization process, B) after decellularization process.

Figure 15 depicts the images obtained by confocal fluorescence microscopy of native and decellularized arteries (DNase 4 ºC, DNase room temperature (RT), and DNase RT with agitation) stained with Hoechst. These three conditions were tested since the optimal temperature for DNase I activity remains unknown. In the native condition is possible to observe a high amount of cell nucleus compared with all the decellularized tissues. The 4 ºC condition was the one with less DNA present in the matrix. For the room temperature condition with and without agitation, even though the number of nucleus was less than in the native matrix, it was the decellularized condition with more DNA remnant. The lack of visible nuclear material for the 4 ºC condition satisfied one of the minimal criteria to satisfy the intent of decellularization [25]. These results suggested that the activity of the enzyme was more efficient at 4 ºC than at RT.

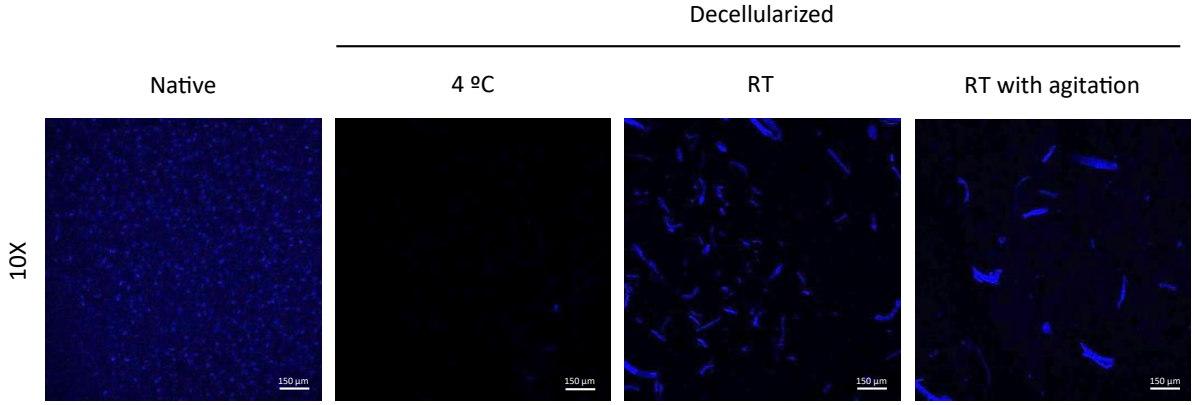


Figure 15 – Confocal imagens of native and decellularized arteries treated with DNase 4 ºC, room temperature (RT) without and with agitation stained in Hoechst.

To further verify the decellularization method, the DNA was quantified (Figure 16). The difference between Nanodrop and Qubit values was elevated, which can be explained by the fact that Nanodrop is not a very reliable technique to quantify DNA, when it is presented in low amounts [241]. Moreover, the DNA quantification was performed before and after DNA extraction being obtained similar values. This confirmed that DNA was not lost in the used extraction protocol and also the specificity of the Qubit fluorophore, since it was not affected by the presence of other tissue components (proteins, GAGs) before extraction. The values of DNA remnant in the dArteries at 4 ºC were smaller than both RT and RT with agitation conditions. In fact, only a mean of 8.5 % and 5.3 % DNA was remnant in 4 ºC condition for Qubit before and after extraction, respectively. For this matter, the DNase treatment at 4 ºC was the selected condition since it is the closer value to the minimal criteria.

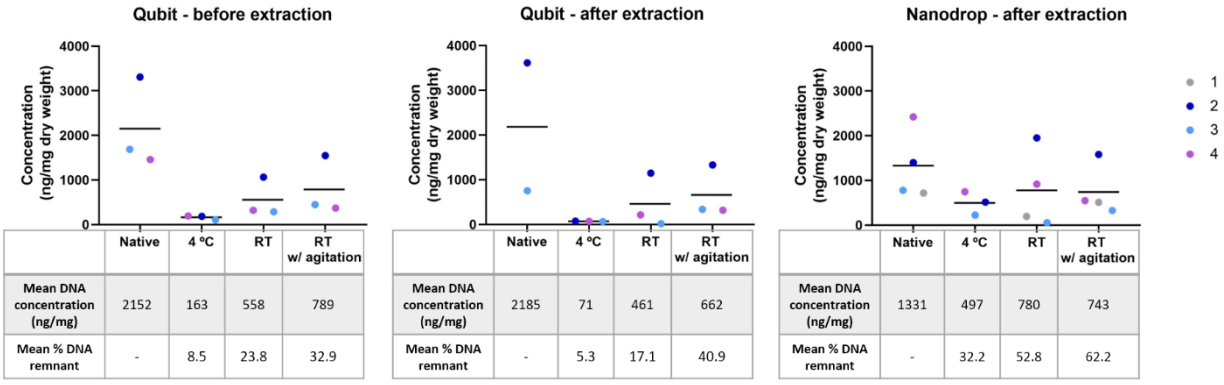


| | Native | 4 ºC | RT | RT w/ agitation |
|---|---|---|---|---|
| Mean DNA concentration (ng/mg) | 2152 | 163 | 558 | 789 |
| Mean % DNA remnant | - | 8.5 | 23.8 | 32.9 |

| | Native | 4 ºC | RT | RT w/ agitation |
|---|---|---|---|---|
| Mean DNA concentration (ng/mg) | 2185 | 71 | 461 | 662 |
| Mean % DNA remnant | - | 5.3 | 17.1 | 40.9 |

| | Native | 4 ºC | RT | RT w/ agitation |
|---|---|---|---|---|
| Mean DNA concentration (ng/mg) | 1331 | 497 | 780 | 743 |
| Mean % DNA remnant | - | 32.2 | 52.8 | 62.2 |

Figure 16 - DNA quantification with two methods: Qubit before and after extraction and Nanodrop for the four conditions: native, and decellularized at 4 ºC, RT and RT with agitation. Each color represents a different vessel and the bar the mean values.

This amount of DNA, 163.3 ± 38.2 ng/mg and 70.5 3 ± 4.9 ng/mg, for DNase at 4 ºC before and after extraction, respectively, is superior to the one obtained for acellular carotids which measured DNA concentration after extraction with PureLink Genomic DNA Kits, Invitrogen after 1 % SDS treatment with 1.37 ± 0.51 ng/mg and, after 0.05 % Trypsin and 1 % Triton X-100 treatment, 0.69 ± 0.06 ng/mg [242]. Comparing the amount of DNA in decellularized arteries obtained by DNase treatment at 4 ºC with other tissues, it is for the most part, lower than the ones previously reported in the literature that vary between 82.8-764.1 ng/mg depending on the decellularization method used [42]. The values obtained from Qubit after extraction for room temperature (558.2 ± 359.4 ng/mg) and RT with agitation (789.3 ± 536.8 ng/mg) are in accordance with the values obtained in another study [70]. Nevertheless, these values remain very high. In order to consider an efficient decellularization, independently of the original tissue and final application, the DNA concentration should be close to 50 ng/mg ECM dry weight [25] to decrease the negative immune response *in vivo* [241]. Our results showed that the DNase had a better performance at 4 ºC without agitation. Hence, the following tests were performed in dArteries treated in this condition.

### 3.3.2 GBM-containing dArteries

As can be seen in Figure 17, native tissue does not exhibit collagen fibers, whereas the uncoated decellularized arteries (dArteries) had these fibers completely exposed. The decellularized arteries were combined with 3 different GBMs using 3 different methods, namely perfusion, pressure inside the dArtery and, finally, pressure and perfusion. For all the tested conditions the collagen fibers were completely covered by GBM coating, even after PBS perfusion, showing the coating stability in all the tested conditions.

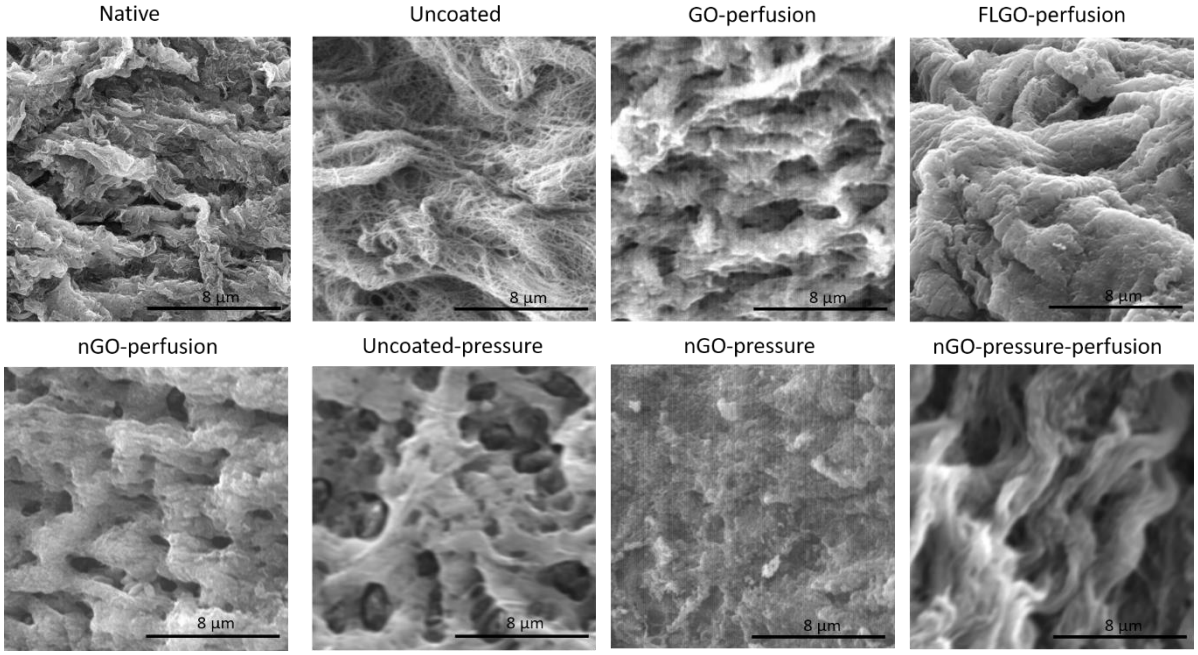


Figure 17 - Scanning Electron Microscopy (SEM) of the native artery, dArteries uncoated and dArteries with the different treatments: GO-coated, FLGO-coated, nGO-coated, uncoated-pressure, nGO-pressure and nGO-pressure-coated.

Since each artery has unique mechanical features, in order to minimize the effect of these natural variability, each dArtery was cut in different pieces, being all the comparisons between the treatments performed into the same decellularized artery. Then, the different pieces of each dArteries with each incorporated GBM were cut into rings of 3 mm, being the mechanical properties in circumferential hoop tension mode measured. The obtained values were represented as percentage of increase comparing with the respective uncoated dArteries. In this way, it was possible to compare the different treatments made in all the decellularized arteries, taking into consideration the fact that the isolated vessels are always different.

As can be seen in Figure 18, the maximum force (Fmax) of dArteries perfused with different GBMs: GO, nGO and FLGO did not affect the mechanical properties of dArteries, being the percentage of increase near 0. Since stability and properties of GO may vary along between batches, 2 GO batches were tested, despite similar mechanical properties were observed.

Regarding nGO, it had a smaller lateral size than the size of the holes created by the exposed collagen fibers of the dArteries. As such, we hypothesised, that it would be capable of better penetration inside the decellularized artery, further improving the mechanical properties. For this coating, different methods of incorporation were tested: perfusion, pressure and pressure + perfusion. In this case, pressure was tested since the idea was that the pressure would expand the matrix, allowing a better penetration of the nGO. However, once more, none were able to improve the mechanical property of the decellularized artery. Upon incorporation of nGO (99 nm of lateral size) under pressure, the Fmax of dArteries remained unchanged when comparing with uncoated and uncoated pressure (Figure 18).

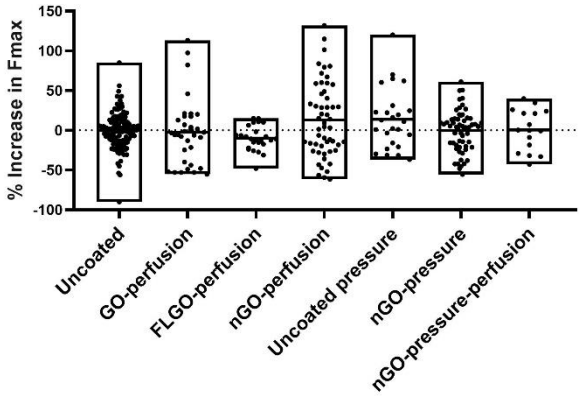


Figure 18 - Fmax of decellularized vessels before and after incorporation of GBMs: uncoated, GO-perfusion, FLGO-perfusion, nGO-perfusion, uncoated pressure, nGO-pressure and nGO-perfusion-pressure. (Kruskall-Wallis test; $p < 0.05$); n = 13 vessels with > 14 rings in each condition (each dot corresponds to one ring).

Besides the maximum force, the burst pressure, strain, and compliance were also assessed for some of the conditions: FLGO, uncoated-pressure and nGO-pressure (Figure 19). The values obtained for the burst pressure were 1159.7 ± 386.2 mmHg for the uncoated, 1029.1 ± 271.4 mmHg for the FLGO -coated, 995.2 ± 426.9 mmHg for the uncoated-pressure and 1002.2 ± 439.8 mmHg for the nGO-pressure, which are far from the values of the gold standard vessels, the saphenous arteries and internal thoracic arteries (ITA) which have a burst pressure of 2134 mmHg and 3073 mmHg, respectively [12, 243, 244]. Concerning the compliance, 12.2 ± 6.9 %/100 mmHg for the uncoated and 17.5 ± 10.2 %/100 mmHg for the FLGO -coated. These values were higher than the ITA compliance, 11.5 %/100 mmHg, which could prevent intima hyperplasia, except for the pressure conditions but remained lower than the compliance of the saphenous vein, 25.6 %/100 mmHg. However, it is important to point out that upon the conditions under pressure, the compliance values decreased significantly comparing to dArteries for 5.8 ± 2.7 %/100 mmHg (uncoated-pressure) and 6.7 ± 3.5 %/100 mmHg (nGO-pressure), which could be associated with the rupture of fibers, such as elastin, due to the applied pressure. These results are not in agreement with other studies that report the incorporation of GBM in decellularize extracellular tissues, since they always report an improvement in their mechanical properties upon GBM incorporation [196, 198, 207]. Moreover, these results were even more surprising since in the previous work performed in our group, an increase of the mechanical properties was observed with GO-coating. Nevertheless, it is important to denote that the lateral size of the GO used in this previous work performed in our group is smaller (1.5 µm) than the one used in this study (11.25 µm), which can have led to a better incorporation of the material during the perfusion process. This difference may explain the contradictory results. In the case of nGO incorporation, its lateral size is much smaller (~0.099 µm) than the GO used in the previous work

which may explain the lack of mechanical properties observed. Even though it is capable of efficacity penetrating the dArteries, its much smaller lateral size is incapable of improving the mechanical properties.

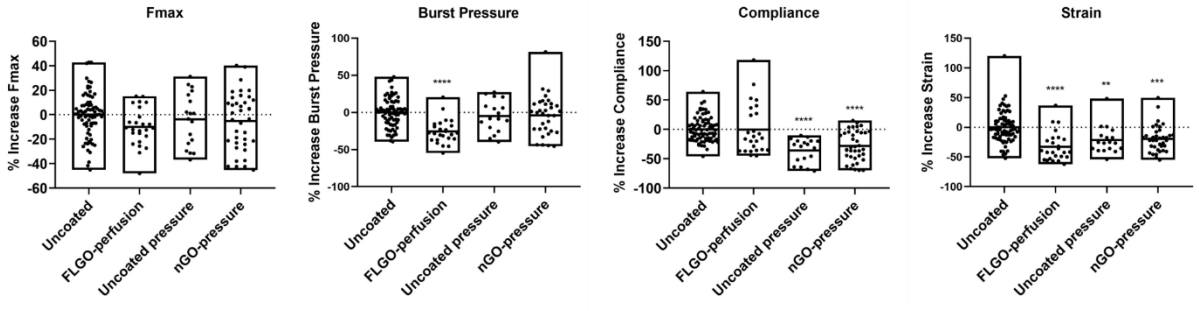


Figure 19 – Fmax, burst pressure, compliance and strain of decellularized vessels before and after incorporation of GBMs: uncoated, FLGO-perfusion, uncoated pressure, and nGO-pressure. (Kruskall-Wallis test, ** $p < 0.05$, *** $p < 0.005$, **** $p < 0.0001$); n = 7 vessels with > 14 rings in each condition (each dot corresponds to one ring).

Since the setting used to measure the mechanical properties was new in our laboratory, in order to verify the data, some samples were sent to Vienna (Figure 20). In Vienna, the values obtained for the burst pressure were 1891.2 ± 685.5 mmHg for the uncoated, 1568.4 ± 568.2 mmHg for the GO-coated and 1556.3 ± 584.1 mmHg for the nGO-coated. Regarding the compliance, 17.0 ± 5.6 %/100 mmHg for the uncoated, 14.8 ± 4.3 %/100 mmHg for the GO-coated and 13.0 ± 4.3 %/100 mmHg for the nGO-coated. The mechanical properties were not increased with GO-perfusion nor nGO-perfusion, which confirmed that the problem would be the coating rather than the set up in our laboratory, which is reliable.

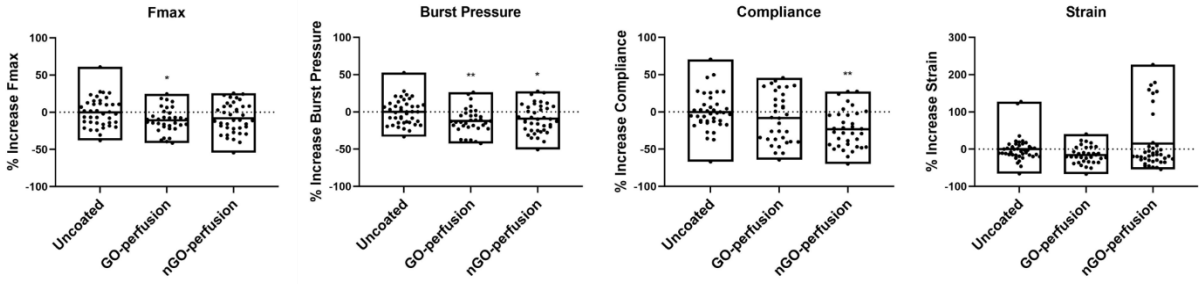


Figure 20 - Fmax, burst pressure, compliance and strain of decellularized vessels before and after incorporation of GBMs: uncoated, GO-perfusion and nGO-perfusion conditions tested by our collaborators in Vienna. (One-Way ANOVA test for Fmax and Burst pressure, Kruskall-Wallis test for Compliance and Strain, * $p < 0.5$; ** $p < 0.05$); n = 3 vessels with > 38 rings in each condition (each dot corresponds to one ring).

## 3.3.3 Hemocompatibility of GBM-coated dArteries

Due to collagen exposure, dArteries have been associated with high thrombogenicity. Heparin is an anticoagulant and its effect in the dArteries avoids coagulation of the matrices where it is incorporated [245]. In this study, the combination of dArteries with heparin was proposed to increase

their thrombogenicity. Figure 21 shows that upon heparinization both uncoated and GO-coated dArteries showed a smoother surface.

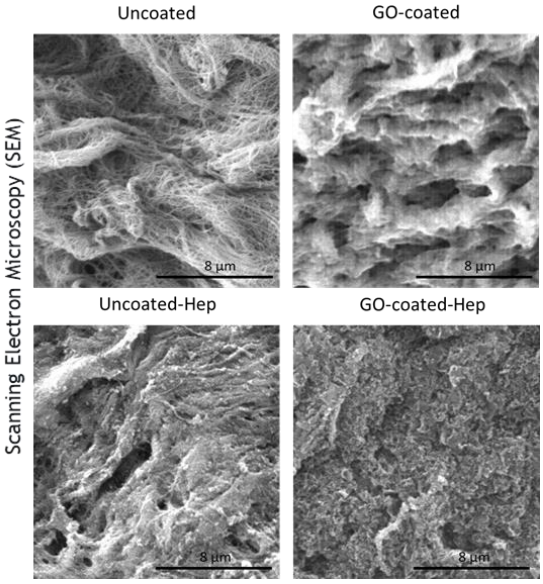


Figure 21 - Scanning Electron Microscopy uncoated and GO coated decellularized arteries, before and after heparinization.

The coagulation test allowed to assess the thrombogenic potential of the dArteries. The different conditions were put in a recalcified human plasma solution. After 20 minutes, the glass, the uncoated and the GO-coated dArteries were completely clotted since a gel was formed (Figure 22). However, in the case of the heparinized uncoated and GO-coated matrices, after 30 hours, the longest time point acquired, neither clotted, suggesting that they are non-thrombogenic (Figure 22).

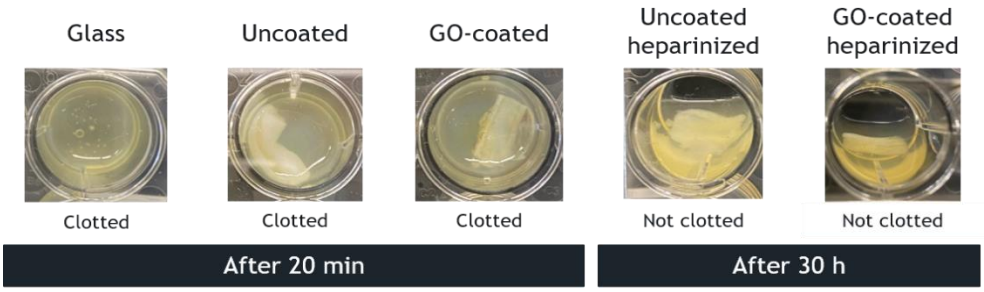


Figure 22 - Coagulation test of Glass, Uncoated, GO-coated, Uncoated heparinized and GO-coated heparinized decellularized arteries.

## 3.4 Summary

The umbilical cord arteries were successfully decellularized. From the 3 DNase treatments adopted to remove the DNA, the one at 4 ºC was the most efficient, being achieved a DNA remotion of 91.5 %, comparing with RT (76.2 %) and RT with agitation (67.1 %).

Different GBMs: GO, nGO and FLGO were successfully incorporated in dArteries being obtained a homogeneous coating that completely covered the exposed collagen fibers. However, none of tested conditions improved the mechanical properties of the dArteries, being observed for some conditions even a decrease in the Fmax, burst pressure, compliance and strain comparing with dArteries.

Nonetheless, heparinization of the uncoated and GO-coated dArteries improved their hemocompatibility.

# Chapter 4

# GBM-reinforced ECM-derived hydrogel

## 4.1 Introduction

Hydrogels are hydrophilic chemical or physical crosslinked macromolecular networks and have multiple biomedical applications such as drug delivery and tissue regeneration [246, 247]. Due to their high water content, hydrogels are able to provide a microenvironment [248] similar to tissues capable of supporting cells growth [249].

Hydrogels obtained from decellularized extracellular matrices have gelation temperature at 37 ºC and have been described with promising features for tissue regeneration since they preserve some elements from native tissues such as collagen and GAG along with other biochemical components like growth factors [250, 251]. This microenvironment is capable of supporting multiple biological processes like angiogenesis, epithelization and neovascularization [10, 11]. Placental membranes namely human amnion and chorion membranes are allografts that have been applied in periodontics, surgical wound treatment (chemical or thermal burns and ulcer sites), ocular surface (correction of corneal epithelial defects, leaking blebs after glaucoma surgery, reconstruction of conjunctival and ocular surfaces) for over 70 years (reviewed by [252]). They have been described with antimicrobial properties and high amount of protein, which facilitates cell migration in the defect [253]. Amnion membranes are composed by collagen type I, III, IV, V and VI, which are bioabsorbable and have hemostatic properties, proteoglycans that provide resistance to compressional forces due to their hydration and swelling pressure properties, laminin capable of promoting cell attachment, growth and differentiation, and fibronectin, a protein involved in cell migration and adhesion [252]. Amnion has also multiple growth factors capable of stimulating epithelization [254] and promotion of tissue repair instead of scar formation [100, 255]. Chorion membranes are composed by collagen type I, III, IV, V and VI, proteoglycans, laminin and fibronectin in their layers of placental membrane [252].

However, the mechanical properties of ECM-derived hydrogels are very weak. This characteristic inhibits their use in load-bearing fields. Nevertheless, it may be surpassed with the incorporation of GBMs in their network. An increase of mechanical properties can be observed when GBMs are

incorporated in ECM-derived materials [198, 256, 257]. In Fu *et al* study [198], the coated matrices with rGO and GO had a higher Young's modulus (0.19 and 0.13 MPa), ultimate tensile stress (5.55 and 4.55 MPa), and strain at failure (28.27 and 20.03 %) than matrices without GBM previously incorporated (0.09 MPa, 4.11 MPa, and 15.13 %). This incorporation may be covalent with chemical modification, or non-covalent, with hydrophilic reactions like hydrogen bonds or hydrophobic reactions such as π-π interactions. The reinforcement allows delay of hydrogel failure and decrease of crack propagation.

In this dissertation work, a GBM reinforced ECM-derived hydrogel was attempted in order to assess its use as SDVGs or as injectable hydrogel. The decellularization process was optimized and different concentrations of GO: 1 % and 10 % added. Rheological tests were performed in order to determine the gelation time, the elastic (G') and viscous (G'') component of the different hydrogels after 30 minutes at 37 ºC.

## 4.2 Methodology

### 4.2.1 Decellularized human placental hydrogel

#### 4.2.1.1 Isolation

Human placenta and umbilical cord tissues of cesarean births were obtained from Centro Hospitalar de S. João, Porto with the ethical committee approval and the informed donor's consent. The amnion and chorion fetal membranes were removed from the placenta manually. The amnion is the external membrane of the placenta and is possible to remove easily and the chorion is the following membrane where the vasculature is, and it is possible to isolate manually with the help of a scalpel by shaving and scrapping the basal tissue. Then, the residual blood is rinsed with PBS and tissues stored at -20 ºC until further use.

#### 4.2.1.2 Decellularization

##### a) Method A

After isolation, amnion and chorion tissues were decellularized using two different methods. Method A was performed as described in the literature [71, 258] with minor modifications. Briefly, amnion and chorion tissues were thawed in PBS and cut in 2 cm squares. Afterwards, they were put in flasks where they were stirred for 48h in 1 % SDS in PBS. Afterwards, the tissues were stirred in 1 % Triton X-100 and 0.02 % EDTA solution overnight followed by rinsing with PBS for three days. Finally, to sterilize the tissue, they were put in a 0.1 % peracetic acid and 4 % ethanol solution, with stirring, for 4 hours. Tissues were subsequently washed with PBS and $dH_2O$ for 40 minutes. Finally, decellularized amnion and chorion membranes were lyophilized and stored at -20 ºC.

### b) Method B

The amnion and chorion membranes were decellularized as described by the University of Vienna, a project partner. Briefly, the samples were stored in the freezer at -80 ºC for more than 24 hours. Afterwards, while still frozen, samples were cut in small pieces of around 2 cm and washed in $dH_2O$ for 1 hour, changing the solution at 30 minutes. Subsequently, tissues were stirred for 1 hour in 1.4 % NaCl followed with strain and rinsing with $dH_2O$. Then the membranes were put in 2 % Triton X-100 and 0.02 % EDTA solution for 1 hour with stirring. Then, for four days a cycle of the same treatment was performed where the samples were rinsed with $dH_2O$, stirred with PBS for one hour and put in 2 % Triton X-100 and 0.02 % EDTA solution, stirring for 20-24 hours. After that, the tissues were rinsed with $dH_2O$ for 1 hour, ensuring no formation of bubbles and transferred to PBS with 0.5 % Pen/Strep solution, with stirring for 2-3 days at 4 ºC. To finalize the decellularization process, the tissues were relocated in PBS + Calcium + Magnesium (PBS +/+) with Pen/Strep and changed to DNase I solution exploring two different concentrations 1.2 % or 0.04 % in PBS +/+ for 4 hours with stirring and then transferred to a chamber at 4 ºC overnight, with stirring. To sterilize the samples, they were rinsed with $dH_2O$ and put in a 4.8 % ethanol and 0.02 % peracetic acid solution for 2.5 hours at room temperature and stirred overnight at 4 ºC with $dH_2O$ with Pen/Strep. Finally, the samples were lyophilized and stored at -20 ºC.

## 4.2.1.3 DNA quantification

The DNA amount in native and decellularized amnion and chorion tissues for both methods, was quantified after tissue digestion using Qubit™ 1X dsDNA HS Assay Kits before DNA extraction. After lyophilization, the different samples were put overnight in a buffer solution composed by Tris, NaCl, EDTA, Proteinase K and SDS at 55 ºC in order to disrupt the membranes and cells present in each sample. The DNA quantification was performed using the Qubit 3.0 Fluorometer and Qubit dsDNA HS Assay Kit (Life Technologies, Carlsbad, California, US), according to the instructions of the producer before DNA pellet extraction.

## 4.2.1.4 ECM-derived hydrogel production

Hydrogel was produced as described by our collaborators at University of Vienna. Briefly, the lyophilized decellularized amnion and chorion tissues were milled into ECM-derived powder and stored at -20 ºC until further use. Firstly, 4 % (w/v) of dECM was added to a solution containing 0.1M hydrochloric acid and 5 % of pepsin ($w/w_{dECM}$). The mix was left for 48 hours with magnetic stirring at room temperature to allow tissue digestion. Finally, neutralization was performed by adjusting the pH with NaOH to 7.4 and the pre-gel was stored at 4 ºC. The hydrogel gelation was further promoted by incubating it at 37 ºC overnight.

## 4.2.2 Graphene-based material incorporation

The GO used in this strategy is the same as the GO used in the previous chapter, described in section 3.2.2.1. Two different concentrations of graphene oxide 1 % (w/v) GO and 10 % (w/v) GO were tested. Graphene oxide suspensions were freeze dried to obtain a powder. The GO powder was

weighted and added to the pre-gel solution either before or after dECM digestion. When added after digestion, it was magnetic stirred for 20/30 minutes, until a homogeneous solution was reached. Afterwards, one of the GO-pre-gel solutions was sonicated while the other had no additional treatment.

### 4.2.3 Mechanical Characterization

All hydrogel samples were rheologically characterized using a Kinexus Rheometer at 25 ºC and 37 ºC to test the gelation capacity. Small-amplitude oscillatory shear (SAOS) test was performed where a small quantity, under 75 µl, was put between the parallel disks and a small amplitude torsional oscillation generated a shear flow in the sample. SAOS can be monitored with time, which is important to assess the gelation time of the hydrogel [259].

Firstly, the pre-gel samples performed oscillation tests to determine the linear-viscoelastic (LVE) regime. They were put in the rheometer plate at 25 ºC and the test geometry of 8 mm diameter and lowered to the defined 1000 µm gap. Since the dECM would be composed with collagen, the values of the parameters chosen were based in the values observed in the literature and slightly modified [259]. After loading the sample (75 µl), the sequence was defined for each hydrogel.

In a first instance, the test was performed to compare two GO incorporation timepoints: before and after digestion. The values of strain and frequency used for the time sweeps performed with the optimal LVE values are shown in Table 3 for the different conditions.

Afterwards, different concentrations of GO: 1 % and 10 % were compared. For this, two time sweeps were performed: with the optimal LVE parameters and the LVE adjusted values of a strain and frequency which can be maintained in all conditions for direct comparison (Table 3). The time sweeps tests were performed in triplicate.

For all these samples, the testing time was short not needing to humidify the chamber (maximum 30 minutes).

Table 3 – Rheometer parameters used for testing decellularized extracellular matrix (dECM): dECM, dECM-sonicated, 1 % GO, 1 % GO-sonicated, 10 % GO and 10 % GO-sonicated.

| Hydrogel | Condition | Parameter | Strain Sweep | Frequency Sweep | Time Sweep | |
|---|---|---|---|---|---|---|
| | | | | | LVE optimal | LVE adjusted |
| dhpcECM | dECM<br>dECM-sonicated<br>1 % GO | Temperature (ºC) | 25 | 25 | 37 | 37 |
| | | Gap size (µm) | 1000 | 1000 | 1000 | 1000 |
| | | Time (min) | 10 | 30 | 30 | 30 |
| | | Frequency (Hz) | 1 | 0.01-100 | 1 | 1 |
| | | % Strain | 0.1-100 | 2 | 2 | 1 |
| | 1 % GO - sonicated | Temperature (ºC) | 25 | 25 | 37 | 37 |
| | | Gap size (µm) | 1000 | 1000 | 1000 | 1000 |
| | | Time (min) | 10 | 30 | 30 | 30 |
| | | Frequency (Hz) | 1.5 | 0.01-100 | 1.5 | 1 |
| | | % Strain | 0.1-100 | 2 | 2 | 1 |
| | 10 % GO<br>10 % GO sonicated | Temperature (ºC) | 25 | 25 | 37 | 37 |
| | | Gap size (µm) | 1000 | 1000 | 1000 | 1000 |
| | | Time (min) | 10 | 30 | 30 | 30 |
| | | Frequency (Hz) | 1 | 0.01-100 | 1 | 1 |
| | | % Strain | 0.1-100 | 0.25 | 0.25 | 1 |

## 4.3 Results and Discussion

### 4.3.1 Decellularized human placenta amnion and chorion

The decellularization process was verified macroscopically with the whitening of the original reddish matrix for the different methods (Figure 23).

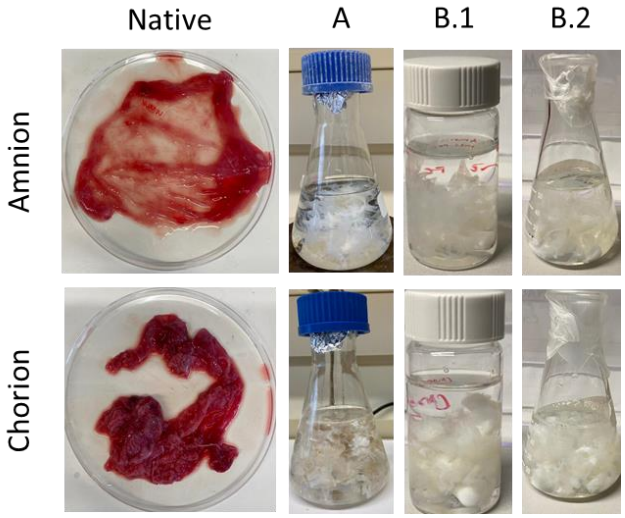


Figure 23 - Isolated amnion and chorion tissues in the native form and after the three decellularization processes: A) method A, B.1) method B with 1.2 % DNase and B.2) method B with 0.04 % DNase.

DNA content of the decellularized human placenta amnion and chorion tissues was assessed for resulting dECM of the three decellularized methods: method A and method B with 1.2 % or 0.04 % DNase. For this, the tissues were digested, and DNA amount quantified using the qubit assay kit, since it was previously demonstrated to be the best method to quantify DNA of decellularized tissues (section 3.3.1). As can be seen in Figure 24, the dECM resulting from method A showed high amount of DNA of 54.9 % for amnion and 103.8 % for chorion, revealing to be an insufficient for tissue decellularization. For method B with 1.2 % DNase, the amniotic tissue had 1.4 % DNA remnant and for method B with 0.04 % DNase it had 1.7 % DNA remnant, revealing similar efficiency. For the chorion membranes the same tendency can be observed, with method B.1 (1.2 % DNase) having 0.5 % of remnant DNA and for the method B.2 (0.04 % DNase), 2.2 % DNA remained. These results showed that the intent of decellularization was correctly executed for method B with 1.2 % and 0.04 % DNase, with a final concentration inferior to the minimal criteria (50 ng/mg ECM dry weight) for both methods B [25].

The decellularization efficiency of method B was higher than the one described by Leonel *et al* [30], where the remnant DNA concentration in fetal membranes was higher (418 ng/ml and 1 125 ng/ml) for both protocols tested in the study with SDS and Triton (Figure 24). The method B.1 (1.2 % DNase) had the best outcome with an optimal DNA removal. Even though the use of 1.2 % DNase and

0.04 % DNase led to similar DNA removal, due to convenience of having the ECM-derived powders prepared with 1.2 % DNase in higher amount, the following tests were performed after this treatment.

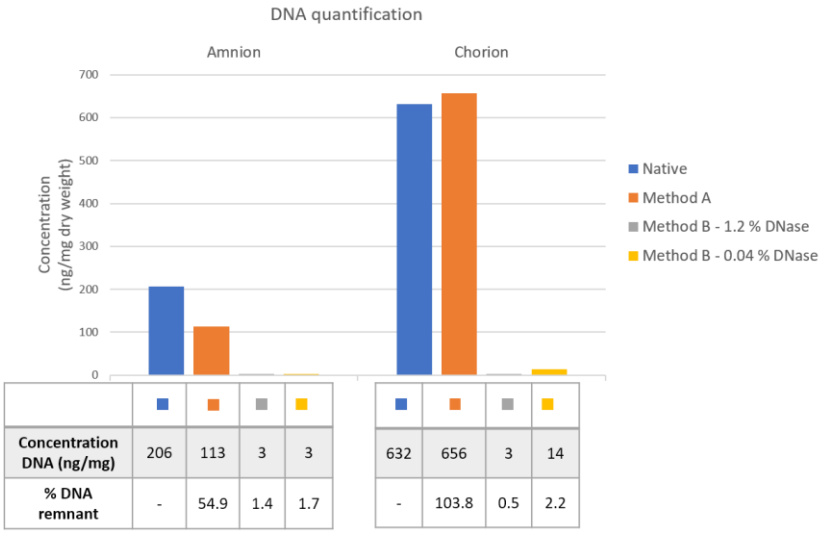


| | | | | | | | | |
|---|---|---|---|---|---|---|---|---|
| Concentration DNA (ng/mg) | 206 | 113 | 3 | 3 | 632 | 656 | 3 | 14 |
| % DNA remnant | - | 54.9 | 1.4 | 1.7 | - | 103.8 | 0.5 | 2.2 |

Figure 24 – DNA quantification of amnion and chorion for the three decellularization methods: A, B with 1.2 % DNase and B with 0.04 % DNase.

## 4.3.2 Hydrogel production and characterization

The incorporation of GO in the hydrogel was tested in two different stages of dECM hydrogel production: before and after digestion. When GO was added before digestion, it mixed at the same time as the ECM-derived powder, being the pepsin digestion performed afterwards.

The strain and frequency sweep tests allowed to determine the values in the linear viscoelastic (LVE) behavior for each hydrogel (Figure 25). The strain sweep test was performed with strains ranging from 0.1 to 100 % strain, with 1 Hz of frequency defined, for all conditions. For dECM, 1 % GO added before and after ECM digestion, a linear constant region was reached at 2 % of strain.

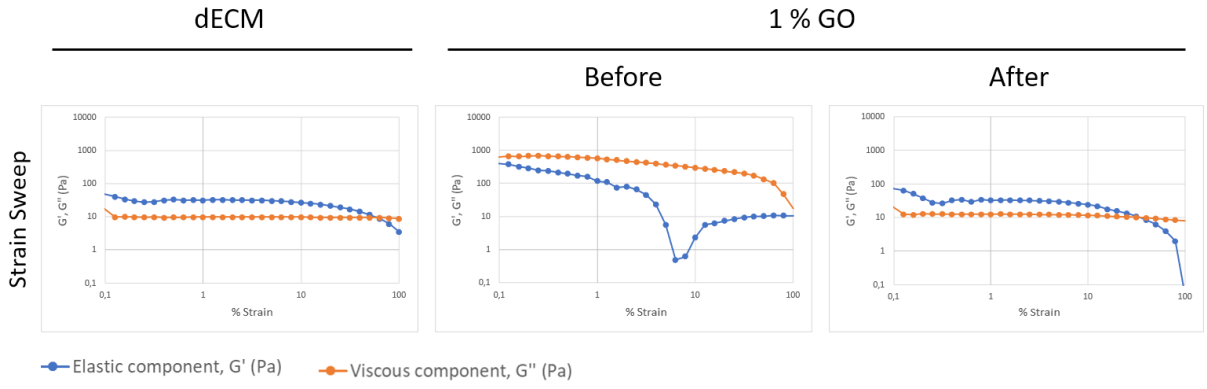


Figure 25 – Strain sweeps performed with optimal LVE (1 Hz) from 0.1 to 100 % of strain for dECM, 1 % GO added before and after digestion.

The frequency sweeps were performed in a range between 0.01 to 100 Hz in order to obtain the low frequency plateau, which allows the monitorization of the gel formation with small amplitude oscillatory shear (SAOS) (Figure 26). The value of the strain used in this test (2 % strain) was the one defined in the strain sweep tests performed previously (Table 3). The selected frequency was defined as 1 Hz for all conditions, representing a step where the G' values were constant.

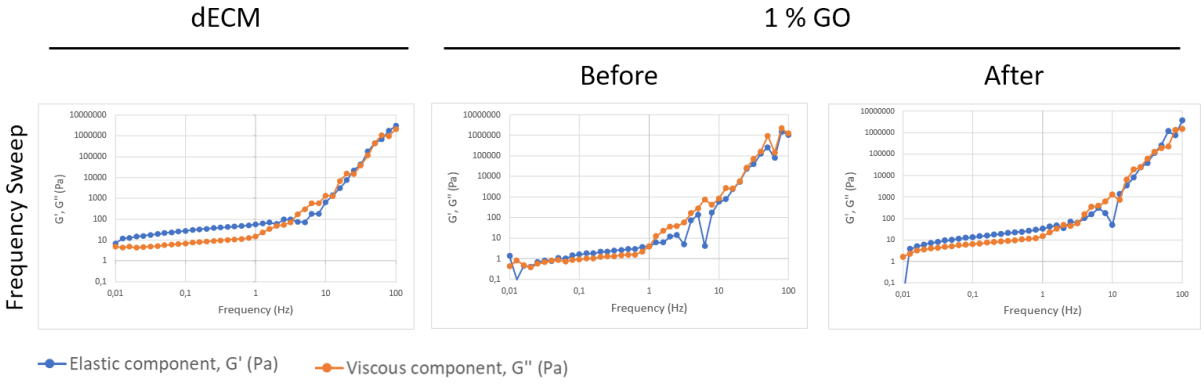


Figure 26 – Frequency sweeps performed with optimal LVE (2 % strain) from 0.01 to 100 Hz for dECM, 1 % GO added before and after digestion.

A time sweep was then performed with the previously determined strain and frequency optimal LVE values (Figure 27), showing that the resulting mechanical properties (elastic and viscous moduli) were overall higher when 1 % GO was added after digestion comparing to 1 % GO added before digestion. This may be explained since when GO is added during tissue digestion, it could react with the pepsin and hinder the correct digestion of the dECM matrix.

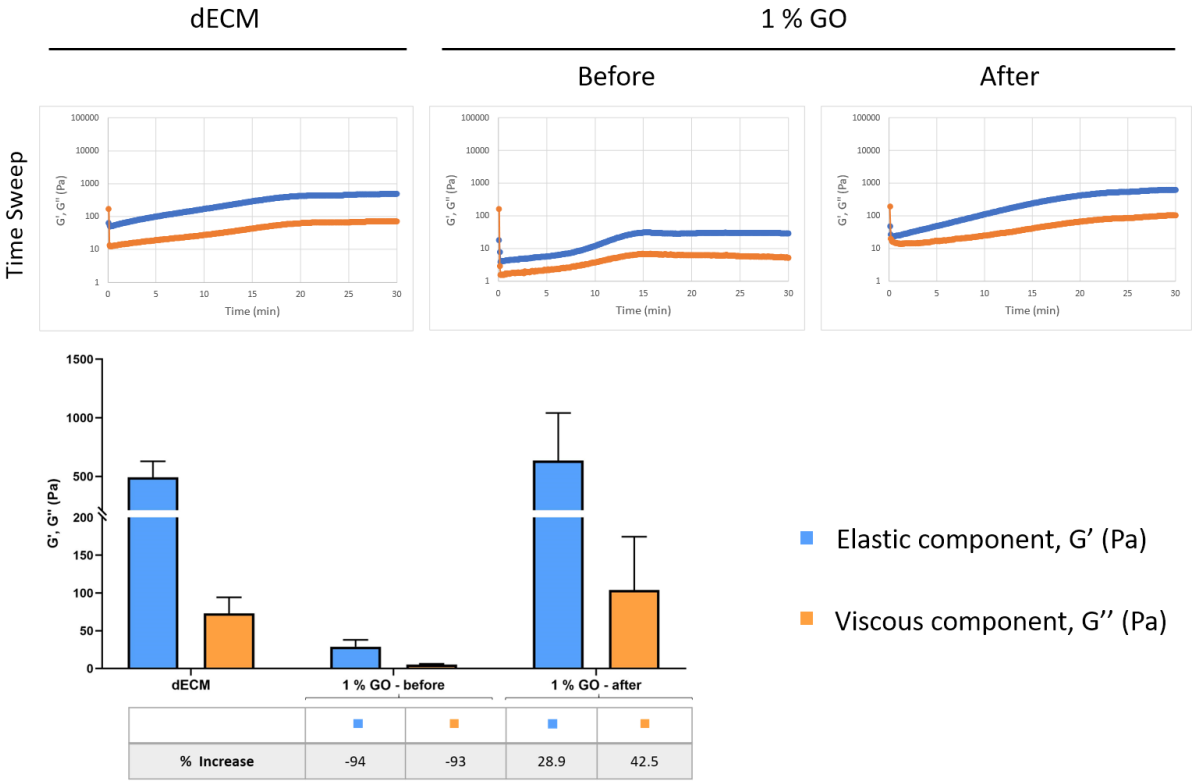


Figure 27 – Time Sweep and elastic component (G') and viscous component (G'') values after 30 min at 37 ºC for dECM, 1 % GO added before and after digestion. Percentage of increase relatively to dECM is presented in the table.

The rheological properties of the dECM hydrogels containing different amounts of GO incorporated after digestion, namely 1 % and 10 %, with or without sonication, were assessed. In a first instance the strain sweep between 0.1 – 100 % strain was also performed for all the conditions in order to determine a percentage of strain in the LVE region (Figure 28). For this test, the frequencies fixed were 1 Hz for untreated, untreated-sonicated, 1 % GO, 10 % GO and 10 % GO-sonicated and 1.5 Hz for 1 % GO-sonicated (Table 3). For all the conditions, except 10 % GO, a linear strain region was reached at 2 % of strain. For the 10 % GO sonicated and not sonicated, this was reached at 0.25 %. These strain values (2 % and 0.25 %) are used as optimal LVE, whereas adjusted LVE values of 1 % strain will be used to compare all materials subjected to the same strain. Moreover, once more, all conditions showed a steep drop in both elastic and viscous moduli after a certain yield strain. The value of percentage of strain before the steep drop is lower for the 10 % GO condition, which suggests that the material is easier to inject than the other conditions, theoretically.

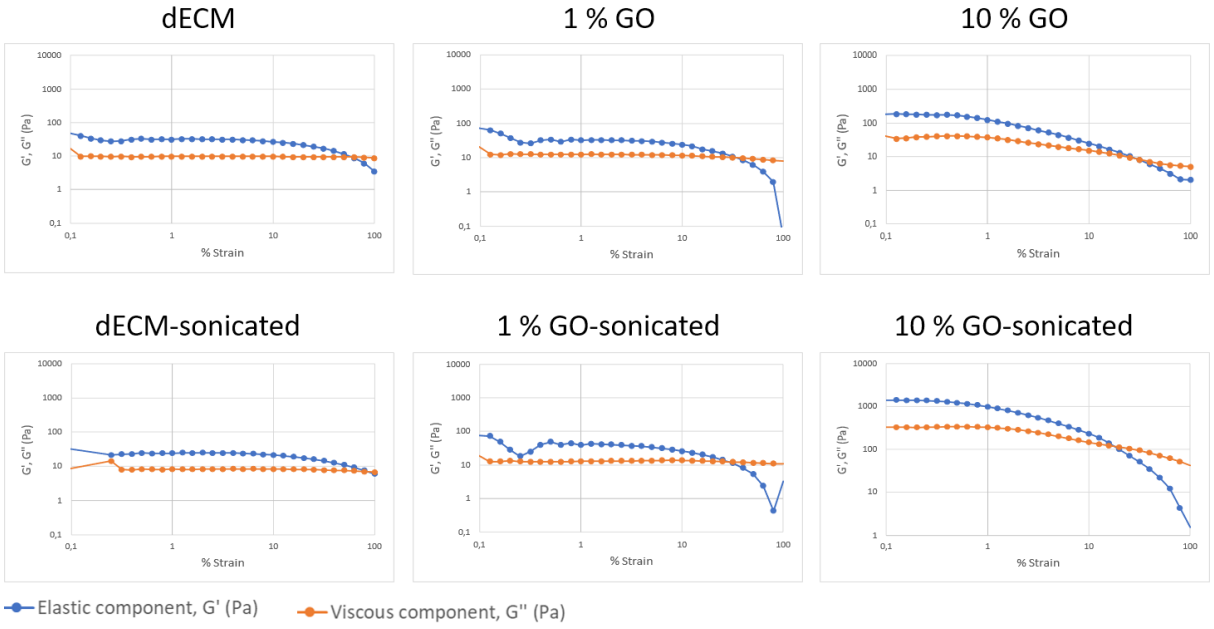


Figure 28 - Strain sweeps from 0.1 to 100 % of strain at 25 ºC, with optimal LVE values of frequency (Table 3) for all ECM-derived hydrogel conditions.

The frequency sweeps were performed again between 0.01 to 100 Hz with the value of the strain defined in Table 3. The selected optimal LVE frequency was defined as 1 Hz for all conditions except for 1 % GO-sonicated which was 1.5 Hz (Figure 29), being G' constant in these frequencies. When adjusted values are required to compare all materials, 1 Hz of frequency is used. Both conditions of 10 % GO: sonicated and not, have very low values of frequency in the plateau which leads to a more readily flow hydrogel, easier to inject [259].

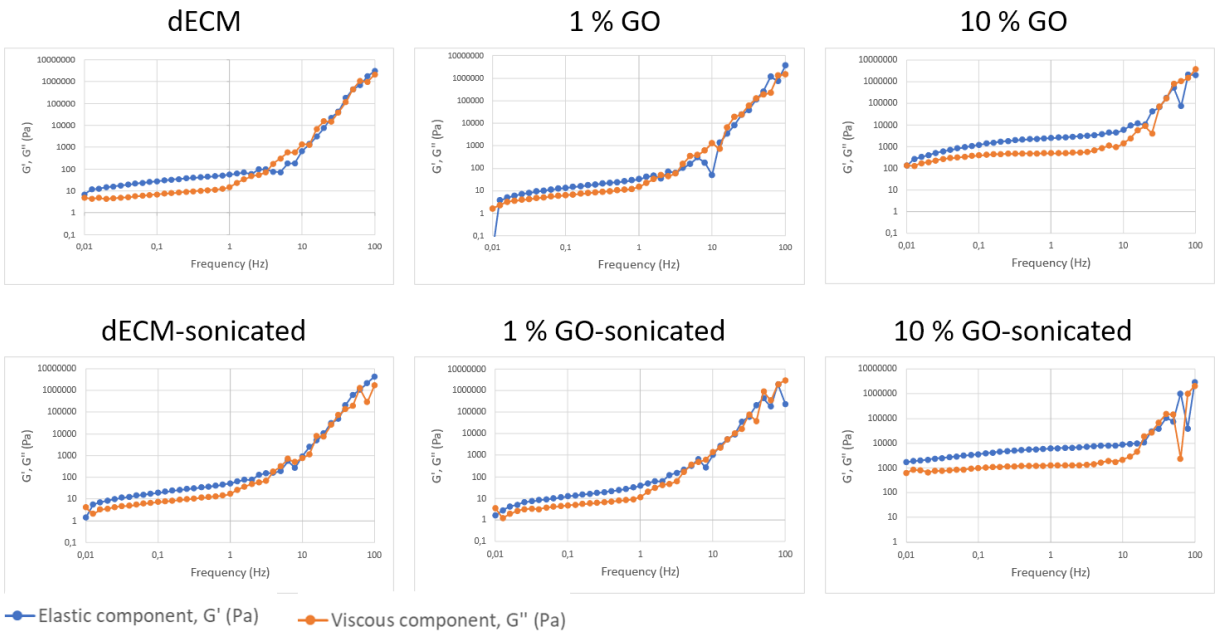


Figure 29 - Frequency sweeps from 0.01 to 100 Hz at 25 ºC, with optimal LVE values of strain (Table 3) for dECM with different concentrations of GO with or without sonication.

The time sweep with the optimal LVE values, allowed to assess elastic and viscous moduli of the ECM-derived hydrogels after being 30 minutes at 37 ºC. For all the conditions, after 30 minutes, the hydrogels behaved already as a solid-like material (Figure 30) since gelation (G' > G'') occurred after 15 sec. Moreover, the viscous (G') and elastic (G'') moduli were much higher for the 10 % condition not sonicated (16.52 kPa and 4.06 kPa) and sonicated (8.43 kPa and 1.88 kPa) comparing to the dECM without GO (0.49 kPa and 0.07 kPa), which results in an enhancement of the mechanical properties of the ECM-derived hydrogel (Figure 30).

Nevertheless, it is important to denote that when 10 % GO sonicated is compared to its control group, dECM-sonicated, the percentage of increase of G' (1889 %) and G'' (5940 %) were similar to the increase percentage obtained for 10% GO without sonication relatively to dECM (G' and G'' values of 2535 % and 5429 %). Hence, sonication is the process which is decreasing the viscous and elastic components of the obtained ECM-derived hydrogel.

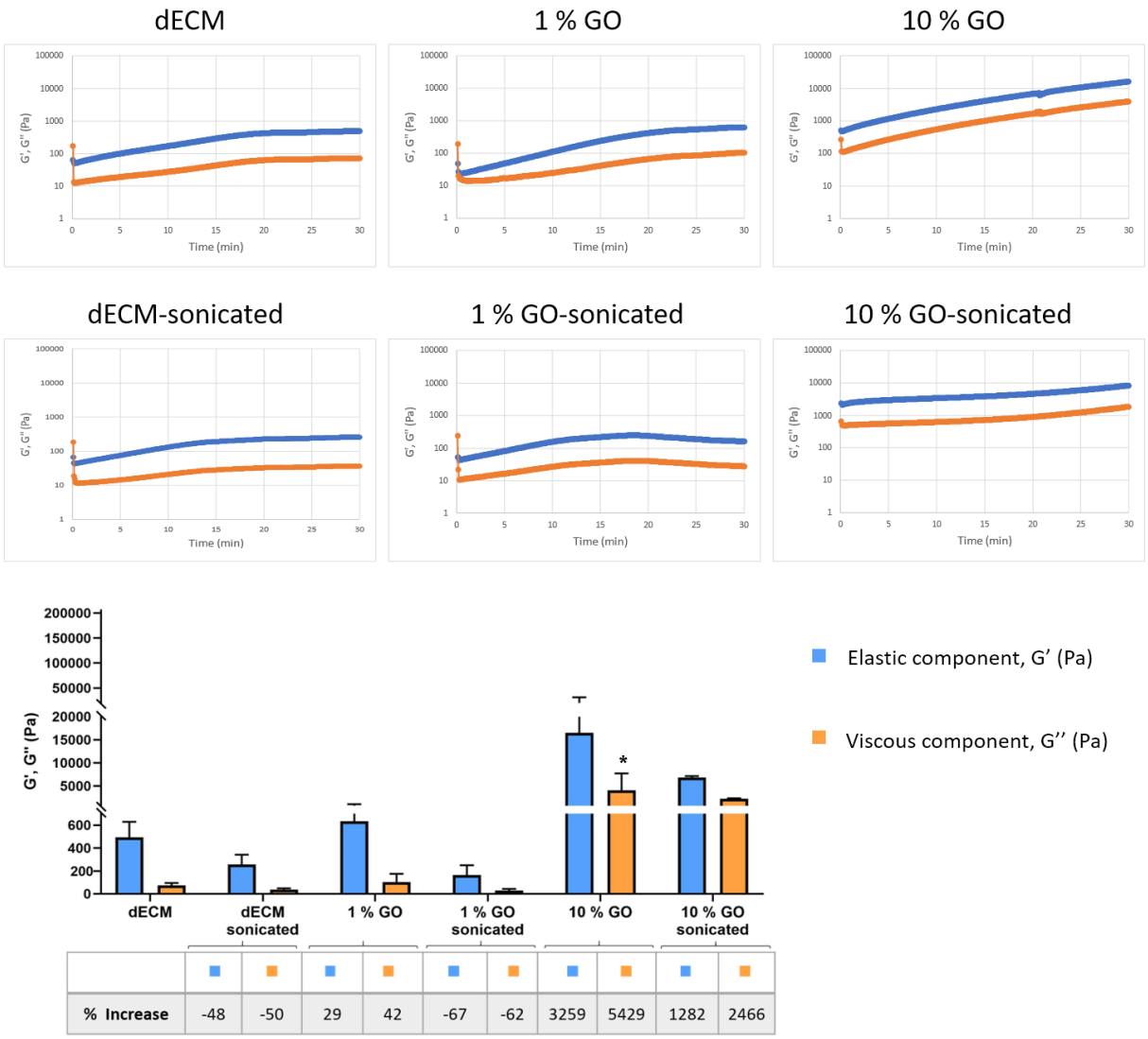


Figure 30 - Time sweeps and Elastic component (G') and viscous component (G'') values after 30 min at 37 ºC with the optimal LVE values from Table 3, for dECM with different concentrations of GO with or without sonication. Percentage of increase relatively to dECM is presented in the table. (One-Way ANOVA test, $p < 0.5$); n = 3.

In order to compare the different gelation times when hydrogels are submitted to the same strain and frequency, a general percentage of strain of 1 % and frequency of 1 Hz was defined (Figure 31). These values correspond to an adjusted linear phase for all the hydrogels. In a first instance, the time sweep with the adjusted LVE parameters allowed to assess the gelation of the hydrogels and then the final elastic and viscous moduli when put at 37 ºC for 30 minutes. For all the conditions except 10 % GO, the gelation time was almost instantaneous and the hydrogel, when put in 37 ºC, had a solid-like behavior (G' > G'') almost since the beginning (after 15 sec), which tended to increase. For the 10 % GO condition, the hydrogel had a solid-like behavior since the beginning of the sequence. This hydrogel behaved already as a solid-like material (Figure 31). An increase of the elastic component was observed for the 10 % GO not sonicated condition (1.50 kPa) as well as for 10 % GO sonicated (0.94 kPa) (Figure 31). These findings show a decrease of the G' and G'' components when tested with the adjusted LVE values: 1 Hz and 1 % strain, despite the trends are maintained. For all the

conditions, when the solution was not sonicated, it led to a higher improvement of the G' and G'' components.

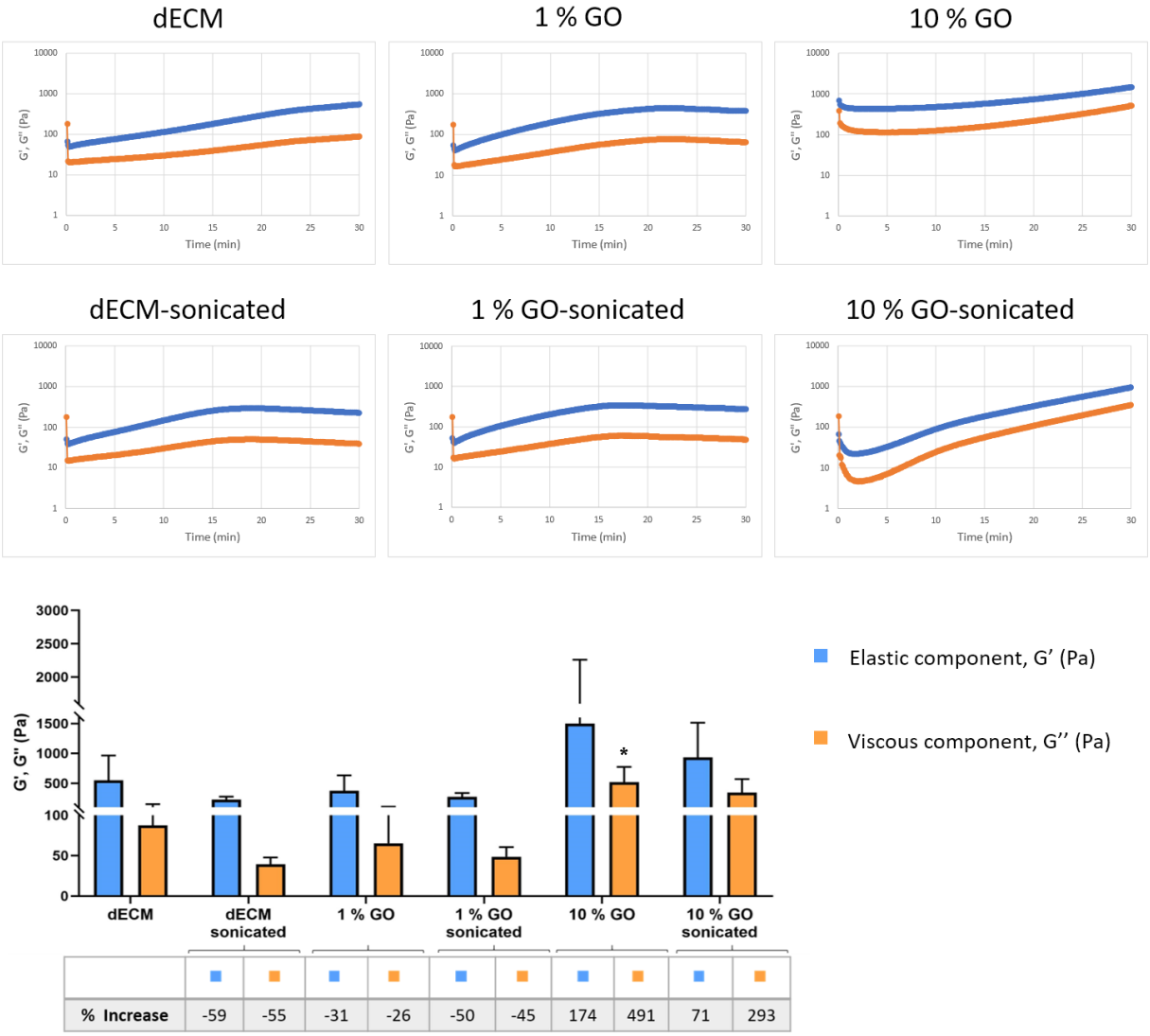


Figure 31 - Elastic component (G') and viscous component (G'') values after 30 min at 37 ºC with the adjusted LVE values from Table 3, for dECM with different concentrations of GO with or without sonication. Percentage of increase relatively to dECM is presented in the table. (One-Way ANOVA test, $p < 0.5$); n = 3.

Finally, the rheological characterization was also performed with 10 % GO after the gel storage for two weeks at 4 ºC and the different tests were compared to freshly prepared 10 % GO hydrogel. The strain and frequency values chosen were the same as for 10 % GO: 0.25 % of strain and 1 Hz (Figure 32).

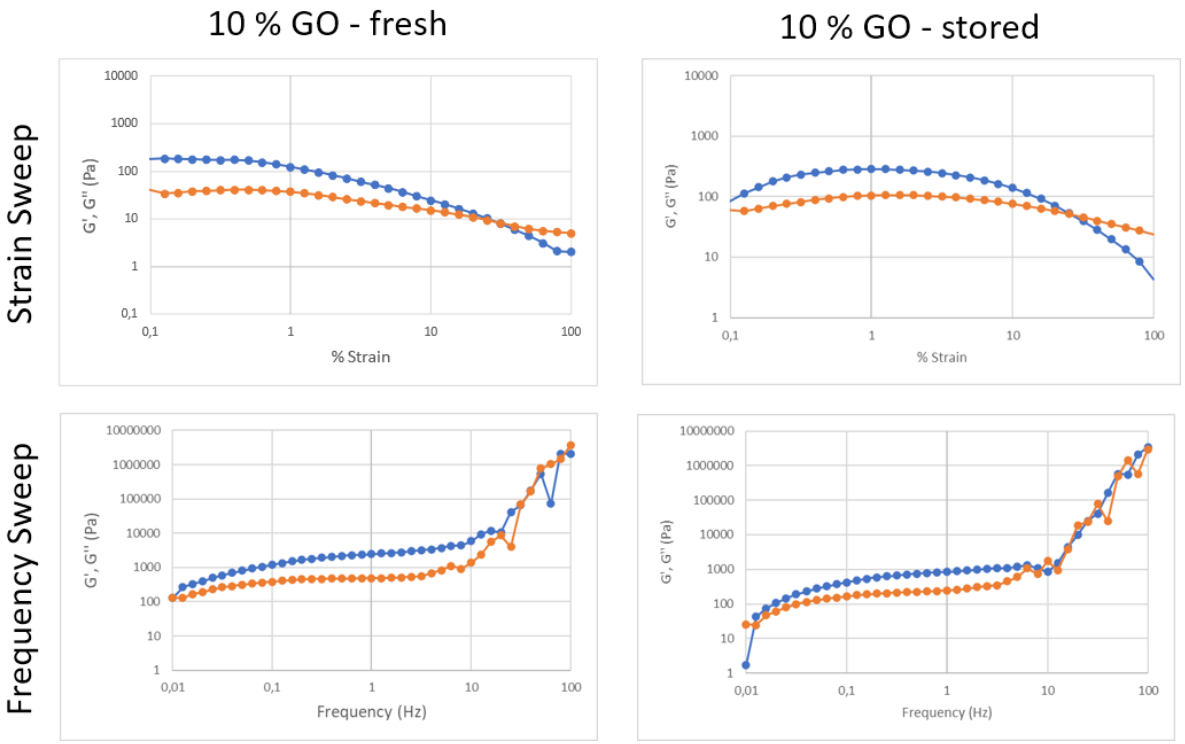


Figure 32 – Frequency and strain time sweeps performed for the 10 % GO hydrogels: fresh and stored for 2 weeks conditions.

An initial decrease in the mechanical properties for the time sweep was observed. This could be explained by some degradation/oxidation of ECM components, since hydrogels are preserved at 4 ºC inside of scintillation vials in a non-sterile environment. Nevertheless, after 30 min at 37 ºC, the G' and G'' for both, fresh (16.53 kPa and 4.06 kPa) and stored (8.63 kPa and 3.09 kPa) hydrogels tend to reach similar values (Figure 33).

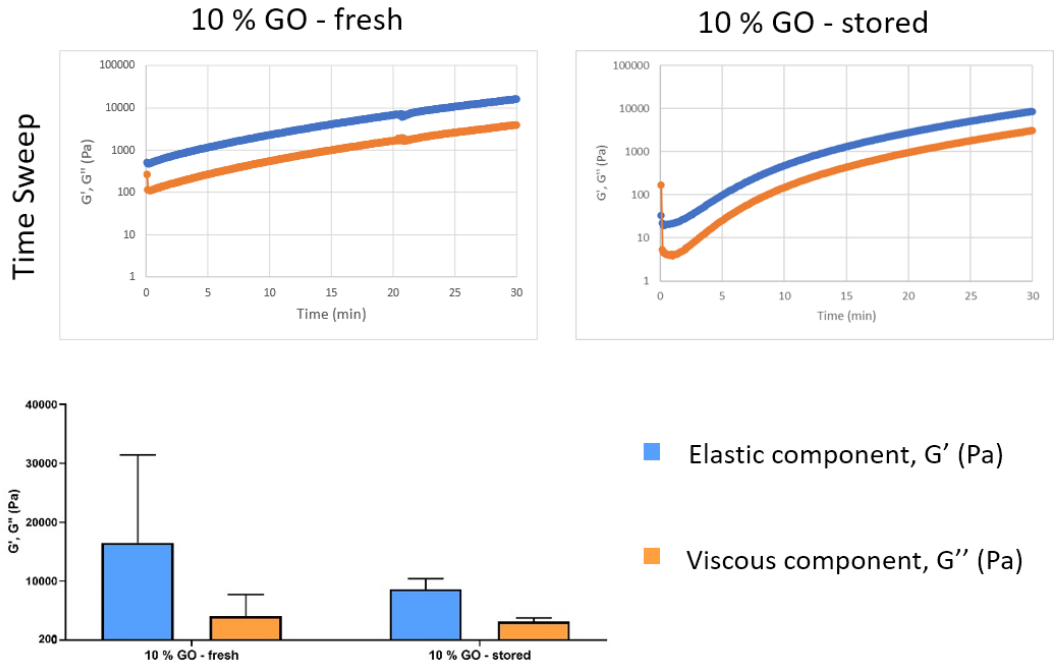


Figure 33 – Time Sweep with elastic component (G') and viscous component (G'') values after 30 min at 37 °C, for the 10 % GO hydrogels freshly prepared and stored for 2 weeks. Time sweep was performed with optimal LVE obtained from Figure 33 and described in Table 3.

## 4.4 Summary

In this second strategy, a successful decellularization method for placental membrane tissues were achieved by freeze/thaw cycle, following the combination of multiple cycles using 2 % Triton X-100 and rinsing, and the use of DNase at 1.2 % (Method B1) and 0.04 % (Method B2). For these two methods the percentage of DNA remnant was, for amnion, 1.4 % and 1.7 % DNA, respectively, and for chorion, 0.5 % and 2.2 %, respectively.

Two different concentrations of GO: 1 % and 10 % were homogeneously incorporated in chorion dECM-derived hydrogels. A significant mechanical reinforcement of 3259 % of elastic (G') and 5429 % of viscous moduli (G'') was observed upon incorporation of 10 % GO without sonication (values obtained using optimal LVE strain and frequency). When using adjusted LVE values, a reinforcement of 174 % (G') and 491 % (G'') was observed for the same 10 % GO concentration. Additionally, it was verified that both sonication and storage (for 2 weeks) decreased the mechanical resistance of the hydrogels, as well as hydrogel

This dissertation work showed that a reinforced ECM-derived hydrogel is obtained with the incorporation of 10 % GO after digestion of the dECM hydrogel, showing promising features to be used as an injectable hydrogel in future research.

# Chapter 5

# Discussion

Decellularization methods need to be optimized and adapted to each raw tissue. In this study, three tissues: umbilical cord arteries, placental amnion and chorion were decellularized using methods adapted from the literature. In order to decellularize umbilical cord arteries, freeze/thaw cycle, hypertonic/hypotonic solution, 1 % Triton X-100 with 0.02 % EDTA and DNase at 4 ºC were promoted [39]. Additionally, the sterilization was performed with peracetic acid and ethanol. The efficiency of this decellularization method was verified by DNA staining and quantification being since the remaining concentration of DNA was close to the minimal criteria of decellularization intent (50 ng/mg DNA), being 163 ng/mg [25]. Nevertheless, other strategies may be performed to further decrease these values and improve the decellularization efficiency, such as using higher concentration of Triton X-100 (e.g. 2 %) and of DNase (e.g. 1.2 %). Accordingly, the decellularization methods of the human placenta amnion and chorion tissues were verified with DNA quantification. For these tissues, two methods were tested. Method A was performed with cycles of 1 % SDS and 1 % Triton X-100 with EDTA. Method B was very similar to the one used for umbilical cord arteries with freeze/thaw cycles, hypertonic/hypotonic solutions. However, there were more cycles, 2 % Triton X-100 was used and DNase 0.04 % or 1.2 % was utilized. The results which better followed the minimal criteria previously mentioned was with method B with 1.2 % DNase, obtaining 3 ng/mg of DNA for both amnion and chorion tissues. Nonetheless, similar results were also obtained with method B with 0.04 % DNase, which can be an interesting option since much less DNase is spent to decellularize a given tissue.

The incorporation of different GBMs in the dArteries: GO, nGO and FLGO was done with perfusion, pressure or pressure following perfusion were tested, aiming to improve the mechanical properties of the decellularized arteries. All the conditions allowed the achievement of a homogeneous coverage of the exposed collagen fibers of the decellularized arteries. As said previously, the mechanical properties of the resulting grafts should match the burst pressure, compliance and strain values of the final recipient since when not respected, graft failure can occur [225, 230]. To have a comparison basis, the values should be compared to the gold standard vessels used: saphenous vein with 2134 mmHg) and internal thoracic artery with 3073 mmHg [12, 243, 244] . For the different conditions tested, none could attain an optimal value for the burst pressure value close to the gold standard vessels used. Nevertheless, a better compliance, higher than the compliance of ITA (11.5 %/100 mmHg) was reached for almost all the conditions: uncoated, GO-coated, nGO-coated and FLGO-coated. When submitted to pressure (uncoated pressure and nGO-pressure), the compliance was lower than the ITA values which may be explained since the pressure may have ruptured the elastin and collagen fibers.

Furthermore, the uncoated and coated dArteries were intended for use as SDVG. As such, a heparinization was needed to assure hemocompatibility if a pos-implantation endothelialization is

envisaged. Heparin is a well-known anticoagulant, used currently in the market [245]. The heparinized conditions were able to avoid clot formation when human recalcified plasma was added whereas the other conditions completely clotted.

The incorporation of GO in ECM-derived hydrogels was tested before and after tissue digestion. When GO was added after digestion, it led to a higher improvement in the mechanical properties. Furthermore, the mechanical properties of ECM-derived hydrogels with/without GO were also assessed with or without sonication, since it has been described that sonication allow a better dispersion of GBM particles in hydrogels matrices. However, our results pointed out that a better reinforcement was achieved when the hydrogels were not sonicated. This could be associated with some dECM protein denaturation or degradation that could occur during the sonication step. The viscous (G'') and elastic (G') components increased after being at 37 ºC for 30 minutes when 10 % GO concentration was added to the ECM-derived hydrogel. Moreover, for all of the conditions, the ECM-derived hydrogel had an almost instantaneous solid-like behavior (G'>G''). Normally, an ECM-derived hydrogel is mainly composed by collagen [260]. Hence, the G' values obtained in our study can be compared to the collagen hydrogel from Zuidema *et al* [259] where G' tended to 0.12 kPa after 30 minutes at 37 ºC. In our work, after 30 minutes at 37 ºC, the G' values were 0.49 kPa for dECM, 0.63 kPa for 1 % GO and 16.53 kPa for 10 % GO. These last values are much higher than the one obtained for the collagen derived hydrogel in [259].

Regarding the use of these reinforced ECM-derived hydrogels with GO, its use as SDVG may be challenging since despite the reinforcement they are still not very consistent, and their printing into the shape of a tubular conduit would be difficult. Nevertheless, these ECM-derived hydrogels could be used as a cell-laden construct combined with a polymeric framework such as polycaprolactone (PCL) as used in for bioprinting with extrusion in a syringe [71]. The principal criterion which needs to be assured is that the material needs to be easily injected by the nozzle with minimal shear force applied in order to avoid cell damage and reduce cell viability [261]. Moreover, the elastic component needs to be superior to the viscous moduli which was observed for all the hydrogels after being 30 minutes at 37 ºC. Another possible application is as injectable hydrogels which are widely reported in literature to promote tissue regeneration once it is possible to deliver them with minimally invasive techniques [246]. One of the possible approaches is to use the body temperature (37 ºC) to trigger the hydrogels gelation. However, the gelation process has to be well tuned, since an incorrect gelation time can lead to rapid material dispersion, when it takes too long [262], or to needle clogging before hydrogel injection, when it is too fast [263]. Their application in the regeneration of heart tissue upon myocardium infarction could be envisioned, since these hydrogels have high amounts of growth factors, pro-regenerative, pro-angiogenic, anti-scarring, anti-inflammatory, and stem cell-recruiting factors, and other ECM components such as collagen, laminin and fibronectin [101]. In this strategy, the incorporation of GO in ECM-derived hydrogels could also be used for its antimicrobial properties [16].

# Chapter 6

# Conclusions and Future Work

## 6.1 Conclusions

Literature review allowed to conclude that the decellularization processes begins with membrane disruption and weakening of cell adhesion (physical and chemical processes), followed by DNA hydrolysis (biological). The protocols used need to be adapted to the native tissue since there is no optimal decellularization method. Nevertheless, upon decellularization process, the resulting matrices observe a decrease in their mechanical properties. Thus, it is important to tune these characteristics of dECM to obtain a performance similar to that of the original tissue. One of the strategies to improve these properties is the incorporation of GBMs. In the few studies where GBM was incorporated in dECM, an increase of the mechanical properties in 2-60 % was observed.

In this study, umbilical cord arteries, placental amnion and chorion were decellularized efficiently being obtained a DNA removal of 91.5 %, 98.6 % and 99.5 %, respectively.

The incorporation of the GBM in the dArteries was successfully performed, covering the exposed collagen fibers of the dArteries. Despite the coating did not increase the mechanical properties, the uncoated, GO-coated, nGO-coated and FLGO-coated decellularized arteries exhibited a higher compliance than the internal thoracic artery that is used for coronary bypass grafting. Regarding hemocompatibility, even though coating with GBM decreased the collagen exposure, when recalcified human plasma was added to uncoated and GO-coated vessels, a clot formation occurred. The heparinization of the dArteries, both uncoated and GO-coated, allowed the enhancement of their hemocompatibility by avoiding the clot formation.

Regarding the ECM-derived hydrogels, after 30 min at 37 ºC, the incorporation of 10 % GO was able to increase the elastic component (G') values by 174 % when the adjusted LVE values (1 Hz and 1 % strain) were used, and by 3259 % when the optimal LVE values (1 Hz and 0.25 % strain) were used, reaching values of 1.50 kPa and 16.52 kPa, respectively. GBM incorporation in ECM-derived hydrogels revealed to be a promising approach to increase their mechanical properties enabling its use as bioprinted hydrogels with tubular geometry or as injectable hydrogels with antimicrobial properties.

## 6.2 Future Work

For future work in GBM-coated dArteries, the GBM incorporation in dArteries still needs to be optimized in order to increase the mechanical properties allowing their use as small diameter vascular grafts. For that, another possible coating may be attempted with rGO or a covalent link between dECM and GBM performed as strategies to enhance the mechanical reinforcement with GBM. The

hemocompatibility of heparinized dArteries should be verified and tested *in vitro* and *in vivo*. Moreover, the preservation of the ECM components could be evaluated by GAGs and collagen quantification using 1,9-dimethylmethylene blue solution and hydroxyproline assay, respectively. To further verify collagen preservation, Masson's trichrome staining or immunohistochemical staining with monoclonal antibodies against elastin, fibronectin, collagen I, collagen IV, EVG, and Van Kossa may be performed.

Additionally, in terms of the ECM-derived hydrogel, further studies may be performed in order to assess the incorporation of GO in the matrix, namely by evaluation of surface topography, GBM distribution in matrix and swelling capacity. The remaining GAGs and collagen presence in the hydrogel should be quantified, after decellularization. The cytotoxicity of the ECM-derived hydrogel containing different concentrations of GO should be assessed by its incubation with, for example, endothelial cells. Moreover, other concentrations of GO should be tested to ensure optimal mechanical reinforcement and handling. Rheological properties of the reinforced ECM-derived hydrogels should be performed upon gelation. Finally, hemocompatibility of the resulting GBM-reinforced ECM-derived hydrogel should be assessed with a coagulation test.

# References


1. Chambless, L., et al., *Population versus clinical view of case fatality from acute coronary heart disease: results from the WHO MONICA Project 1985-1990. Multinational MONItoring of Trends and Determinants in CArdiovascular Disease.* Circulation, 1997. **96**(11): p. 3849-59.
2. Lu, L., et al., *Myocardial Infarction: Symptoms and Treatments.* Cell Biochem Biophys, 2015. **72**(3): p. 865-7.
3. *Oral Health-Related Quality of Life*. 2020.
4. Bergmeister, H., et al., *Tissue engineering of vascular grafts.* European Surgery, 2013. **45**: p. 187-193.
5. Caliskan, E., et al., *Saphenous vein grafts in contemporary coronary artery bypass graft surgery.* Nat Rev Cardiol, 2020. **17**(3): p. 155-169.
6. Kimicata, M., P. Swamykumar, and J.P. Fisher, *Extracellular Matrix for Small-Diameter Vascular Grafts.* Tissue Engineering Part A, 2020. **26**(23-24): p. 1388-1401.
7. Hiob, M.A., et al., *Biomaterials and Modifications in the Development of Small-Diameter Vascular Grafts.* ACS Biomaterials Science & Engineering, 2017. **3**(5): p. 712-723.
8. Elliott, M.B., et al., *Regenerative and durable small-diameter graft as an arterial conduit.* Proceedings of the National Academy of Sciences, 2019. **116**(26): p. 12710.
9. Boccafoschi, F., et al., *Preparation and characterization of a scaffold for vascular tissue engineering by direct-assembling of collagen and cells in a cylindrical geometry.* Macromol Biosci, 2007. **7**(5): p. 719-26.
10. Hoganson, D.M., et al., *The retention of extracellular matrix proteins and angiogenic and mitogenic cytokines in a decellularized porcine dermis.* Biomaterials, 2010. **31**(26): p. 6730-7.
11. Lei, P., H. You, and S.T. Andreadis, *Bioengineered skin substitutes.* Methods Mol Biol, 2013. **1001**: p. 267-78.
12. Pashneh-Tala, S., S. MacNeil, and F. Claeyssens, *The Tissue-Engineered Vascular Graft-Past, Present, and Future.* Tissue Engineering Part B-Reviews, 2016. **22**(1): p. 68-100.
13. Schneider, K.H., et al., *Decellularized human placenta chorion matrix as a favorable source of small-diameter vascular grafts.* Acta Biomater, 2016. **29**: p. 125-134.
14. Lin, C.H., et al., *In Vivo Performance of Decellularized Vascular Grafts: A Review Article.* International Journal of Molecular Sciences, 2018. **19**(7).
15. Papageorgiou, D.G., I.A. Kinloch, and R.J. Young, *Mechanical properties of graphene and graphene-based nanocomposites.* Progress in Materials Science, 2017. **90**: p. 75-127.
16. Henriques, P.C., et al., *Fabrication and antimicrobial performance of surfaces integrating graphene-based materials.* Carbon, 2018. **132**: p. 709-732.
17. Gomes, R.N., et al., *Antimicrobial graphene nanoplatelets coatings for silicone catheters.* Carbon, 2018. **139**: p. 635-647.
18. Allaire, E., et al., *The immunogenicity of the extracellular matrix in arterial xenografts.* Surgery, 1997. **122**(1): p. 73-81.
19. *Partos nos hospitais: total e por tipo.*
20. Manabe, R., et al., *Transcriptome-based systematic identification of extracellular matrix proteins.* Proc Natl Acad Sci U S A, 2008. **105**(35): p. 12849-54.

21. Sellaro, T.L., et al., *Maintenance of hepatic sinusoidal endothelial cell phenotype in vitro using organ-specific extracellular matrix scaffolds.* Tissue Eng, 2007. **13**(9): p. 2301-10.
22. Giancotti, F.G. and E. Ruoslahti, *Integrin signaling.* Science, 1999. **285**(5430): p. 1028-32.
23. Adachi, E., I. Hopkinson, and T. Hayashi, *Basement-membrane stromal relationships: interactions between collagen fibrils and the lamina densa.* Int Rev Cytol, 1997. **173**: p. 73-156.
24. Keane, T.J., I.T. Swinehart, and S.F. Badylak, *Methods of tissue decellularization used for preparation of biologic scaffolds and in vivo relevance.* Methods, 2015. **84**: p. 25-34.
25. Crapo, P.M., T.W. Gilbert, and S.F. Badylak, *An overview of tissue and whole organ decellularization processes.* Biomaterials, 2011. **32**(12): p. 3233-3243.
26. Heath, D.E., *A Review of Decellularized Extracellular Matrix Biomaterials for Regenerative Engineering Applications.* Regenerative Engineering and Translational Medicine, 2019. **5**(2): p. 155-166.
27. Lin, C.H., et al., *An investigation on the correlation between the mechanical property change and the alterations in composition and microstructure of a porcine vascular tissue underwent trypsin-based decellularization treatment.* J Mech Behav Biomed Mater, 2018. **86**: p. 199-207.
28. Rahman, S., et al., *Optimising the decellularization of human elastic cartilage with trypsin for future use in ear reconstruction.* Sci Rep, 2018. **8**(1): p. 3097.
29. Sánchez, J.C., et al., *Decellularization and In Vivo Recellularization of Abdominal Porcine Fascial Tissue.* Tissue Eng Regen Med, 2020.
30. Leonel, L., et al., *Decellularization of placentas: establishing a protocol.* Braz J Med Biol Res, 2017. **51**(1): p. e6382.
31. Bakhtiar, H., et al., *Optimizing Methods for Bovine Dental Pulp Decellularization.* J Endod, 2021. **47**(1): p. 62-68.
32. Chen, R.N., et al., *Process development of an acellular dermal matrix (ADM) for biomedical applications.* Biomaterials, 2004. **25**(13): p. 2679-86.
33. Stenn, K.S., et al., *Dispase, a neutral protease from Bacillus polymyxa, is a powerful fibronectinase and type IV collagenase.* J Invest Dermatol, 1989. **93**(2): p. 287-90.
34. Gubareva, E., et al., *Non-human primate oesophagus decellularization.* Genes and Cells, 2014. **9**: p. 64-69.
35. Mendoza-Novelo, B., et al., *Decellularization of pericardial tissue and its impact on tensile viscoelasticity and glycosaminoglycan content.* Acta Biomaterialia, 2011. **7**(3): p. 1241-1248.
36. Liao, J., E.M. Joyce, and M.S. Sacks, *Effects of decellularization on the mechanical and structural properties of the porcine aortic valve leaflet.* Biomaterials, 2008. **29**(8): p. 1065-1074.
37. Pan, M.X., et al., *An efficient method for decellularization of the rat liver.* Journal of the Formosan Medical Association = Taiwan yi zhi, 2014. **113**(10): p. 680-687.
38. Zheng, Z.W., et al., *Development of an Accurate and Proactive Immunomodulatory Strategy to Improve Bone Substitute Material-Mediated Osteogenesis and Angiogenesis.* Theranostics, 2018. **8**(19): p. 5482-5500.
39. Schneider, K.H., et al., *Acellular vascular matrix grafts from human placenta chorion: Impact of ECM preservation on graft characteristics, protein composition and in vivo performance.* Biomaterials, 2018. **177**: p. 14-26.
40. Grauss, R.W., et al., *Histological evaluation of decellularised porcine aortic valves: matrix changes due to different decellularisation methods☆.* European Journal of Cardio-Thoracic Surgery, 2005. **27**(4): p. 566-571.
41. Syed, O., et al., *Evaluation of decellularization protocols for production of tubular small intestine submucosa scaffolds for use in oesophageal tissue engineering.* Acta Biomaterialia, 2014. **10**(12): p. 5043-5054.
42. Poornejad, N., et al., *The impact of decellularization agents on renal tissue extracellular matrix.* 2016. **31**(4): p. 521-533.
43. Gilbert, T.W., et al., *Collagen fiber alignment and biaxial mechanical behavior of porcine urinary bladder derived extracellular matrix.* Biomaterials, 2008. **29**(36): p. 4775-4782.
44. Hodde, J. and M. Hiles, *Virus safety of a porcine-derived medical device: Evaluation of a viral inactivation method.* 2002. **79**(2): p. 211-216.

45. Flynn, L.E., *The use of decellularized adipose tissue to provide an inductive microenvironment for the adipogenic differentiation of human adipose-derived stem cells.* Biomaterials, 2010. **31**(17): p. 4715-4724.
46. Brown, B.N., et al., *Comparison of three methods for the derivation of a biologic scaffold composed of adipose tissue extracellular matrix.* Tissue Eng Part C Methods, 2011. **17**(4): p. 411-21.
47. Lumpkins, S.B., N. Pierre, and P.S. McFetridge, *A mechanical evaluation of three decellularization methods in the design of a xenogeneic scaffold for tissue engineering the temporomandibular joint disc.* Acta Biomaterialia, 2008. **4**(4): p. 808-816.
48. Levy, R.J., et al., *Inhibition of cusp and aortic wall calcification in ethanol- and aluminum-treated bioprosthetic heart valves in sheep: background, mechanisms, and synergism.* J Heart Valve Dis, 2003. **12**(2): p. 209-16; discussion 216.
49. Srinivasan, M., D. Sedmak, and S. Jewell, *Effect of fixatives and tissue processing on the content and integrity of nucleic acids.* Am J Pathol, 2002. **161**(6): p. 1961-71.
50. Xu, C.C., R.W. Chan, and N. Tirunagari, *A biodegradable, acellular xenogeneic scaffold for regeneration of the vocal fold lamina propria.* Tissue Eng, 2007. **13**(3): p. 551-66.
51. Reing, J.E., et al., *The effects of processing methods upon mechanical and biologic properties of porcine dermal extracellular matrix scaffolds.* Biomaterials, 2010. **31**(33): p. 8626-8633.
52. Prasertsung, I., et al., *Development of acellular dermis from porcine skin using periodic pressurized technique.* 2008. **85B**(1): p. 210-219.
53. Gorschewsky, O., et al., *Quantitative analysis of biochemical characteristics of bone-patellar tendon-bone allografts.* Biomed Mater Eng, 2005. **15**(6): p. 403-11.
54. He, M. and A. Callanan, *Comparison of methods for whole-organ decellularization in tissue engineering of bioartificial organs.* Tissue engineering. Part B, Reviews, 2013. **19**(3): p. 194-208.
55. Rieder, E., et al., *Decellularization protocols of porcine heart valves differ importantly in efficiency of cell removal and susceptibility of the matrix to recellularization with human vascular cells.* J Thorac Cardiovasc Surg, 2004. **127**(2): p. 399-405.
56. Zhou, J., et al., *Impact of heart valve decellularization on 3-D ultrastructure, immunogenicity and thrombogenicity.* Biomaterials, 2010. **31**(9): p. 2549-2554.
57. Petersen, T.H., et al., *Matrix Composition and Mechanics of Decellularized Lung Scaffolds.* Cells Tissues Organs, 2012. **195**(3): p. 222-231.
58. Nakayama, K.H., et al., *Decellularized rhesus monkey kidney as a three-dimensional scaffold for renal tissue engineering.* Tissue Eng Part A, 2010. **16**(7): p. 2207-16.
59. Meyer, S.R., et al., *Comparison of aortic valve allograft decellularization techniques in the rat.* 2006. **79A**(2): p. 254-262.
60. White, L.J., et al., *The impact of detergents on the tissue decellularization process: A ToF-SIMS study.* Acta Biomaterialia, 2017. **50**: p. 207-219.
61. Cartmell, J.S. and M.G. Dunn, *Effect of chemical treatments on tendon cellularity and mechanical properties.* 2000. **49**(1): p. 134-140.
62. Uygun, B.E., et al., *Organ reengineering through development of a transplantable recellularized liver graft using decellularized liver matrix.* Nature Medicine, 2010. **16**(7): p. 814-820.
63. Vavken, P., S. Joshi, and M.M. Murray, *TRITON-X is most effective among three decellularization agents for ACL tissue engineering.* 2009. **27**(12): p. 1612-1618.
64. Choi, J.S., et al., *Bioengineering endothelialized neo-corneas using donor-derived corneal endothelial cells and decellularized corneal stroma.* Biomaterials, 2010. **31**(26): p. 6738-6745.
65. Fernández-Pérez, J. and M. Ahearne, *The impact of decellularization methods on extracellular matrix derived hydrogels.* Scientific Reports, 2019. **9**(1): p. 14933.
66. Lynch, A.P., S.L. Wilson, and M. Ahearne, *Dextran Preserves Native Corneal Structure During Decellularization.* Tissue Eng Part C Methods, 2016. **22**(6): p. 561-72.
67. Gonzalez-Andrades, M., et al., *Generation of bioengineered corneas with decellularized xenografts and human keratocytes.* Invest Ophthalmol Vis Sci, 2011. **52**(1): p. 215-22.

68. Pang, K., L. Du, and X. Wu, *A rabbit anterior cornea replacement derived from acellular porcine cornea matrix, epithelial cells and keratocytes.* Biomaterials, 2010. **31**(28): p. 7257-65.
69. Sasaki, S., et al., *In vivo evaluation of a novel scaffold for artificial corneas prepared by using ultrahigh hydrostatic pressure to decellularize porcine corneas.* Mol Vis, 2009. **15**: p. 2022-8.
70. Elder, B.D., S.V. Eleswarapu, and K.A. Athanasiou, *Extraction techniques for the decellularization of tissue engineered articular cartilage constructs.* Biomaterials, 2009. **30**(22): p. 3749-56.
71. Pati, F., et al., *Printing three-dimensional tissue analogues with decellularized extracellular matrix bioink.* Nat Commun, 2014. **5**: p. 3935.
72. Gratzer, P.F., R.D. Harrison, and T. Woods, *Matrix alteration and not residual sodium dodecyl sulfate cytotoxicity affects the cellular repopulation of a decellularized matrix.* Tissue Eng, 2006. **12**(10): p. 2975-83.
73. O'Neill, J.D., et al., *Decellularization of human and porcine lung tissues for pulmonary tissue engineering.* Ann Thorac Surg, 2013. **96**(3): p. 1046-55; discussion 1055-6.
74. Cebotari, S., et al., *Detergent Decellularization of Heart Valves for Tissue Engineering: Toxicological Effects of Residual Detergents on Human Endothelial Cells.* 2010. **34**(3): p. 206-210.
75. Nonaka, P.N., et al., *Effects of freezing/thawing on the mechanical properties of decellularized lungs.* 2014. **102**(2): p. 413-419.
76. Dahl, S.L., et al., *Decellularized native and engineered arterial scaffolds for transplantation.* Cell Transplant, 2003. **12**(6): p. 659-66.
77. Cox, B. and A. Emili, *Tissue subcellular fractionation and protein extraction for use in mass-spectrometry-based proteomics.* Nature Protocols, 2006. **1**(4): p. 1872-1878.
78. Bhattacharya, S., *Cryoprotectants and Their Usage in Cryopreservation Process*. 2018: IntechOpen.
79. Pulver, A., et al., *Production of Organ Extracellular Matrix Using a Freeze-thaw Cycle Employing Extracellular Cryoprotectants.* Cryo letters, 2014. **35**: p. 400-406.
80. Huang, H., et al., *Effects of repetitive multiple freeze-thaw cycles on the biomechanical properties of human flexor digitorum superficialis and flexor pollicis longus tendons.* Clin Biomech (Bristol, Avon), 2011. **26**(4): p. 419-23.
81. Yang, B., et al., *Development of a porcine bladder acellular matrix with well-preserved extracellular bioactive factors for tissue engineering.* Tissue Eng Part C Methods, 2010. **16**(5): p. 1201-11.
82. Keane, T.J., et al., *Preparation and characterization of a biologic scaffold and hydrogel derived from colonic mucosa*. 2017. **105**(2): p. 291-306.
83. Baiguera, S., et al., *Tissue engineered human tracheas for in vivo implantation.* Biomaterials, 2010. **31**(34): p. 8931-8938.
84. Montoya, C.V. and P.S. McFetridge, *Preparation of ex vivo-based biomaterials using convective flow decellularization.* Tissue Eng Part C Methods, 2009. **15**(2): p. 191-200.
85. Karabekmez, F.E., A. Duymaz, and S.L. Moran, *Early clinical outcomes with the use of decellularized nerve allograft for repair of sensory defects within the hand.* Hand (N Y), 2009. **4**(3): p. 245-9.
86. Remlinger, N.T., et al., *Hydrated xenogeneic decellularized tracheal matrix as a scaffold for tracheal reconstruction.* Biomaterials, 2010. **31**(13): p. 3520-3526.
87. Stern, M.M., et al., *The influence of extracellular matrix derived from skeletal muscle tissue on the proliferation and differentiation of myogenic progenitor cells ex vivo.* Biomaterials, 2009. **30**(12): p. 2393-2399.
88. Keane, T.J., et al., *Preparation and characterization of a biologic scaffold from esophageal mucosa.* Biomaterials, 2013. **34**(28): p. 6729-6737.
89. Bolland, F., et al., *Development and characterisation of a full-thickness acellular porcine bladder matrix for tissue engineering.* Biomaterials, 2007. **28**(6): p. 1061-1070.
90. Funamoto, S., et al., *The use of high-hydrostatic pressure treatment to decellularize blood vessels.* Biomaterials, 2010. **31**(13): p. 3590-3595.
91. Zambon, A., et al., *Dry acellular oesophageal matrix prepared by supercritical carbon dioxide.* The Journal of Supercritical Fluids, 2016. **115**: p. 33-41.

92. Sawada, K., et al., *Cell removal with supercritical carbon dioxide for acellular artificial tissue*. 2008. **83**(6): p. 943-949.
93. Casali, D.M., et al., *A novel supercritical CO2-based decellularization method for maintaining scaffold hydration and mechanical properties*. The Journal of Supercritical Fluids, 2018. **131**: p. 72-81.
94. Guler, S., et al., *Supercritical Carbon Dioxide-Assisted Decellularization of Aorta and Cornea*. Tissue Eng Part C Methods, 2017. **23**(9): p. 540-547.
95. Chen, Y., et al., *Current advances in the development of natural meniscus scaffolds: innovative approaches to decellularization and recellularization*. Cell and Tissue Research, 2017. **370**(1): p. 41-52.
96. Mao, Y. and J.E. Schwarzbauer, *Stimulatory effects of a three-dimensional microenvironment on cell-mediated fibronectin fibrillogenesis*. J Cell Sci, 2005. **118**(Pt 19): p. 4427-36.
97. Simsa, R., et al., *Systematic in vitro comparison of decellularization protocols for blood vessels*. PLoS One, 2018. **13**(12): p. e0209269.
98. Cornwell, K.G., A. Landsman, and K.S. James, *Extracellular matrix biomaterials for soft tissue repair*. Clin Podiatr Med Surg, 2009. **26**(4): p. 507-23.
99. Hao, Y., et al., *Identification of antiangiogenic and antiinflammatory proteins in human amniotic membrane*. Cornea, 2000. **19**(3): p. 348-52.
100. Tseng, S.C., D.Q. Li, and X. Ma, *Suppression of transforming growth factor-beta isoforms, TGF-beta receptor type II, and myofibroblast differentiation in cultured human corneal and limbal fibroblasts by amniotic membrane matrix*. J Cell Physiol, 1999. **179**(3): p. 325-35.
101. Francis, M.P., et al., *Human placenta hydrogel reduces scarring in a rat model of cardiac ischemia and enhances cardiomyocyte and stem cell cultures*. Acta Biomaterialia, 2017. **52**: p. 92-104.
102. Duplock, E.J., M. Scheffler, and P.J.D. Lindan, *Hallmark of Perfect Graphene*. Physical Review Letters, 2004. **92**(22): p. 225502.
103. Sheehy, D.E. and J. Schmalian, *Optical transparency of graphene as determined by the fine-structure constant*. Physical Review B, 2009. **80**(19): p. 193411.
104. Dreyer, D.R., et al., *The chemistry of graphene oxide*. Chemical Society Reviews, 2010. **39**(1): p. 228-240.
105. Lukowiak, A., A. Kedziora, and W. Strek, *Antimicrobial graphene family materials: Progress, advances, hopes and fears*. Adv Colloid Interface Sci, 2016. **236**: p. 101-12.
106. Wick, P., et al., *Classification Framework for Graphene-Based Materials*. 2014. **53**(30): p. 7714-7718.
107. Barbolina, I., et al., *Purity of graphene oxide determines its antibacterial activity*. 2D Materials, 2016. **3**: p. 025025.
108. Kovtyukhova, N., et al., *Layer-by-Layer Assembly of Ultrathin Composite Films from Micron-Sized Graphite Oxide Sheets and Polycations*. 1999. **11**: p. 771-778.
109. Liu, J., J. Tang, and J.J. Gooding, *Strategies for chemical modification of graphene and applications of chemically modified graphene*. Journal of Materials Chemistry, 2012. **22**(25): p. 12435-12452.
110. Choi, W., et al., *Synthesis of Graphene and Its Applications: A Review*. Critical Reviews in Solid State and Materials Sciences, 2010. **35**(1): p. 52-71.
111. Zhang, Q., et al., *Graphene oxide-modified electrospun polyvinyl alcohol nanofibrous scaffolds with potential as skin wound dressings*. RSC Advances, 2017. **7**(46): p. 28826-28836.
112. Smith, A.T., et al., *Synthesis, properties, and applications of graphene oxide/reduced graphene oxide and their nanocomposites*. Nano Materials Science, 2019. **1**(1): p. 31-47.
113. Maggio, M., et al., *Thermally stable, solvent resistant and flexible graphene oxide paper*. RSC Advances, 2016. **6**(50): p. 44522-44530.
114. Hu, W., et al., *Graphene-based antibacterial paper*. ACS Nano, 2010. **4**(7): p. 4317-23.
115. Cai, D., et al., *High performance polyurethane/functionalized graphene nanocomposites with improved mechanical and thermal properties*. Composites Science and Technology, 2012. **72**(6): p. 702-707.
116. Lim, H.N., N.M. Huang, and C.H. Loo, *Facile preparation of graphene-based chitosan films: Enhanced thermal, mechanical and antibacterial properties*. 2012. **358**: p. 525.
117. Yousefi, M., et al., *Anti-bacterial activity of graphene oxide as a new weapon nanomaterial to combat multidrug- resistance bacteria*. Materials Science and Engineering C, 2017. **74**.

118. Lee, C., et al., *Measurement of the elastic properties and intrinsic strength of monolayer graphene*. Science, 2008. **321**(5887): p. 385-8.
119. Dikin, D.A., et al., *Preparation and characterization of graphene oxide paper*. Nature, 2007. **448**(7152): p. 457-60.
120. Xu, Z., et al., *Ultrastrong fibers assembled from giant graphene oxide sheets*. Advanced materials (Deerfield Beach, Fla.), 2013. **25**(2): p. 188-193.
121. Jalili, R., et al., *Scalable One-Step Wet-Spinning of Graphene Fibers and Yarns from Liquid Crystalline Dispersions of Graphene Oxide: Towards Multifunctional Textiles*. 2013. **23**(43): p. 5345-5354.
122. Huang, G., et al. *Highly strong and elastic graphene fibres prepared from universal graphene oxide precursors*. Scientific reports, 2014. **4**, 4248 DOI: 10.1038/srep04248.
123. Seyedin, S., et al., *Towards the Knittability of Graphene Oxide Fibres*. Sci Rep, 2015. **5**: p. 14946.
124. Xiang, C., et al., *Large Flake Graphene Oxide Fibers with Unconventional 100% Knot Efficiency and Highly Aligned Small Flake Graphene Oxide Fibers*. 2013. **25**(33): p. 4592-4597.
125. Suk, J.W., et al., *Mechanical Properties of Monolayer Graphene Oxide*. ACS Nano, 2010. **4**(11): p. 6557-6564.
126. Gómez-Navarro, C., M. Burghard, and K. Kern, *Elastic Properties of Chemically Derived Single Graphene Sheets*. Nano Letters, 2008. **8**(7): p. 2045-2049.
127. Zandiatashbar, A., et al., *Effect of defects on the intrinsic strength and stiffness of graphene*. Nature Communications, 2014. **5**(1): p. 3186.
128. Jiang, L., et al., *Preparation and characterization of graphene/poly(vinyl alcohol) nanocomposites*. 2010. **118**(1): p. 275-279.
129. Yang, X., et al., *Well-Dispersed Chitosan/Graphene Oxide Nanocomposites*. ACS Applied Materials & Interfaces, 2010. **2**(6): p. 1707-1713.
130. Liang, J., et al., *Molecular-Level Dispersion of Graphene into Poly(vinyl alcohol) and Effective Reinforcement of their Nanocomposites*. 2009. **19**(14): p. 2297-2302.
131. Zhang, P., et al., *Fracture toughness of graphene*. Nature Communications, 2014. **5**(1): p. 3782.
132. Jung, G., Z. Qin, and M.J. Buehler, *Molecular mechanics of polycrystalline graphene with enhanced fracture toughness*. Extreme Mechanics Letters, 2015. **2**: p. 52-59.
133. Pugno †, N.M. and R.S. Ruoff ‡, *Quantized fracture mechanics*. Philosophical Magazine, 2004. **84**(27): p. 2829-2845.
134. Zhang, B., L. Mei, and H. Xiao, *Nanofracture in graphene under complex mechanical stresses*. 2012. **101**(12): p. 121915.
135. Ky, M.-N. and Y.-J. Yum, *Mode I fracture toughness analysis of a single-layer grapheme sheet*. Journal of Mechanical Science and Technology, 2014. **28**(9): p. 3645-3652.
136. Fadeel, B., et al., *Safety Assessment of Graphene-Based Materials: Focus on Human Health and the Environment*. ACS Nano, 2018. **12**(11): p. 10582-10620.
137. Pinto, A.M., I.C. Gonçalves, and F.D. Magalhães, *Graphene-based materials biocompatibility: a review*. Colloids Surf B Biointerfaces, 2013. **111**: p. 188-202.
138. Bianco, A., *Graphene: safe or toxic? The two faces of the medal*. Angew Chem Int Ed Engl, 2013. **52**(19): p. 4986-97.
139. Lalwani, G., et al., *Toxicology of graphene-based nanomaterials*. Adv Drug Deliv Rev, 2016. **105**(Pt B): p. 109-144.
140. Bullock, C.J. and C. Bussy, *Biocompatibility Considerations in the Design of Graphene Biomedical Materials*. 2019. **6**(11): p. 1900229.
141. Piperno, A., et al., *Cellular Signaling Pathways Activated by Functional Graphene Nanomaterials*. Int J Mol Sci, 2018. **19**(11).
142. Wang, W., Y. Zhang, and W. Liu, *Bioinspired fabrication of high strength hydrogels from non-covalent interactions*. Progress in Polymer Science, 2017. **71**(Supplement C): p. 1-25.
143. Martinez Paino, I.M., F. Santos, and V. Zucolotto, *Biocompatibility and toxicology effects of graphene oxide in cancer, normal, and primary immune cells*. J Biomed Mater Res A, 2017. **105**(3): p. 728-736.
144. Cheng, C., et al., *Biopolymer functionalized reduced graphene oxide with enhanced biocompatibility via mussel inspired coatings/anchors*. Journal of Materials Chemistry B, 2013. **1**(3): p. 265-275.

145. Pinto, A.M., et al., *Smaller particle size and higher oxidation improves biocompatibility of graphene-based materials.* Carbon, 2016. **99**: p. 318-329.
146. Kurapati, R., et al., *Covalent chemical functionalization enhances the biodegradation of graphene oxide.* 2D Materials, 2017. **5**(1): p. 015020.
147. Jaworski, S., et al., *In vitro evaluation of the effects of graphene platelets on glioblastoma multiforme cells.* Int J Nanomedicine, 2013. **8**: p. 413-20.
148. Ou, L., et al., *Toxicity of graphene-family nanoparticles: a general review of the origins and mechanisms.* Part Fibre Toxicol, 2016. **13**(1): p. 57.
149. Kenry, et al., *When stem cells meet graphene: Opportunities and challenges in regenerative medicine.* Biomaterials, 2018. **155**: p. 236-250.
150. Kotchey, G.P., et al., *The enzymatic oxidation of graphene oxide.* ACS Nano, 2011. **5**(3): p. 2098-108.
151. Kurapati, R., et al., *Dispersibility-Dependent Biodegradation of Graphene Oxide by Myeloperoxidase.* Small, 2015. **11**(32): p. 3985-94.
152. Mukherjee, S.P., et al., *Graphene oxide is degraded by neutrophils and the degradation products are non-genotoxic.* Nanoscale, 2018. **10**(3): p. 1180-1188.
153. Li, Z., et al., *Elastic Cu@PPy sponge for hybrid device with energy conversion and storage.* Nano Energy, 2019. **58**: p. 852-861.
154. Ma, J., et al., *Crucial Role of Lateral Size for Graphene Oxide in Activating Macrophages and Stimulating Pro-inflammatory Responses in Cells and Animals.* ACS Nano, 2015. **9**(10): p. 10498-515.
155. Russier, J., et al., *Evidencing the mask effect of graphene oxide: a comparative study on primary human and murine phagocytic cells.* Nanoscale, 2013. **5**(22): p. 11234-47.
156. Sasidharan, A., et al., *Hemocompatibility and macrophage response of pristine and functionalized graphene.* Small, 2012. **8**(8): p. 1251-63.
157. Li, Y., et al., *The triggering of apoptosis in macrophages by pristine graphene through the MAPK and TGF-beta signaling pathways.* Biomaterials, 2012. **33**(2): p. 402-11.
158. Zhou, H., et al., *The interactions between pristine graphene and macrophages and the production of cytokines/chemokines via TLR- and NF-κB-related signaling pathways.* Biomaterials, 2012. **33**(29): p. 6933-42.
159. Mukherjee, S.P., M. Bottini, and B. Fadeel, *Graphene and the Immune System: A Romance of Many Dimensions.* Front Immunol, 2017. **8**: p. 673.
160. Liu, J.H., et al., *Effect of size and dose on the biodistribution of graphene oxide in mice.* Nanomedicine (Lond), 2012. **7**(12): p. 1801-12.
161. Zhang, X., *Distribution and biocompatibility studies of graphene oxide in mice after intravenous administration.* Carbon, 2011. **v. 49**(no. 3): p. pp. 986-995-2011 v.49 no.3.
162. Yin, P.T., et al., *Design, Synthesis, and Characterization of Graphene–Nanoparticle Hybrid Materials for Bioapplications.* Chemical Reviews, 2015. **115**(7): p. 2483-2531.
163. Palmieri, V., et al., *Graphene oxide touches blood: in vivo interactions of bio-coronated 2D materials.* Nanoscale Horizons, 2019. **4**(2): p. 273-290.
164. Kenry, K.P. Loh, and C.T. Lim, *Molecular Hemocompatibility of Graphene Oxide and Its Implication for Antithrombotic Applications.* Small, 2015. **11**(38): p. 5105-17.
165. Singh, S.K., et al., *Amine-Modified Graphene: Thrombo-Protective Safer Alternative to Graphene Oxide for Biomedical Applications.* ACS Nano, 2012. **6**(3): p. 2731-2740.
166. Feng, R., et al., *Impact of graphene oxide on the structure and function of important multiple blood components by a dose-dependent pattern.* J Biomed Mater Res A, 2015. **103**(6): p. 2006-14.
167. Yang, M.C., et al., *Electrochemical Polymerization of PEDOT-Graphene Oxide-Heparin Composite Coating for Anti-fouling and Anti-clotting of Cardiovascular Stents.* Polymers (Basel), 2019. **11**(9).
168. Henriques, P.C., et al., *Graphene Surfaces Interaction with Proteins, Bacteria, Mammalian Cells, and Blood Constituents: The Impact of Graphene Platelet Oxidation and Thickness.* ACS Applied Materials & Interfaces, 2020. **12**(18): p. 21020-21035.
169. Williams, D.F., *Challenges With the Development of Biomaterials for Sustainable Tissue Engineering.* Front Bioeng Biotechnol, 2019. **7**: p. 127.
170. Kenry, K.P. Loh, and C.T. Lim, *Molecular interactions of graphene oxide with human blood plasma proteins.* Nanoscale, 2016. **8**(17): p. 9425-9441.

171. Orecchioni, M., et al., *Graphene and the immune system: Challenges and potentiality.* Adv Drug Deliv Rev, 2016. **105**(Pt B): p. 163-175.
172. Liu, S., et al., *Antibacterial activity of graphite, graphite oxide, graphene oxide, and reduced graphene oxide: membrane and oxidative stress.* ACS Nano, 2011. **5**(9): p. 6971-80.
173. Gurunathan, S., et al., *Oxidative stress-mediated antibacterial activity of graphene oxide and reduced graphene oxide in Pseudomonas aeruginosa.* Int J Nanomedicine, 2012. **7**: p. 5901-14.
174. Zheng, H., et al., *Antibacterial applications of graphene oxides: structure-activity relationships, molecular initiating events and biosafety.* Science Bulletin, 2018. **63**(2): p. 133-142.
175. Shi, L., et al., *The Antibacterial Applications of Graphene and Its Derivatives.* Small, 2016. **12**(31): p. 4165-84.
176. Singh, S.P., et al., *Laser-Induced Graphene Layers and Electrodes Prevents Microbial Fouling and Exerts Antimicrobial Action.* ACS Applied Materials & Interfaces, 2017. **9**(21): p. 18238-18247.
177. Pham, V.T., et al., *Graphene Induces Formation of Pores That Kill Spherical and Rod-Shaped Bacteria.* ACS Nano, 2015. **9**(8): p. 8458-67.
178. Ghosal, K. and K. Sarkar, *Biomedical Applications of Graphene Nanomaterials and Beyond.* ACS Biomaterials Science & Engineering, 2018. **4**(8): p. 2653-2703.
179. Gong, F., et al., *Recent Advances in Graphene-Based Free-Standing Films for Thermal Management: Synthesis, Properties, and Applications.* Coatings, 2018. **8**: p. 63.
180. Nguyen, S.T., *Graphene/Carbon Nanotube Aerogels*. 2018: CRC Press.
181. Priyadarsini, S., et al., *Graphene and graphene oxide as nanomaterials for medicine and biology application.* Journal of Nanostructure in Chemistry, 2018. **8**(2): p. 123-137.
182. Tadyszak, K., J.K. Wychowaniec, and J. Litowczenko, *Biomedical Applications of Graphene-Based Structures.* Nanomaterials (Basel, Switzerland), 2018. **8**(11): p. 944.
183. Shin, Y.C., et al. *Multifaceted Biomedical Applications of Functional Graphene Nanomaterials to Coated Substrates, Patterned Arrays and Hybrid Scaffolds*. Nanomaterials (Basel, Switzerland), 2017. **7**, DOI: 10.3390/nano7110369.
184. Mohan, V.B., et al., *Graphene-based materials and their composites: A review on production, applications and product limitations.* Composites Part B: Engineering, 2018. **142**: p. 200-220.
185. Cunha, C., S. Panseri, and S. Antonini, *Emerging nanotechnology approaches in tissue engineering for peripheral nerve regeneration.* Nanomedicine, 2011. **7**(1): p. 50-9.
186. Wang, Q.L., et al., *The application of graphene oxidized combining with decellularized scaffold to repair of sciatic nerve injury in rats.* Saudi Pharmaceutical Journal, 2017. **25**(4): p. 469-476.
187. Niu, Q.F., et al., *Adsorptive properties of graphene oxide on vitamin B12 and their effect on the promotion of peripheral nerve regeneration.* Neurological Research, 2019. **41**(3): p. 282-288.
188. Duran, N., et al., *Graphene Oxide: A Carrier for Pharmaceuticals and a Scaffold for Cell Interactions.* Current topics in medicinal chemistry, 2015. **15**.
189. Guo, X. and N. Mei, *Assessment of the toxic potential of graphene family nanomaterials.* J Food Drug Anal, 2014. **22**(1): p. 105-115.
190. Çelik, M., et al., *Involuntary movements associated with vitamin B12 deficiency.* Parkinsonism & Related Disorders, 2003. **10**(1): p. 55-57.
191. Mancini, F., et al., *Prevalence and features of peripheral neuropathy in Parkinson's disease patients under different therapeutic regimens.* Parkinsonism Relat Disord, 2014. **20**(1): p. 27-31.
192. Jorfi, M. and E.J. Foster, *Recent Advances in Nanocellulose for Biomedical Applications.* Journal of Applied Polymer Science, 2015. **132**: p. 41719.
193. Hickey, R.J. and A.E. Pelling, *Cellulose Biomaterials for Tissue Engineering.* 2019. **7**(45).
194. Namvar, F., et al., *Potential Use of Plant Fibres and their Composites for Biomedical Applications.* Bioresources, 2014. **9**.
195. Rojas, J., *Current trends in the production of cellulose nanoparticles and nanocomposites for biomedical applications.* Cellulose - Fundamental Aspects and Current Trends, 2015.
196. Toker, M., et al., *Decellularization and characterization of leek: a potential cellulose-based biomaterial.* Cellulose, 2020. **27**(13): p. 7331-7348.

197. Tarassoli, S.P., et al., *Skin tissue engineering using 3D bioprinting: An evolving research field.* Journal of Plastic, Reconstructive & Aesthetic Surgery, 2018. **71**(5): p. 615-623.
198. Fu, J.P., et al., *Reduced Graphene Oxide Incorporated Acellular Dermal Composite Scaffold Enables Efficient Local Delivery of Mesenchymal Stem Cells for Accelerating Diabetic Wound Healing.* Acs Biomaterials Science & Engineering, 2019. **5**(8): p. 4054-4066.
199. Srivastava, A., et al., *Use of porcine acellular dermal matrix as a dermal substitute in rats.* Annals of surgery, 2001. **233**(3): p. 400-408.
200. Zhang, Q., et al., *Reduction pathway-dependent cytotoxicity of reduced graphene oxide.* Environmental Science: Nano, 2018. **5**(6): p. 1361-1371.
201. Thi Tran, T.T., et al., *Tithonia diversifolia pectin – reduced graphene oxide and its cytotoxic activity.* Materials Letters, 2016. **183**: p. 127-130.
202. Mukherjee, S., et al., *Graphene Oxides Show Angiogenic Properties.* Adv Healthc Mater, 2015. **4**(11): p. 1722-32.
203. Chakraborty, S., et al., *Reduced graphene oxide-loaded nanocomposite scaffolds for enhancing angiogenesis in tissue engineering applications.* Royal Society Open Science, 2018. **5**: p. 172017.
204. Kang, Y., et al., *Graphene oxide and reduced graphene oxide induced neural pheochromocytoma-derived PC12 cell lines apoptosis and cell cycle alterations via the ERK signaling pathways.* International journal of nanomedicine, 2017. **12**: p. 5501-5510.
205. Nie, W., et al., *Three-dimensional porous scaffold by self-assembly of reduced graphene oxide and nano-hydroxyapatite composites for bone tissue engineering.* Carbon, 2017. **116**: p. 325-337.
206. Syama, S., et al., *Nano-bio compatibility of PEGylated reduced graphene oxide on mesenchymal stem cells.* 2D Materials, 2017. **4**(2): p. 025066.
207. Jafarkhani, M., et al., *Graphene functionalized decellularized scaffold promotes skin cell proliferation.* Canadian Journal of Chemical Engineering, 2019.
208. Tuan, R.S., A.F. Chen, and B.A. Klatt, *Cartilage regeneration.* J Am Acad Orthop Surg, 2013. **21**(5): p. 303-11.
209. Makris, E.A., et al., *Repair and tissue engineering techniques for articular cartilage.* Nat Rev Rheumatol, 2015. **11**(1): p. 21-34.
210. Gong, M., et al., *Graphene oxide-modified 3D acellular cartilage extracellular matrix scaffold for cartilage regeneration.* Materials Science & Engineering C-Materials for Biological Applications, 2021. **119**.
211. Kang, H., et al., *In vivo cartilage repair using adipose-derived stem cell-loaded decellularized cartilage ECM scaffolds.* J Tissue Eng Regen Med, 2014. **8**(6): p. 442-53.
212. Murphy, C.M., et al., *Cell-scaffold interactions in the bone tissue engineering triad.* Eur Cell Mater, 2013. **26**: p. 120-32.
213. Sutherland, A.J., et al., *The bioactivity of cartilage extracellular matrix in articular cartilage regeneration.* Adv Healthc Mater, 2015. **4**(1): p. 29-39.
214. Huo, D., et al., *Construction of Antithrombotic Tissue-Engineered Blood Vessel via Reduced Graphene Oxide Based Dual-Enzyme Biomimetic Cascade.* Acs Nano, 2017. **11**(11): p. 10964-10973.
215. Zhang, Y., et al., *Assembly of graphene oxide-enzyme conjugates through hydrophobic interaction.* Small, 2012. **8**(1): p. 154-9.
216. Jin, L., et al., *Functionalized graphene oxide in enzyme engineering: a selective modulator for enzyme activity and thermostability.* ACS Nano, 2012. **6**(6): p. 4864-75.
217. Wilczek, P., et al., *Thrombogenicity and biocompatibility studies of reduced graphene oxide modified acellular pulmonary valve tissue.* Mater Sci Eng C Mater Biol Appl, 2015. **53**: p. 310-21.
218. Singh, S.K., et al., *Thrombus inducing property of atomically thin graphene oxide sheets.* ACS Nano, 2011. **5**(6): p. 4987-96.
219. Obiweluozor, F.O., et al., *Considerations in the Development of Small-Diameter Vascular Graft as an Alternative for Bypass and Reconstructive Surgeries: A Review.* Cardiovascular Engineering and Technology, 2020. **11**(5): p. 495-521.
220. Weiss, A.J. and A. Elixhauser, *Trends in Operating Room Procedures in U.S. Hospitals, 2001–2011: Statistical Brief #171*, in *Healthcare Cost and Utilization Project (HCUP) Statistical Briefs*. 2006, Agency for Healthcare Research and Quality (US): Rockville (MD).

221. Devine, C., B. Hons, and C. McCollum, *Heparin-bonded Dacron or polytetrafluoroethylene for femoropopliteal bypass grafting: a multicenter trial.* J Vasc Surg, 2001. **33**(3): p. 533-9.
222. Tschoeke, B., et al., *Tissue-engineered small-caliber vascular graft based on a novel biodegradable composite fibrin-polylactide scaffold.* Tissue Eng Part A, 2009. **15**(8): p. 1909-18.
223. Hamaguchi, M., et al., *Short-term thrombogenicity and patency of expanded polytetrafluoroethylene (ePTFE) vascular grafts with varying wall structure.* 1994. **23**: p. 832-837.
224. Huang, A.H. and L.E. Niklason, *Engineering of arteries in vitro.* Cell Mol Life Sci, 2014. **71**(11): p. 2103-18.
225. Catto, V., et al., *Vascular Tissue Engineering: Recent Advances in Small Diameter Blood Vessel Regeneration.* ISRN Vascular Medicine, 2014. **2014**: p. 923030.
226. Seifu, D.G., et al., *Small-diameter vascular tissue engineering.* Nature Reviews Cardiology, 2013. **10**(7): p. 410-421.
227. Ishino, N. and T. Fujisato, *Decellularization of porcine carotid by the recipient's serum and evaluation of its biocompatibility using a rat autograft model.* J Artif Organs, 2015. **18**(2): p. 136-42.
228. Nagaoka, Y., et al., *Reconstruction of small diameter arteries using decellularized vascular scaffolds.* J Med Dent Sci, 2014. **61**(1): p. 33-40.
229. Amensag, S., et al., *Pilot assessment of a human extracellular matrix-based vascular graft in a rabbit model.* J Vasc Surg, 2017. **65**(3): p. 839-847.e1.
230. Haruguchi, H. and S. Teraoka, *Intimal hyperplasia and hemodynamic factors in arterial bypass and arteriovenous grafts: a review.* J Artif Organs, 2003. **6**(4): p. 227-35.
231. Zeng, W., et al., *The use of BDNF to enhance the patency rate of small-diameter tissue-engineered blood vessels through stem cell homing mechanisms.* Biomaterials, 2012. **33**(2): p. 473-84.
232. Koobatian, M.T., et al., *Successful endothelialization and remodeling of a cell-free small-diameter arterial graft in a large animal model.* Biomaterials, 2016. **76**: p. 344-58.
233. Kong, X., et al., *The use of heparin, bFGF, and VEGF 145 grafted acellular vascular scaffold in small diameter vascular graft.* J Biomed Mater Res B Appl Biomater, 2019. **107**(3): p. 672-679.
234. Andreia T. Pereira, et al., *Graphene oxide-reinforced poly(2-hydroxyethyl methacrylate) hydrogels with extreme stiffness and high-strength.* Composites Science and Technology,, 2019. **Volume 184**.
235. Wendel, H.P. and G. Ziemer, *Coating-techniques to improve the hemocompatibility of artificial devices used for extracorporeal circulation.* Eur J Cardiothorac Surg, 1999. **16**(3): p. 342-50.
236. Morinha, F., et al., *DNA sampling from body swabs of terrestrial slugs (Gastropoda: Pulmonata): a simple and non-invasive method for molecular genetics approaches.* Journal of Molluscan Studies, 2014. **80**(1): p. 99-101.
237. Timochenco, L., et al., *High-Yield Production of Nano-Lateral Size Graphene Oxide by High-Power Ultrasonication.* Materials (Basel), 2021. **14**(8).
238. Bergmeister, H., et al., *Healing characteristics of electrospun polyurethane grafts with various porosities.* Acta Biomater, 2013. **9**(4): p. 6032-40.
239. Bergmeister, H., et al., *In vivo remodeling of decellularized xenogeneic arteries: Impact of heparin-crosslinking on graft stability.* Journal of Heart and Lung Transplantation - J HEART LUNG TRANSPLANT, 2007. **26**.
240. Gonçalves, I.C., et al., *Protein adsorption and clotting time of pHEMA hydrogels modified with C18 ligands to adsorb albumin selectively and reversibly.* Biomaterials, 2009. **30**(29): p. 5541-51.
241. Ungerleider, J.L., et al., *Fabrication and characterization of injectable hydrogels derived from decellularized skeletal and cardiac muscle.* Methods, 2015. **84**: p. 53-9.
242. Mancuso, L., et al., *Decellularized ovine arteries as small-diameter vascular grafts.* Biomedical Materials, 2014. **9**(4).
243. Konig, G., et al., *Mechanical properties of completely autologous human tissue engineered blood vessels compared to human saphenous vein and mammary artery.* Biomaterials, 2009. **30**(8): p. 1542-50.

244. Lamm, P., et al., *Autologous endothelialized vein allograft: a solution in the search for small-caliber grafts in coronary artery bypass graft operations.* Circulation, 2001. **104**(12 Suppl 1): p. I108-14.
245. Hao, C., et al., *Heparin: An essential drug for modern medicine.* Prog Mol Biol Transl Sci, 2019. **163**: p. 1-19.
246. Guvendiren, M., H.D. Lu, and J.A. Burdick, *Shear-thinning hydrogels for biomedical applications.* Soft Matter, 2012. **8**(2): p. 260-272.
247. Burdick, J.A. and G.D. Prestwich, *Hyaluronic acid hydrogels for biomedical applications.* Adv Mater, 2011. **23**(12): p. H41-56.
248. Ananthanarayanan, B., Y. Kim, and S. Kumar, *Elucidating the mechanobiology of malignant brain tumors using a brain matrix-mimetic hyaluronic acid hydrogel platform.* Biomaterials, 2011. **32**(31): p. 7913-23.
249. Zuidema, J.M., et al., *Fabrication and characterization of tunable polysaccharide hydrogel blends for neural repair.* Acta Biomaterialia, 2011. **7**(4): p. 1634-1643.
250. Taylan, E. and K. Oktay, *Application of Decellularized Tissue Scaffolds in Ovarian Tissue Transplantation.* Methods Mol Biol, 2018. **1577**: p. 177-181.
251. Zhang, Y., et al., *Preparation of a nano- and micro-fibrous decellularized scaffold seeded with autologous mesenchymal stem cells for inguinal hernia repair.* Int J Nanomedicine, 2017. **12**: p. 1441-1452.
252. Gupta, A., S.D. Kedige, and K. Jain, *Amnion and Chorion Membranes: Potential Stem Cell Reservoir with Wide Applications in Periodontics.* Int J Biomater, 2015. **2015**: p. 274082.
253. Chen, E. and A. Tofe, *A literature review of the safety and biocompatibility of amnion tissue. – ScienceOpen.* The Journal of Implant &
Advanced Clinical Dentistry. **2**.
254. Koizumi, N.J., et al., *Growth factor mRNA and protein in preserved human amniotic membrane.* Curr Eye Res, 2000. **20**(3): p. 173-7.
255. Lee, S.B., et al., *Suppression of TGF-beta signaling in both normal conjunctival fibroblasts and pterygial body fibroblasts by amniotic membrane.* Curr Eye Res, 2000. **20**(4): p. 325-34.
256. Liu, S.K., et al., *Off-the-Shelf Biomimetic Graphene Oxide-Collagen Hybrid Scaffolds Wrapped with Osteoinductive Extracellular Matrix for the Repair of Cranial Defects in Rats.* Acs Applied Materials & Interfaces, 2018. **10**(49): p. 42948-42958.
257. Liu, S.K., et al., *Biocompatible graphene oxide-collagen composite aerogel for enhanced stiffness and in situ bone regeneration.* Materials Science & Engineering C-Materials for Biological Applications, 2019. **105**.
258. Ott, H.C., et al., *Perfusion-decellularized matrix: using nature's platform to engineer a bioartificial heart.* Nat Med, 2008. **14**(2): p. 213-21.
259. Zuidema, J.M., et al., *A protocol for rheological characterization of hydrogels for tissue engineering strategies.* J Biomed Mater Res B Appl Biomater, 2014. **102**(5): p. 1063-73.
260. Claudio-Rizo, J.A., et al. *Chapter 1 Decellularized ECM-Derived Hydrogels : Modification and Properties*. 2018.
261. Derby, B., *Printing and prototyping of tissues and scaffolds.* Science, 2012. **338**(6109): p. 921-6.
262. Hillel, A.T., et al., *Photoactivated composite biomaterial for soft tissue restoration in rodents and in humans.* Sci Transl Med, 2011. **3**(93): p. 93ra67.
263. Martens, T.P., et al., *Percutaneous cell delivery into the heart using hydrogels polymerizing in situ.* Cell Transplant, 2009. **18**(3): p. 297-304.